SF 298 MASTER COPY KEEP THIS COPY FOR REPRODUCTION PURPOSES

REPORT DOCUMENTATION PAGE

Form Approved
OMB NO. 0704-0188

1. AGENCY USE ONLY *(Leave blank)*	2. REPORT DATE	3. REPORT TYPE AND DATES COVERED
	August 1998	Final 7/1/95 - 7/9/98

4. TITLE AND SUBTITLE

Analysis of Advanced Direct-Injection Diesel Engine Development Strategies

5. FUNDING NUMBERS

DAAH04-95-1-0430

6. AUTHOR(S)

K. T. Rhee

7. PERFORMING ORGANIZATION NAMES(S) AND ADDRESS(ES)

Rutgers, The State University of New Jersey
College of Engineering
Mechanical and Aerospace Engineering
Piscataway, NJ 08854

8. PERFORMING ORGANIZATION REPORT NUMBER

9. SPONSORING / MONITORING AGENCY NAME(S) AND ADDRESS(ES)

U.S. Army Research Office
P.O. Box 12211
Research Triangle Park, NC 27709-2211

10. SPONSORING / MONITORING AGENCY REPORT NUMBER

ARO 34452.4-EG

11. SUPPLEMENTARY NOTES

The views, opinions and/or findings contained in this report are those of the author(s) and should not be construed as an official Department of the Army position, policy or decision, unless so designated by other documentation.

12a. DISTRIBUTION / AVAILABILITY STATEMENT

Approved for public release; distribution unlimited.

13. ABSTRACT *(Maximum 200 words)*

The methodology of achieving a high power density (HPD, or brake mean effective pressure) direct-injection Diesel engine has been studied, which is directed to using high fuel/air ratio, high-speed and ceramic engine components. Among the main thrust to achieve these engine changes for an advanced Diesel engine is the design of a high injection pressure (HIP) fuel system. During the course of the present study, two Cummins 903 engines mated with a Rutger-built HIP were employed to investigate the engine response to HIP and in-cylinder processes by using the Rutgers high-speed infrared (IR) spectral digital imaging system.

Five separate technical publications were prepared to report results obtained from the study. The main findings include: The HIP system permits engine operation at an air/fuel ratio of as rich as 18 to 1 with smoke emission not worse than with the conventional mechanical (low pressure) injection system; A high injection pressure improves HPD of a Diesel engine; A HIP unit promotes the (invisible) preflame reactions during the ignition delay period; The formation of the very first flame kernel is significantly affected by a cetane improver (fuel additive); The new three-color method developed in the present study was used to determine simultaneous distributions of temperature, soot and water vapor in the engine cylinder; and more. The techniques developed on the present ARO-sponsorship were employed in other engine studies and carried out under the sponsorship of industrial members and other US governmental components.

14. SUBJECT TERMS	15. NUMBER IF PAGES
High power density, Direct-injection, Diesel Combustion, Spectral IR images, Quantitative imaging.	70
	16. PRICE CODE

17. SECURITY CLASSIFICATION OR REPORT	18. SECURITY CLASSIFICATION OF THIS PAGE	19. SECURITY CLASSIFICATION OF ABSTRACT	20. LIMITATION OF ABSTRACT
UNCLASSIFIED	UNCLASSIFIED	UNCLASSIFIED	UL

Table of Content

Analysis of Advanced Direct-Injection Diesel Engine Development Strategies

Executive Summary

The methodology of achieving a high power density (HPD, or high brake mean effective pressure) direct-injection Diesel engine has been studied, which is directed to using high fuel/air ratio, high-speed and ceramic engine components.

Among the main thrust to achieve these engine changes for an advanced Diesel engine is the design of a high injection pressure (HIP) fuel system. During the course of the present study, two Cummins 903 engines mated with a Rutger-built HIP were employed to investigate the engine response to HIP and in-cylinder processes by using the Rutgers high-speed infrared (IR) spectral digital imaging system (which was referred to as the Super Imaging System, SIS by others).

Five separate technical publications were prepared to report results obtained from the study. The main findings include: The HIP system permits engine operation at an air/fuel ratio of as rich as 18 to 1 with smoke emission not worse than with the conventional mechanical (low pressure) injection system; A high injection pressure improves HPD of a Diesel engine; A HIP unit promotes the (invisible) preflame reactions during the ignition delay period; The formation of the very first flame kernel is significantly affected by a cetane improver (fuel additive); The new three-color method developed in the present study was used to determine simultaneous distributions of temperature, soot and water vapor in the engine cylinder; and more. The techniques developed on the present ARO-sponsorship were employed in other engine studies and carried out under the sponsorship of industrial members and other US governmental components.

Analysis of Advanced Direct-Injection Diesel Engine Development Strategies

K. T. Rhee
Department of Mechanical and Aerospace Engineering
Rutgers, The State University of New Jersey
Piscataway, New Jersey 08855-0909

1. Introduction

Technology advancement of Diesel engines, the main power plant utilized in US Army ground vehicles, has an emphasis on designing high mean-effective-pressure (BMEP) and high fuel-efficiency systems. Many different paths are taken to achieve this goal at present, which needs further analysis.

Direct Injection Diesel Engine. A direct injection (DI) compression ignition (CI) engine has advantages over an indirect injection (IDI) engine, including higher efficiency and power density. The engine's simple induction system and open chamber for rapid heat release, however, produce low gas motions. This requires a greater role by the fuel injection unit for improved mixing, particularly if a high smoke-limited power output is to be obtained. A "better" injector is, therefore, desired for increasing the over-all fuel/air ratio, engine speed and induction pressure which are typical design practices employed for achieving a high BMEP or higher power-density.

Some Advanced Diesel Technology Strategies. Any measure of improving the engine performance, however, is only useful when the new engine meets the regulatory emission standards and other desirable characteristics, e.g. low noise and easy starting. In developing an improved DI-CI engine that delivers those desirable engine characteristics, some of which are mutually exclusive with each other, many unconventional changes in the engine-fuel system are implemented, such as: very high pressure fuel injection (HPI); multiple fuel injections per cycle; pilot injection; adiabatic engine; new fuel additives; fuel reformulation (e.g. oxygenated fuels having high cetane number), and even oxygen-enrichment of the intake air. In view of the ever growing demand for an improved engine by the law as well as engine-users, such radical changes in both the engine and fuels will continue to be explored in the future.

Note that some of those methods have already offered promising improvement: For example, a tailored-double fuel-injection (achieved by an electronic-controlled injector) produced low emissions of both NOx and particulates. The HPI, a similar methodology of tailored-injection, also appears to be an attractive strategy for advancement of Diesel engine technology. It is to complete the fuel injection within a short period of time by starting it relatively late but delivering fuel at a high rate. The method is expected to result in smaller droplets more uniformly spread over a large volume of fuel spray plume, which gives rise to a short ignition delay. The uniform distribution is expected to reduce excessively fuel-rich (high-temperature) pockets. These all would help produce more rapid heat release occurring at a somewhat delayed time, which is expected to improve thermal efficiency and to produce low emissions of NOx and also particulates.

What is Missing? While those developmental measures are incorporated with the system basics of existing DI-CI engines, there is no doubt that the development can be much better facilitated (e.g. design of a new matching combustion chamber) if the in-cylinder reaction processes are better understood when such engine-fuel changes are made.

Probably one of the more important pieces of information missing at present is regarding thermo-chemical behavior as fuel and air are mixed during the period of early fuel injection or ignition delay, particularly when the injector parameters are greatly changed. (It is noted that the same is not well known for the existing engine either.) It is reasonable to predict that the preflame reactions are altered by new advancement strategies, e.g. the HPI highly affect the subsequent in-cylinder processes, which relationships need extensive studies for achieving better engine development.

What is New? In spite of their usefulness in other aspects, the images of very high-temperature reaction zones (during the post flame period), obtained by using conventional high-speed photography (or a visible-range light sensor), do not directly indicate what is happening during the preflame period. In order to help study invisible (low-temperature thermal) as well as visible in-cylinder processes, a new engine/flame diagnostic system has been developed during the last several years [1-4]. The system *simultaneously captures four geometrically identical infrared (IR) images in respective spectral bands at high rates* for quantitative analysis. For convenience of discussion, this system is hereafter called the Rutgers System, or super imaging system (SIS) as referred to by others. This prototype system, made operational in early 1994, has continuously been improved and new data-processing methods have also been developed for its enhanced applications to engine/flame studies.

2. Objectives of the Present Study

The present proposal was to analyze advanced engine and fuel technology strategies being taken for designing a better direct injection compression ignition (DI-CI) engine. This was performed by using a DI-CI engine apparatus equipped with an electronic-controlled new Rutgers-built HIP system and the new Rutgers high-speed multispectral infrared (IR) system (or SIS) combined with new data analysis methods.

3. Discussion of Problems and Methodology

It is not a secret that the methodology of computational analysis of a complex transient multiphase reacting flow, e.g. in-cylinder DI-CI engine processes, needs additional improvement for reasonable applications. Measurements obtained using the conventional diagnostic probes (at a limited number of locations) from such a reaction have been a main source of information for increasing our knowledge about the processes. But, the limitations of those results are well recognized. For example, the species concentration determined using a sampling probe does not help provide us with the overall picture of a rapidly flowing process.

Technology advancements in the electro-optical area achieved in recent years, however, offer new possibilities of *quantitative images* of the complex reactions, i.e., many data points simultaneously obtained over the reactor. Our SIS (the description of the system is made in the Appendix) used in the present study is one of such new tools given rise to by those modern technology advancements. Our engine apparatus (Fig. 1) with new HIP units (two units of HIP built at Rutgers, whose illustration is shown in the Appendix) have the versatility of analyzing in-cylinder processes of engines incorporating recent advanced engine development strategies being taken in the engine community. The cylinder head has an optical access (shaded area) barely big enough to investigate one spray plume as shown in Fig. 2.

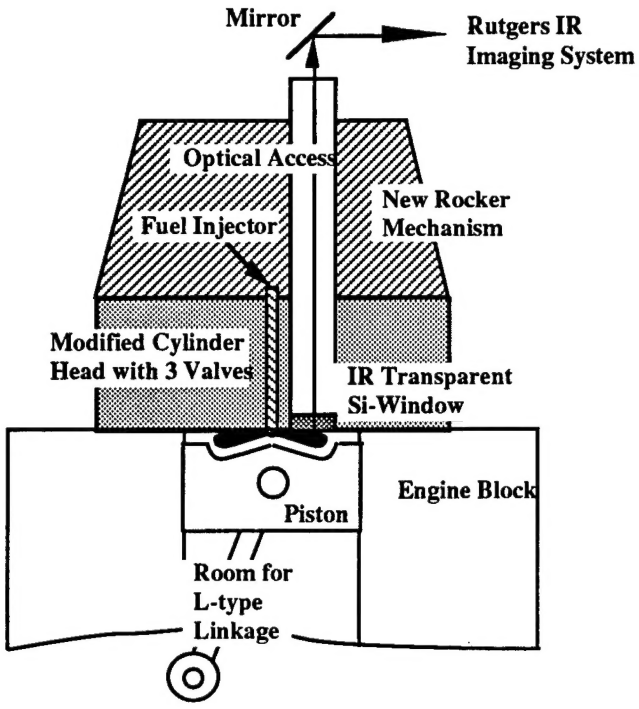

Fig. 1. Single Cylinder Engine Mounted with a Cummins 903 Cylinder Head with Optical Access for the SIS or Rutgers IR System.

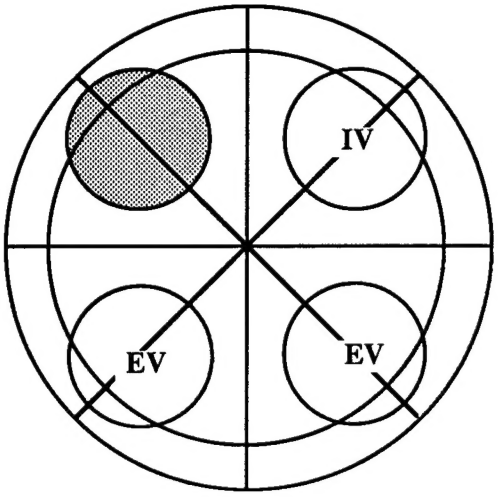

Fig. 2. Optical Access (shaded area) with respect to Spray Plume Axes.

3-1. Why Spectral IR Images at High Rates?

Thermally Important and More. Thanks to revealing fingerprints exhibited by the vibrational molecular excitation in the region of relatively low-level quantum energies, infrared (IR) spectrometry is often employed for various analytical and quantitative purposes *in the thermal regime*. The key to achieving the quantitative imaging is to combine our SIS technology with traditional spectrometry. Such unique advantages are not readily attainable by a visible-range system because the "fingerprint" in the emission (or absorption) spectrum (produced by the object) is not obvious in the visible range.

Furthermore, during the process of our exploratory study of the in-cylinder processes of our CI-DI engine equipped with a HIP unit, something quite unexpected was discovered: When high-speed spectral IR images were obtained (from the engine described in Fig. 1 through the optical access depicted in Fig. 2) using the SIS in wavelength bands of (A) 2.2-2.5μm and (B) 3.43μm, some obvious preflame reactions were observed to take place during the ignition delay period, which will be further explained below.

Knowing the exact time of fuel injection and comparing the successive images with a pressure-time (p-t) diagram, the first image obtained in 2.2-2.5μm band was inferred to indicate the occurrence of premixed combustion. In the set captured in 3.43μm, however, there are images revealing progressive preflame reactions. It appears that the (invisible) preflame reaction started *immediately* after the fuel injection. As far as we found to date, the early preflame images are interpreted to represent chemiluminescent radiation [6,7].

Among several new findings associated with this phenomenon is that the very center of first (visible) flame kernel seems to be identifiable by looking at the (invisible) preflame images. Extensive discussion on this finding is included elsewhere [6]. Again, the high-speed spectral IR images by our new SIS have helped uncover something unknown in the past.

3-2. What Can be Studied by SIS?

During the course of our continuing engine studies using the SIS, we have come to know that our new tool will permit us to see many invisible processes which have not been observed in the past. They include:

- o. Thermal/chemical state of mixtures during the ignition delay period can be captured, even possibly some specific species distributions.
- o. Whereabouts of (high-temperature) combustion products (with respect to the reactor walls), which become rapidly invisible once the reaction completes, can be mapped out.
- o. Images of unreacted fuel/air mixtures (also the end-gas in SI engine combustion), which are subject to compression attaining high-temperature leading to self-ignition, can be captured.
- o. Residual gas mixtures during the compression stroke may also be imaged using the new tool.
- o. Thermal responses of the reactor wall to the presence of the combustion products can also be determined at the same time.

In addition to those invisible phenomena, there are many (visible) processes that can readily be studied using the new SIS, as listed below.

- o. The very kernel of self-ignition (e.g. exhibited by the presence of water vapor in the combustion product) can be located. (This is facilitated by looking at invisible preflame images)
- o. Propagation of reaction fronts can be traced over the spray.
- o. Distributions of soot can be determined, which may be compared with temperature (and water vapor) distribution.
- o. Temperature distributions over the spray plume can be achieved, and more.

Since, in our SIS system, many of those phenomena are recorded by simultaneously obtaining four spectral (digital) IR images at successive instants of time, their mutual relationships can be studied, e.g. a relationship between the chemiluminescence in the preflame period and the soot distribution in the post flame period.

It is noted that the dynamics of reaction processes can be studied by the successive images captured at high rates. It is our experience that a video display *greatly* helps improve our understanding of a rapidly reacting flow phenomenon, which we can hardly achieve by looking at still pictures.

Because of the SIS's capability of displaying in situ results obtained from an in-cylinder investigation, more consistent investigation can be achieved, e.g. without altering the engine operational condition.

3-3. Method

The methods to be employed in the present study were mostly experimental, and were was augmented by the (computational) spectrometric (data) analysis method. The present section, therefore, includes some description of the engine apparatus, the Rutgers System or SIS, experimental method and the data processing method.

3-3-1. Engine

Engine. The single-cylinder DI-CI engine, which was used for the present study, was constructed in collaboration with Power Energy International (Madison, WI) and BKM, Inc. (San Diego, CA), under the sponsorship of the U.S. Department of Defense University Research Initiative. The engine body was constructed to accommodate components from a Cummins 903 engine. It is pointed out that in this new single-cylinder arrangement, the engine (Fig. 1) uses a section of the 903 cylinder head to obtain representative characteristics of the DI-CI engine population. In order to facilitate future investigation of other combustion problems, the new engine design-construction incorporated several flexible design considerations, such as separate control of both coolant and oil flows in the cylinder head and the block, respectively; reserving a large amount of space in the crankcase (e.g. for easy installation of a linkage system that retains thermocouple wires from the piston-crown to the data system outside the engine crankcase).

Some modifications were made on the Cummins engine cylinder head for installing an IR optical window: conversion of one of the intake valves to the optical access; a new rocker-arm mechanism, which provided a cylindrical space for the optical passage; a pressure transducer installed flush with the chamber wall; a measure to use either a Cummins (mechanical) PT unit injector or BKM's Servojet electronic-controlled HPI injector. In addition, since the installation of the IR window was to be made leak-proof, while permitting frequent cleaning of the soot deposit over the surface, an installation method was newly introduced using an o-ring [4]. (The typical time required to complete the window cleaning was about three minutes.) The optical access (with viewing area of 37mm diameter) was made big enough to cover the projected view of a spray plume out of an eight-hole (0.15mm diameter) nozzle, which assumes all spray plumes to be identical.

High-Pressure Injection. In order to compare the in-cylinder processes obtained by the original (mechanical) PT injector mated with the present Cummins 903 engine cylinder head, an electronically controlled HPI system was newly constructed in our laboratory. The new unit was basically a BKM Servojet unit injector of the accumulator type [6]. Because of the crowded engine cylinder head due to new installation of an optical access and a pressure transducer (in addition to the existing components such as the valve train), the relatively bulky Servojet unit was not usable in the apparatus. Keeping the original system design features, an entirely new injector unit was fabricated in our laboratory: Among the key considerations taken into account for this was to use original injector tips of the Cummins PT nozzle, which was to provide technical and economic flexibility in choosing different injector tip geometry. The operation of the injector was performed by using the same electronic package given with the original Servojet unit.

An extensive bench-top characterization of this new injector package was performed in order to determine several important pieces of information about the new HPI, including the relationships of the actual start of fuel injection and the amount of fuel injected per cycle to the input control by the electronic signals, i.e., the pulse width and timing, and the accumulator pressure, respectively. (It is pointed out that the start of injection is defined as the time when the fuel plume tip reached a sensor located about 10mm away from the injector nozzle hole.) The injection (sac) pressure-time history has not been measured in the present characterization, but was inferred to be the same as the original unit [6], which

resembles a spike-shape that collapses rapidly to have a very short residual period of low injection pressure. Based on our experience of fabricating the existing HIP unit in our laboratory, a separate new unit was designed for improved controllability and injector performance.

3-3-2. High-Speed Multispectral Infrared Imaging System.

As mentioned earlier, the "fingerprint" of (both low and high temperature) thermo-chemical molecular characteristics (such as distributions of temperature, reaction fronts and species population) can be found more in the IR domain than the visible range. This fact motivated us to develop a new high-speed spectral IR digital imaging system several years ago. The development of our IR system at Rutgers has been a progressive course of work. The first generation of this research tool captured successive flame images at high rates using only a single camera head [1]. The next system employed two camera heads in order to capture two geometrically (pixel-to-pixel) identical IR images in respective spectral bands, i.e., a two-color system [2,3], which permitted determination of temperature and water vapor distributions in flames [3]. Its prototype electronic systems were all fabricated via hand-wiring directly using many transistor-transistor-logic (TTL) components. One of the main functions of the camera circuits was to generate the timing signals required to operate the charge-coupled-device (CCD). This two-color system was redesigned (using Protel and Orcad design systems) and constructed in printed boards, which included several programmable logic gate arrays (using Max-Plus, Altera Corp.) that replaced most TTL components to take IR images having minimum noise.

In the new SIS, four separate high-speed IR cameras are lined up to a single optical unit, and are simultaneously triggered at successive instants of time by using signals generated from the engine being investigated, which permits capturing a set of four geometrically identical images at each moment. In order to maximize the radiation energy incident on the imagers housed in the liquid-nitrogen cooled Dewars, a large reflective optical head (152mm diameter) was employed which was followed by three pieces of new spectral beam splitters. This divides the IR domain into four ranges for respective imagers. Narrow band filters were installed in front of respective cameras. Among the filters with central wavelengths employed to date are 2.2μm, 2.47μm, 3.43μm, and 3.8μm. In spite of the small amount of radiation passing through those band filters, cryogenically cooled PtSi imagers have sufficiently high sensitivity. Unlike in most high-speed visible-range imaging, no separate (IR) light source was needed. A schematic presentation of the SIS' is made in Fig. 3.

Since the development of our IR imaging system was an unconventional attempt using IR imagers (64x128 PtSi Schottky-barrier detector) other peripheral units were newly designed/fabricated in our laboratory. (Figure 3 shows a block diagram of this four-color system, or SIS.) Those printed in an outlined font in the figure were newly developed at Rutgers because no ready-made substitute was available at reasonable cost on the market. The imaging rate is changeable to obtain over 4 x 1,800 frames/sec and the exposure period can be adjusted at the same time to have as short as 10μsec. The imaging system was integrated with a new package of electronic circuits to independently vary: (1) the start of imaging; (2) the interval of imaging (as individually triggered by the corresponding engine CA markers); and (3) the number of images to be captured per cycle of the engine. As mentioned before, the prototype four-color system which was made operational earlier had many things to be improved upon, which include several modifications in the imager-driving circuits for increased sensitivity, disposal of video signal prior to digitization, and elimination of unwanted charge generated during the off-data acquisition periods.

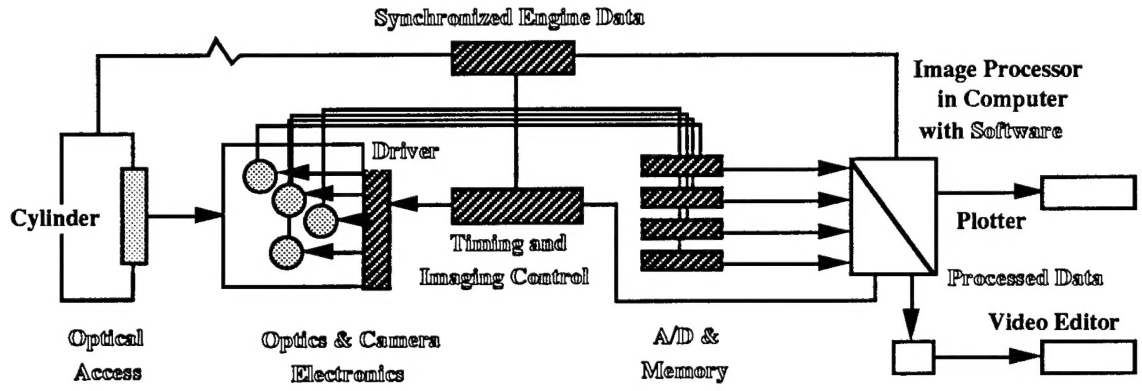

Fig. 3. High-Speed Multispectral IR Imaging System with Data Acquisition-Processing Units.

A parametric study of the new imaging system for characterizing its performance was an important precondition in order to obtain predictable and consistent digital images under various imaging conditions.

Quantitative Imaging. The digital data from individual pixels of spectral images are obtained in a 12-bit dynamic resolution, which are then processed for "quantitative imaging." As briefly mentioned earlier, a separate work is being implemented to develop a new spectrometric data analysis method applicable in the engine/flame environment. Three main computer programs are integrated in the method: (1) the conventional two-color method for determining temperature of a solid wall; (2) the widely known two-color method for determining distributions of temperature and soot in spray combustion [4]; and (3) a new dual band method.

Since the former two methods are relatively well known, the third one will only be mentioned here (More details of the method and results are discussed in Appendix). Some typical problems in the radiation area involve determination of spectral radiation from a given volume of combustion products with known species concentration and temperature. What is being achieved in our new study is determination of species concentration and temperature within the volume for given values of spectral radiation, a reverse problem. Our data-based computer program employs the single-line-group model by Ludwig, et al. [5]. In the present work, the method is extended to its application to the engine environment. This work involves not only development of a new data processing method but also new design and fabrication of a data acquisition system synchronized with the SIS in order to obtain the length of the optical path and the cylinder pressure for corresponding spectral images.

3-3-3. SIS Performance Summary

A brief summary of system performance is included below:

- o. Variable and high frame-rate, up to 4 x 1,800frames/sec.
- o. Variable and short exposure period, as short as 10μsec.
- o. Variable aperture, to obtain images in mutually comparable intensity
- o. Variable and narrow band spectrum image, with range of 2.1-5.5μm
- o. Dynamic resolution, 12-bit resolution
- o. Uniform sensitivity among individual pixels in an imager,. Corrected

o. Spatial resolution, 64 x 128
o. Amount of data storage with computer interface, 256 images per channel
o. Individual images by encoder signals in a controlled manner.

4. Relationship of the Present Study to Other Activities

There have been several main engine-fuel studies being carried out in our laboratory under separate sponsorships (as explained in Appendix). Two separate SI engines with optical access became available under the sponsorship of Ford Motor Company. The first is a single-cylinder unit mated with a Ford 302 cylinder head and the second is a Ford 4.6 modular engine modified to have an optical access. Among the new data to be obtained from this experiment are,

. Fuel spray and reactions during the start-up condition
. Thermal response of Ford 4.6 modular engine
. Engine knock and end gas images
. Residual gas mixtures
. Flame propagation behavior of alternative fuels
. Gas-side heat transfer in the cylinder

In particular, our investigation of the effects of fuel parameters on in-cylinder processes was quite extensively performed in collaboration with another sister project ("Analyzing Alternative Fuels Combustion") being sponsored by the U.S. Department of Energy, Alternative Fuels Utilization Program (AFUP). Development of the SIS and the new data analysis method, which has been possible by the ARO sponsorship in the past, has been an essential key for attracting research participation at Rutgers by Ford, Texaco, and recently DOE AFUP. The new work under the present ARO proposal played the central role by benefiting those engine/flame studies in our laboratory.

5. Results from the Present Study

Five separate publications were generated during the course of the present study as listed next. Note that copies of the papers are included in the Appendix and abstracts of the individual papers are presented below.

1. Campbell, S., Clasen, E., Chang, C., ad Rhee, K. T., "Flames and Liquid Fuel in an SI Engine during Cold Start," SAE Paper-961153, 1996.
2. Clasen, E., Song, K., Campbell, S., and Rhee, K. T., "Fuel Effects on Diesel Combustion Processes," SAE Paper-962066, 1996.
3. Chang, C., Clasen, E., Song, K., Campbell, S., Jiang, H., Rhee, K. T., "Quantitative Imaging of In-cylinder Processes by Multispectral Methods," SAE Paper-970872, 1997.
4. Kajitani, S., Chen, Z., Konno, M., Rhee, K. T., "Engine Performance and Exhaust Characteristics of Direct-injection Diesel Engine Operated with DME." SAE Paper-972973, 1997.
5. Themel, T., Jansons, M., Campbell, S. and Rhee, K. T.," Diesel Engine Response to High Fuel-Injection Pressures," SAE Paper to be presented at International Fuels and Lube Meeting to be held in San Francisco, October 1998.

A. Flames and Liquid Fuel in SI Engine Cylinder during Cold Start
SAE Paper-961153

The flame propagation in the very first firing and the subsequent cycles in an SI engine during the cold start were studied to gain a better understanding of reaction fronts associated with liquid fuel (regular unleaded) layers in the cylinder. This work was performed using the Rutgers high-speed spectral infrared digital imaging system from a single-cylinder engine. It had optical access which was mounted with a production engine cylinder-head mated with a conventional port fuel injection (PFI) system.

In the study, four images in respective spectral bands were simultaneously obtained at successive instants of time during the combustion period, which was done for eight sequential cycles. This multiple-band successive-imaging was repeated in about two-minute interval over a period of more than twenty-five minutes after the engine start. During this experiment, the temperature changes at the intake port, the water jacket and the exhaust gas were monitored. In addition, pressure-time data was obtained in individual cycles in order to gain some insight into the overall cylinder condition. Note that the fuel rate by the PFI for the first set of successive images was about 3.5 times stoichiometric and that for others was near-stoichiometric.

The first firing cycle exhibited almost invariably a weak flame propagation, which was followed by very intense flame fronts in the next cycle. Note that the flame propagation seems to only indicate the consumption of the fuel vapor produced in the cycle. The flames in the third cycle were also intense in some cases, but mostly weaker than those in the second. Upon formation of the flame front in the beginning, some exceedingly strong local reactions started to grow, but no earlier than 15CA after TDC. The reactions appeared to be diffusion reaction fronts around liquid fuel layered over the chamber surfaces. The scale of the local reaction zones decreased with time and exhibited some significant transient changes. This variation continued even though the engine was almost fully warmed. Results from some parametric studies are also reported.

B. Fuel Effects on Diesel Combustion Processes
SAE Paper-962066

The crank angle locations for the *first occurrences* of several main combustion events in a Diesel engine were investigated for varied fuel parameters. The events studied include: preflame reactions; premixed flame propagation; start of pressure rise; maximum rate of pressure rise (dp/dt); and peak cylinder pressure. The fuels employed in the study were in two groups: (1) Base fuel-1 and derivatives prepared by mixing it with small doses of a cetane number (CN) enhancing additive; and (2) Base fuel-2 and those made by adding different amounts of bio-Diesel fuel.

The experiment was performed by using a single-cylinder direct-injection (DI) Diesel engine equipped with an electronically controlled high-pressure fuel injection unit. The in-cylinder processes during the periods of ignition delay and combustion reaction were measured by using a high-speed multispectral infrared (IR) imaging system developed at Rutgers University. The other events were found from the pressure-time history.

The purpose of using these fuels was to investigate: additive effects on the (invisible) preflame reaction and visible premixed flame development; flame behaviors of bio-Diesel fuels; CN effects on in-cylinder reactions; and others. There is some evidence that the formation of the visible flame kernels may not be directly related to the preflame

reactions when the additive is used to increase CN. The reactions during the ignition delay of bio-Diesel fuels were rather unpredictable, therefore requiring additional investigation. Among the most indicative timelines for determining a fuel's CN were those of: the maximum dp/dt; the start of pressure rise; the first premixed flame; and the peak pressure. In particular, the timeline of maximum dp/dt seems to be most insensitive to the variation of injection timing. Some new findings are also reported in the paper.

C. Quantitative Imaging of In-cylinder Processes by Multispectral Methods

SAE Paper-970872

With the objective of achieving better investigation of engines-fuels by obtaining instantaneous quantitative imaging of in-cylinder processes, several steps have been taken for some years at Rutgers University. They are: (1) Construction of a new multispectral high-speed infrared (IR) digital imaging system; (2) Development of spectrometric analysis methods; (3) Application of the above to real-world in-cylinder engine environments and simple flames. This paper reports some of results from these studies.

The one-of-a-kind Rutgers IR imaging system was developed in order to simultaneously capture four geometrically identical (pixel-to-pixel) images in respective spectral bands of IR radiation issued from a combustion chamber at successive instants of time in high rates.

In order to process the raw data gathered by this Rutgers system, three new spectrometric methods have been developed to date: (1) dual-band mapping method; (2) new band-ratio method; and (3) three-band iteration method. The former two methods are developed to obtain instantaneous distributions of temperature and water vapor concentrations, and the latter method is to simultaneously find those of temperature, water vapor and soot in the engine cylinder.

Applications of these techniques were made to both SI and CI engine combustion as well as bench-top burner flames. Discussion is made on the methods and new results.

D. Engine Performance and Exhaust Characteristics of Direct-injection Diesel Engine Operated with DME

SAE Paper-972973

Neat dimethyl ether (DME), as an alternative fuel candidate for Diesel engines, was investigated by measuring primarily engine performance and exhaust gas characteristics. In addition, other responses of the engine to the new fuel were also determined at the same time, including the injector needle lift and heat release. The engine measurements with this fuel were compared with those obtained by using conventional Diesel fuel.

Findings from the present work include: (1) It was necessary to add small amount of lubricating additives to DME, if a conventional fuel injection system is employed. This was to achieve satisfactory injector performance and to minimize some excessive wear. (2) Engine performance for both fuels was basically comparable to each other, except for a better energy conversion efficiency with DME. (3) In the DME-operated engine, emissions of soot and unburned hydrocarbon (UHC) were almost negligible, but NOx emission was about the same as in the Diesel oil operation. (4) The reduction of NOx emission by delaying the injection time was highly significant with DME.

E. Diesel Engine Response to High Fuel-Injection Pressures
SAE 1998 F&L Meeting in San Francisco

A single-cylinder direct-injection (DI) Diesel engine (Cummins 903) equipped with a new laboratory-built electronically controlled high injection pressure fuel unit (HIP) was studied in order to evaluate design strategies for achieving a high power density (HPD) compression ignition (CI) engine.

In performing the present parametric study of engine response to design changes, the HIP was designed to deliver injection pressures variable to over 210 MPa (30,625psi).

Among other parameters investigated for the analysis of the HPD DI-CI engine with an HIP were the air/fuel ratio ranging from 18 to 36, and intake air temperature as high as 205°C (400°F). The high temperatures in the latter were considered in order to evaluate combustion reactions expected in an uncooled (or low-heat-rejection) engine for a HPD, which operates without cooling the cylinder.

Engine measurements from the study include: indicated mean effective pressure, fuel consumption, and smoke emissions.
It was found that a Diesel engine incorporated with an HIP under varied operational conditions, including those encountered in uncooled engine design needs variation of injection parameters, namely the start of injection and the rate shape. When the engine operating condition shifts, the rapid variation of those parameters are needed in order to optimize the engine power delivery and fuel consumption as well as to minimize smoke emissions.

Other engine responses to the varied parameters in this high-pressure Diesel engine are also reported in the paper.

6. References

1. Jiang, H., McComiskey, T., Qian, Y., Jeong, Y.I., Rhee, K.T., and J.C. Kent, "A New High-Speed Spectral Infrared Imaging Device Applied for Imaging Gaseous Mixtures from Combustion Devices," CST, 90, 5-6, p. 341, 1993.
2. McComiskey, T., Jiang, H., Qian, Y., Rhee, K.T., and Kent, J.C., "High-Speed Spectral Infrared Imaging of SI Engine Combustion," SAE Paper- 930865, 1993.
3. Jiang, H., Qian, Y. and Rhee, K.T., "High-Speed Dual- Spectra Infrared Imaging," Optical Engineering, 32 (6), pp. 1281-1289, 1993.
4. Jeong, Y.I., Qian, Y., Campbell, S. and Rhee, K.T., "Investigation of a DI Diesel Engine by High-Speed Spectral IR Imaging..," SAE Paper-941732, 1994.
5. Ludwig, C.B., Malkmus, W., Reardon, J.E., and Thomson, J.A.L., Handbook of Infrared Radiation from Combustion Gases, NASA SP-3080, 1973.
6. Clasen, E., Campbell, S. and Rhee, K.T., "Spectral IR Images of Direct-Injection Diesel Combustion by High-pressure Fuel Injection," SAE Paper-950605, 1995.
6. Abata, D., Stroia, B.J., Beck, N.J., and Roach, A.R., "Diesel Engine Flame Photographs with High Pressure Injection," SAE Paper-880298, 1988.
7. Gaydon, A.G. and Wolfhard, H.D., Flames, *Their structure, radiation and temperature*, Chapman and Hall, Ltd., London, 1970.
8. Shimada, T., Shoji, T., and Takeda, Y., "The Effect of Fuel Injection Pressure on Diesel Engine Performance," SAE Paper-901919, 1989.
9. Tow, T.C., Pierpont, D.A. and Reitz, R.D., "Reducing Particulate and NOx Emissions

by using Multiple Injections in a Heavy Duty D.I. Diesel Engine," SAE Paper-940897.
10. Shundoh, S., Komori, M., Tsujimur, K., Kobayashi, S., "NOx Reduction from Diesel Combustion using Pilot Injection with HPI," SAE Paper-920461, 1992.
11. Wood, M.E., Bryzik, W., and Schwarz, E., "100 Hour Endurance Testing of High Output Adiabatic Diesel Engine," SAE Paper-940951, 1994.
12. Myers, P.S., an Invited Lecture, Technical Meeting, Central State Section of the Combustion Institute, University of Wisconsin-Madison, June 5-7, 1994.
13. Kajitani, S., Usisaki, H., Clasen, E., Campbell, S. and Rhee, K.T., "MTBE for Improved Diesel Combustion and Emissions?," SAE Paper-941688, 1994.
14. Desai, R.R., Gaynor, E., Watson, H.C., "Giving Standard Diesel Fuels Premium Perfmc. using Oxygen-Enriched Air in Diesel Engines, " SAE Paper-932806, 1993.

961153

Flames and Liquid Fuel in an SI Engine Cylinder during Cold Start

Campbell, S., Clasen, E., Chang, C. and Rhee, K.T.
Department of Mechanical and Aerospace Engineering
Rutgers, The State University of New Jersey
Piscataway, NJ 08855

Abstract

The flame propagations in the very first firing and subsequent cycles in an SI engine during cold start were studied to gain a better understanding of reaction fronts associated with liquid fuel (regular unleaded) in the cylinder. This work was performed using the Rutgers high-speed spectral infrared digital imaging system on a single-cylinder engine with optical access. The engine was mounted with a production engine cylinder-head mated with a conventional port fuel injection (PFI) system.

In the study, four images in respective spectral bands were simultaneously obtained at successive instants of time during the combustion period, which was done for eight sequential cycles. This multiple-band successive-imaging was repeated in intervals of about two minutes over a period of more than twenty-five minutes after the engine start. During this experiment, the temperature changes at the intake port, the water jacket and the exhaust gas were monitored. In addition, pressure-time data was obtained from individual cycles in order to gain some insight into the overall in-cylinder reactions. Note that the fuel rate by the PFI for the first set of successive images was about 3.5 times stoichiometric and that for others was near-stoichiometric.

The first firing cycle exhibited almost invariably weak flame propagation, which was followed by very intense flame fronts in the next cycle. Note that the flame propagation in the first cycle seems to only indicate consumption of the fuel vapor available in the cycle. The flames in the third cycle were also intense in some cases, but mostly weaker than those in the second. Upon formation of the flame front in the beginning of combustion, some exceedingly strong local reactions started to grow, but no earlier than 15CA after TDC. The reactions appeared to be diffusion reaction fronts around liquid fuel layered over the chamber surfaces. The scale of these local reaction zones decreased with time and exhibited some significant transient changes. This variation continued to occur even though the engine was relatively well warmed. Results from some parametric studies are also reported.

Introduction

The large amount of unburned hydrocarbon (UHC) emitted by spark ignition (SI) engines during cold start basically stems from the fact that the liquid fuel introduced into the engine is poorly vaporized. Because of the fuel's low vapor pressure at this time, extra fuel is injected into the engine in order to produce enough vapor to achieve successful development of the flame propagation (with the throttle valve closed). This extra fuel causes accordingly large amounts of liquid fuel layered at the intake port and in the combustion chamber.

Let's consider what may occur during cold start in a typical modern SI engine with a conventional port injection fuel system (PIF). The present discussion concerns reactions during two different time periods from the start: They are: (1) the first period of several seconds, and (2) the early period before attaining a well warmed engine condition. The former is of interest because, in a typical modern SI engine, the over-rich fuel injection ceases immediately after the start. The latter is separately discussed because, during the warm up period, the in-cylinder formation of UHC continues to be high even with the mixture near stoichiometric.

Engine Operation with Extra Fuel. The very first fuel injected, although in an amount sufficient to produce a rich mixture of several times the stoichiometric, will probably not be connected to an immediate flame propagation, but will mostly wet the intake port and the combustion chamber surface. With no ignition occurring in this cycle, both a great amount of fuel vapor and probably even some liquid fuel would be wasted "raw" to the exhaust. In the next cycle, the fuel at the intake port will be added by the next fuel delivery to form a thicker liquid layer of fuel and an increased amount of vapor. When the intake valve opens, more fuel from this accumulation will be combined with the trapped fuel (in the cylinder from the previous cycle), which will also produce thicker layers of liquid fuel over the chamber surface and, of course, an increased amount of vapor. In spite of this, the cycle may not achieve a flame propagation either, and then the same will be

repeated. The process involving wasting and accumulation of the fuel will continue until a sufficiently rich vapor-air mixture is produced near the spark plug for a successful fire ball formation. Even the first firing cycle may not be followed by the same, and then the above process will be repeated as before. The number and mode of such unsuccessful cycles during the start will depend on various factors, e.g. the amount of fuel injection per cycle; fuel distillation characteristics; temperature of the cold start; amount of the residual fuel trapped in the cylinder and the intake port after the previous engine operation. Note that the last is affected by the piston locations, the time period after the previous engine operation, and more.

The combustion, then, will produce the first hot (rushing) back-flow of combustion products, which will alter the thermal condition and fluid flows at the intake port to increase the atomization and vaporization of the liquid fuel deposit. The combustion will also change the transport process over the liquid fuel layers in the cylinder, which increases vapor formation and decreases the amount of liquid fuel loaded over the surface. The waste gas at this time is expected to contain a greater portion of incomplete combustion products for several reasons. For example, there will be over-rich diffusion flame fronts off the liquid layer, and fuel vapor leaving the layer (after the reaction fronts disappear) will not be well oxidized. Note that since the combustion chamber surface is at low temperatures, the wall quenching effects will be highly significant. In addition, the UHC diffused out of the quenched layer will be poorly consumed by the bulk combustion products. Such strong quenching effects and poor post-flame oxidation, plus the raw fuel mentioned above, will become main sources of the engine-out UHC during the cold start. The high complexity of the formation processes may be further realized as considered in the following.

In order to minimize the amount of UHC during this period, several possible injection strategies may be implemented in the very early cycles. As one such strategy, a minimum amount of fuel may be injected to produce a lean vapor-air mixture for a marginal ignition followed by a completing flame propagation, or a large amount of fuel could be injected to produce a near-stoichiometric vapor-air mixture. The first flame propagation by the former strategy is expected to be weak but leave a small amount of unconsumed liquid fuel over the chamber surface. Such a weak (lean-mixture) flame would be subjected to strong quenching effects to cause more incomplete products, but the small amount of liquid fuel is expected to produce less over-rich diffusion reactions and a smaller amount of wasteful fuel vapor before the exhaust-valve-open (EVO). The first flame by the latter method, if properly achieved in a well controlled manner, which depends on the cold start temperature, fuel characteristics and others, will be strong to help the engine to attain a high temperature sooner. This strategy will need fewer cycles of operation than the former before attaining a high temperature, which will additionally bring beneficial aspects such as an active post flame oxidation, but leaves a larger amount of liquid fuel over the surface, a negative factor in achieving low UHC emissions. Regardless of strategies, there will be a significant amount of liquid fuel deposit over the surfaces causing UHC, which would exhibit severe transient and cyclic variations.

The variations would be dependent on the amount of extra fuel, the temperature of the cold start, the engine speed (and change) and more. The massive amount of liquid fuel layers formed over the surface during the cold start may be disposed of in several routes, including: (1) consumed in the following cycles; (2) washed down to the crankcase; (3) vaporized (in the absence of reaction fronts) and wasted during EVO; and (4) carbonized over or within the deposit formation. It is desirable to obtain a better understanding of such in-cylinder events during this over-rich combustion period, particularly the flames (of consuming fuel vapor) and (diffusion) reactions over the liquid layers. In order to minimize negative consequences on not only the UHC but also on others as considered above, a delicate compromise will have to be made among various factors for the PFI control strategy in a prompt manner during the transient period.

The present discussion also is concerned with the number of cycles from the start when the over-rich fuel injection is taken off and a near-stoichiometric mixture is provided. It's importance can be seen from the fact that if the fuel is fully vaporized (upon the over rich injection of several times an amount of fuel in a near stoichiometric mixture) the mixture will be simply too rich to ignite. As the combustion cycle continues, the engine temperature rises to promote the vaporization of the fuel at both the intake port and in the combustion chamber. With the mixture preparation shifted to near stoichiometric, sooner or later, the catalytic converter becomes lit up.

Liquid Layers during the Warm-up Period. When the engine attains a warm condition, the fuel introduced for producing a near stoichiometric mixture may be well vaporized achieving predictable flame propagations. However, only recently, some new evidence came to light suggesting that the regular unleaded gasoline at ignition may not be well vaporized in the combustion chamber even after the engine is relatively well warmed. This poor vaporization may be a significant source of UHC emissions [1]*. This study reports a new discovery of locally reacting centers in the combustion chamber, in which successive images were captured by using our high-speed multispectral IR imaging system. Note that when the engine was warm, these local reactions were mainly found around the intake valve and that they were not found when the same engine was operated by gaseous fuels (namely propane and natural gas). In addition, when the engine was started at room temperature, reaction centers were found at multiple locations, even including the exhaust valve and spark plug. Also, there is some observation suggesting that the formation of local reaction centers may be affected by the distillation characteristics of fuel.

The above observation of local reaction centers, which were considered to occur due to liquid layers formed

*Numbers in parentheses designate references at end of paper.

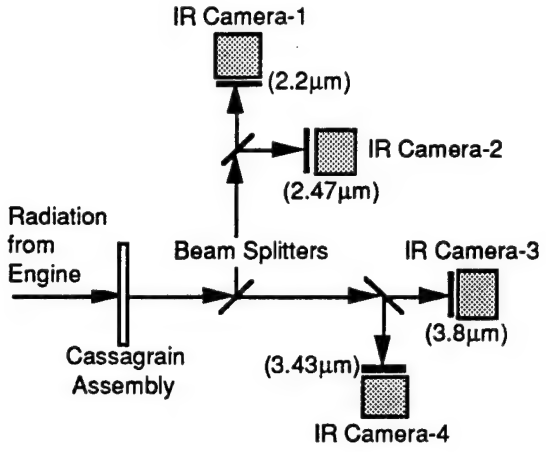

Fig. 1. Schematic Presentation of Rutgers SIS.

over the cylinder head during the intake period, may not be surprising in view that many research individuals report liquid fuel layers or puddles observed at the intake port (in warm SI engines). In addition, the local reaction centers, according to the above study, remain initially a surface phenomenon, which later become a volume phenomenon, i.e., around 70 after top-dead-center (ATDC). The radiation from the local centers was similar to that expected in diffusion flames. Note that an SI engine operated by a gaseous fuel, which did not exhibit any sign of local reactions, produces much lower engine-out UHC than the same engine fueled by regular gasoline. As to the phase of fuel in the mixture when it rushes through the intake port, it is actually desirable to have it only partially vaporized in order to achieve a high brake mean effective pressure (bmep). If, instead, an SI engine is designed to achieve a nearly full vaporization of the fuel at this time, at the expense of bmep, (for example, by excessively heating the port) the liquid fuel layer in a cylinder may not be formed. After finding this liquid burning, a strong need for obtaining better understanding of the phenomenon associated with many issues was pronounced, such as its transient variation and effects of engine-fuel factors.

If the formation of liquid layers is significantly responsible for UHC even in a warm SI engine, it should be reasonable to infer that the same would be a main process of the engine-out UHC during the remaining warm-up period after the over-rich fuel injection ceases at the intake port. It is desirable to investigate the behaviors of flames and diffusion reactions over the liquid layers during this transient period, while the engine is run by a near stoichiometric mixture.

Experiment

Since the present investigation was performed based on findings from the earlier work [1], the same apparatus were used. They include (1) high-speed multispectral IR imaging system and (2) SI engine with optical access, which will be only briefly described here. More details of these apparatus may be found elsewhere [1-3].

Table-I. Engine Dimensions

Bore x Stroke (mm),	101.6 x 101.6
Compression Ratio,	9:1
Spark Ignition,	6 BTDC
Valve Timing:	
EVO	135 ATDC
EVC	10 ATDC
IVO	10 BTDC
IVC	135 BTDC
Fuel Rail Pressure	200 kPa

Multispectral IR Imaging System. This is a one-of-a-kind system designed and fabricated at Rutgers University, which is referred to as the Rutgers System or Super Imaging System (SIS). As shown in Fig. 1, this SIS has four high-speed IR digital camera units connected to a single optical train. The radiation passing through the optical access of the engine is collected by a cassegrain assembly consisting of two reflective mirrors, and is then relayed through three different spectral beam splitters. This arrangement produces four geometrically identical (pixel-to-pixel matching) images in respective spectral domains. A narrow-band filter installed in front of each camera further specifies, within the corresponding domain, the spectral nature of the image for the camera.

Some of the performance features of the SIS having Pt-Si imagers (64x128 pixels each) are: imaging rate over 1,800frames/sec per camera; independently variable exposure period as short as 20μsec; spectral range of 1.5-5.5μm; and total 256 images to be captured (in each experiment) per camera. The cameras in the SIS are simultaneously operated according to the predetermined setting, including: the exposure period; the total number of images to be obtained per cycle; the start of imaging (in crank angle, CA) with respect to a reference marker (here top-dead-center, TDC); the interval between successive images in CA.

Four spectrally distinct images simultaneously obtained by the SIS at successive instants of time implies that, ideally, distributions of four different pieces of information may be obtained at the CA of imaging, such as temperature, and concentrations of water vapor and soot. While new data processing methods for achieving such quantitative imaging are being developed at Rutgers, it was found that raw images produced by the SIS permit us to collect new pieces of in-cylinder information, which are difficult to obtain using conventional diagnostic devices. Some of them are reported here.

Engine Apparatus. The apparatus was built on a single-cylinder engine base by mounting a new Ford 302 cylinder head and a matching port-injection fuel system (PIF). Construction of the set-up was performed in an attempt to preserve the representative characteristics of the real-world SI engines. Figure 2 shows the arrangement of the optical access in the engine. Since an in-depth description was made in previous papers, some relevant engine information is summarized in Table-I.

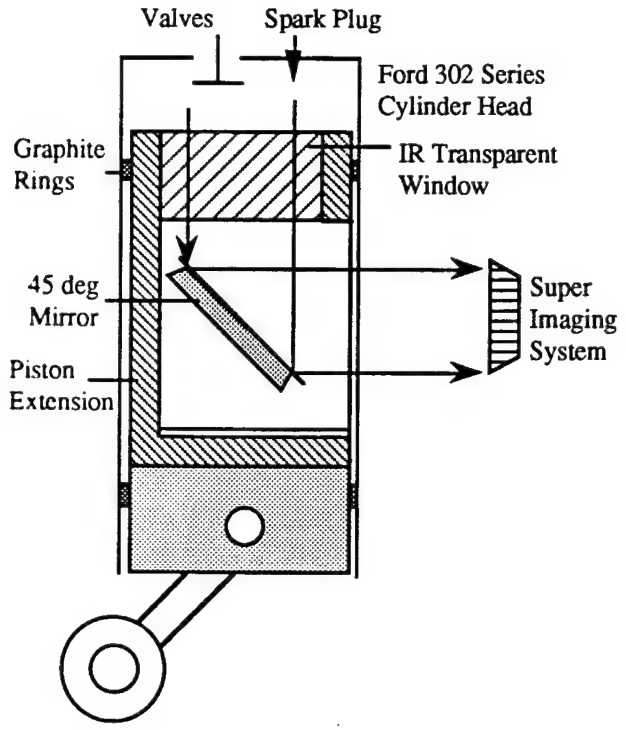

Fig. 2. Spark-Ignition Engine with Optical Access.

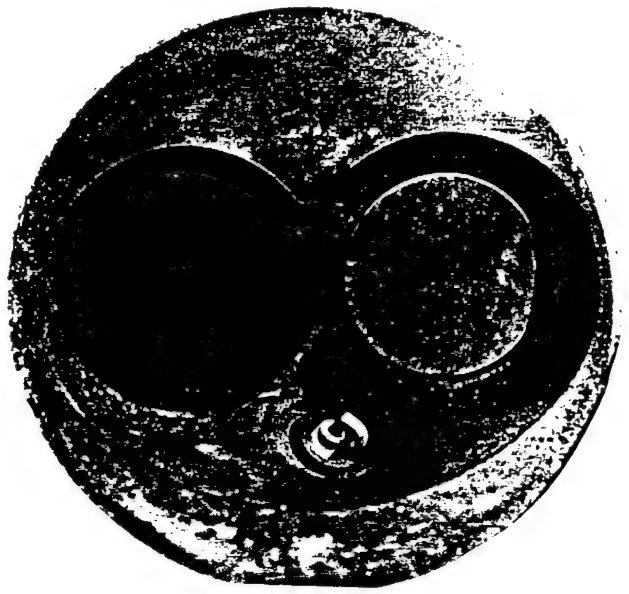

Fig. 3. A Visible-Ray Photograph of the Cylinder Head Exhibiting the Imaging View.

The engine apparatus was sufficiently instrumented in order to obtain consistent results from the experiment. Particularly to monitor the thermal condition of the intake port, thermocouples were installed where deemed appropriate. In addition, cylinder pressure-time (p-t) history was recorded for the corresponding sets of instantaneous images. This was achieved by synchronizing both pressure-time data acquisition and imaging to the same engine encoder.

Figure 3 is included here in order to indicate the imaging view, which shows the intake valve on the left, the exhaust valve on the right and the spark plug in between. This figure will be referred to when the instantaneous spectral images are presented later.

Results and Discussion

The main results from the study are a set of four separate spectral IR digital images simultaneously taken at successive instants of time during the combustion period. This high-speed imaging from a cold engine was done by starting from the very first cycle until the engine was fully warmed up with the intake manifold vacuum maintained at 24kPa. While the imaging was performed, the corresponding pressure-time data was obtained to gain some idea of the overall combustion condition. Temperature changes at the intake-port, the water-jacket (the cylinder heat) and the exhaust gas were recorded. The experiment was performed by using regular unleaded gasoline with ignition time at 6BTDC.

In each imaging, four sets (in spectral bands of 2.2, 2.47, 3.43 and 3.8μm) of thirty-two digital images per cycle, were simultaneously obtained from eight successive cycles, which filled up the memory in the SIS (over four megabytes in 12 bit dynamic resolution). Note that, in a separate run, the imaging was also carried out by obtaining (in each spectral band) eight images per cycle from 32 sequential cycles. In yet another experiment, the same was made to obtain a single image per cycle at 35 ATDC from 256 consecutive cycles. These data were transferred to hard drive to free the SIS memory for the next imaging, a process which typically took about two minutes. That is, in this experiment, such a batch of images was repeatedly obtained in about two-mimute intervals during the warm-up period.

The imaging of combustion events during the cold start was done in two steps in sequence: (1) over-rich mixture imaging; and (2) stoichiometric mixture imaging. In the first step, after the engine was motored to attain a speed of 350rpm. The injection started in an amount of about 3.5times that of a stoichiometric mixture, which seemed to produce a satisfactory start. Note that when a smaller amount of fuel was injected, the first successful firing cycle was not always followed by the same. The SIS was synchronized to capture images from the very first firing and subsequent cycles, which took only a few seconds and were immediately followed by a fuel-injection-rate change to provide a stoichiometric mixture. At this time, the external load was engaged on the engine in such a way that the speed did not exceed 500rpm. As soon as the SIS was ready again for imaging after transferring the first batch of images, the second batch was obtained in the same way using a stoichiometric mixture at constant engine speed of 500rpm.

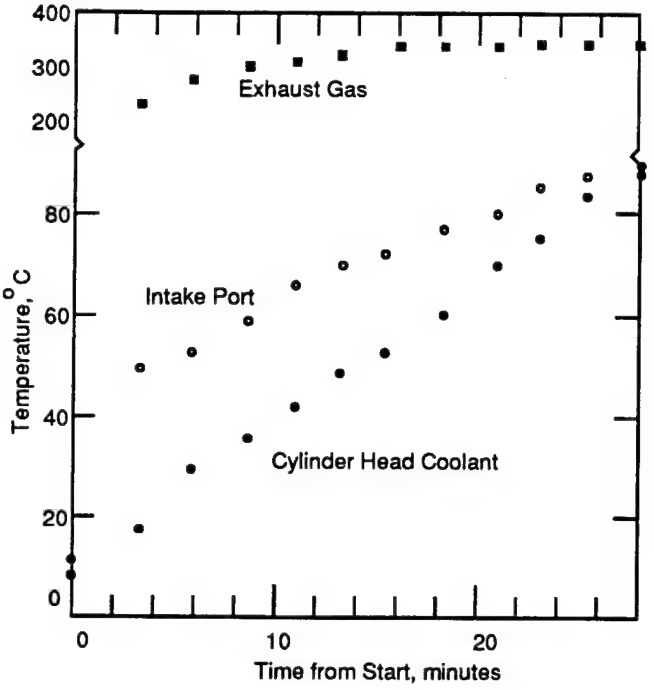

Fig. 4. Temperature-time Data at each Imaging.

Figure 4 summarizes the typical sequence of imaging and temperature measurements in the engine, which, although self-explanatory, still deserves some attention. During the warming period, the temperature at the intake port is consistently higher than at the cylinder head coolant, which is caused by the back-flow of the combustion products. As soon as the imaging from the over-rich starting was done, the heater in the coolant loop was turned on for a while in order to shorten the warm-up period. In this experiment, when the measured temperature at the coolant outlet was near 90°C, the coolant was almost boiling, which may be a condition a bit more over-heated than in a typical engine operation.

It should be added that the engine running for such a long period of time produced a layer of deposit over the optical window, which would have been impossible for visible ray to pass through. But the quality of spectral IR images in the present experiment did not appear to be significantly degraded by the deposit.

A large number of imaging trials were performed. Typical sets of spectral IR images obtained from the very first firing and the following seven cycles are presented in Fig. 5 (A) 3.43μm and (B) 3.8μm. The results obtained thereafter in about two-minute intervals are shown in Fig. 6 by indicating the start time of imaging. They are displayed in pseudo-color in order to enhance the presentation of more local variations. Those images in the former band were expected to indicate radiation from mainly water vapor (and soot if formed), exhibiting the consumption of fuel vapor. Note that this band was also observed to capture radiation from some intermediate species in the preignition zone [1,2]. Since the latter band is transparent to radiation from main combustion products including water vapor and carbon dioxide, it was considered to mostly exhibit those from the cylinder head surface, and since the soot formation was

	a	b	c	d	e	f	g	h
1	-5	TDC	5	10	15	20	25	30
2	35	40	45	50	55	60	65	70
3	75	80	85	90	95	100	105	110

Fig. 7. Look-up-table indicating the Time of Imaging.

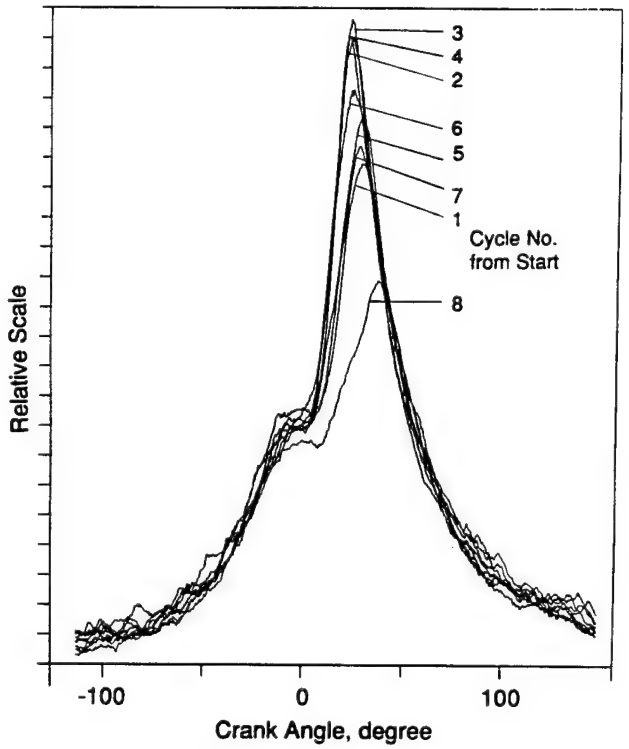

Fig. 8. Pressure-time Recorded in Early Cycles.

expected in very rich or diffusion reactions, it would be also reflected by the results in this band. The sequence of images captured in a 5CA intervals is from the left to the right and goes downward, like in a calendar. In order to indicate the individual times of imaging in CA, a look-up table (LUT) for the images is included in Fig. 7. In addition, Fig. 8 displays the pressure-time (p-t) histories to match with respective imaging cycles.

While in-cylinder events with the over-rich fuel injection (Fig. 5) were meaningful even after 110CA ATDC, as indicated by 3-h of Fig. 7, those with a near-stoichiometric mixture (Fig. 6) did not show such after 70ATDC, as included in the results. Because of the difference in strength of the radiation, imaging was made with the exposure period set to 170μsec for those with the over-rich fuel, and 310μsec for the near-stoichiometric mixture.

Over-Rich Mixture for Start. Discussing the results from the over-rich starting, the images of flame propagation (via 3.43μm) in the very first firing cycle are

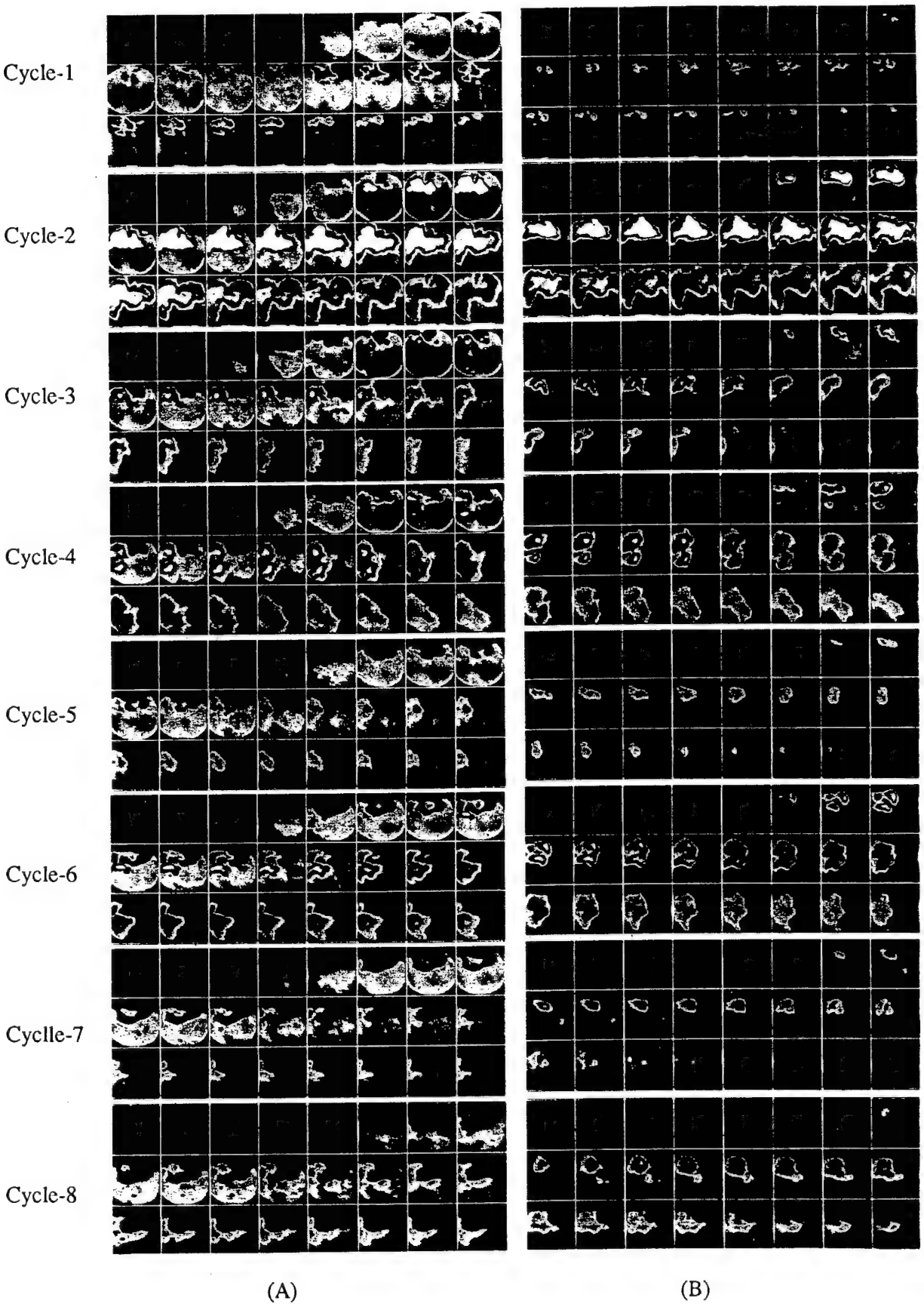

Fig. 5. High-speed Spectral IR Images Obtained at First Eight Sequential Cycles from Start via Bands of: (A) 3.43mm; and (B) 3.8mm.

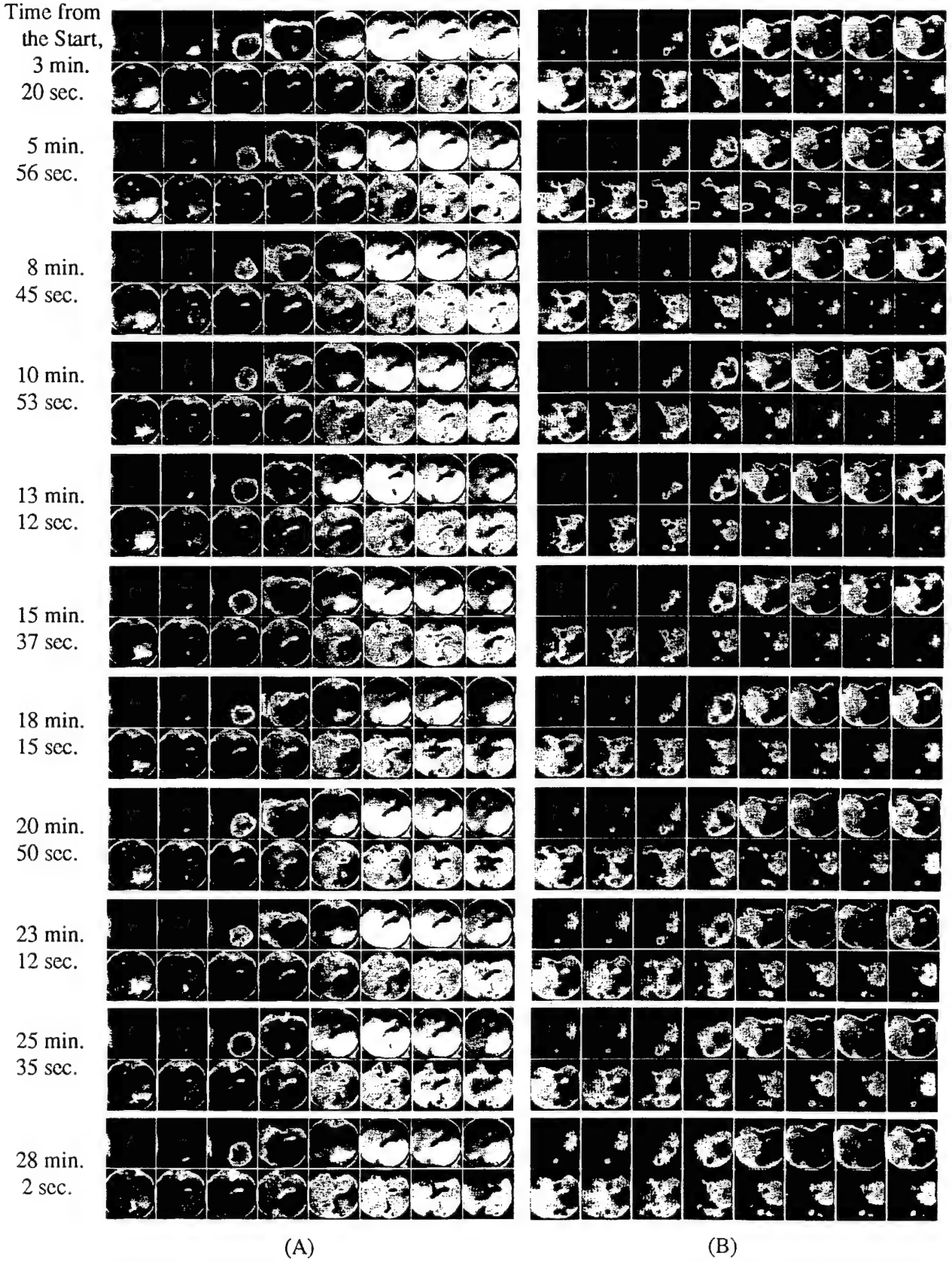

Fig. 6. High-speed Spectral IR Images Obtained during the Warm-up Period via Bands of: (A) 3.43mm; and (B) 3.8mm.

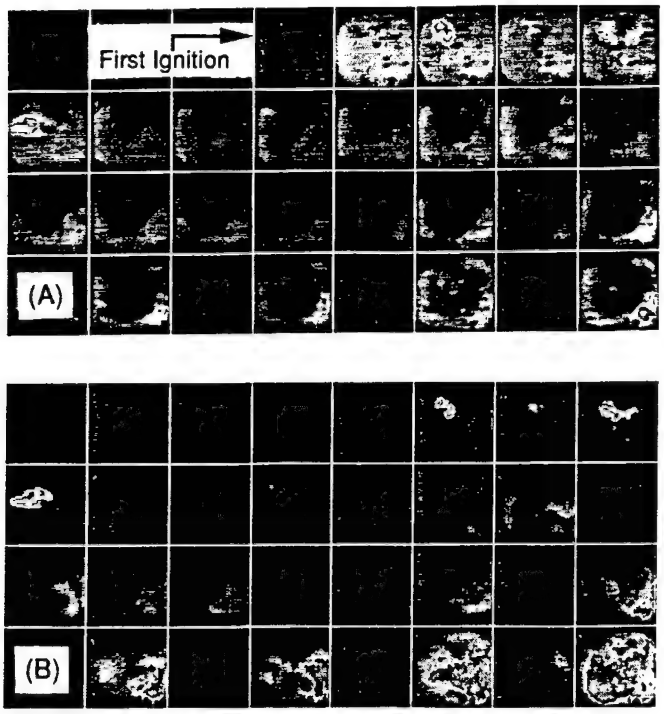

Fig. 9. Images obtained from Successive Cycles: One per cycle at 35CA ATDC: (A) 3.43μm and (B) 3.8μm.

relatively weak (Fig. 5-(A)). This fact seems to suggest that a relatively small amount of vapor was produced prior to ignition in the cycle. This weak flame front, however, became somewhat intense at the later stage of combustion in the cycle, exhibiting a sluggish consumption of fuel, which can be also seen from the p-t history (Fig. 8). Although the actual amount of accumulated fuel in the cylinder prior to the ignition is expected to be large, the energy release in the first cycle is small, which suggests that the unused fuel was either layered over the surface or partially lost (e.g. via wash-down). It is noted that, in the first ignition cycle, the flame fronts are observed over the entire imaging view of the chamber, which suggests that the fuel vapor was accumulated in the zone during the previous (no-ignition) cycles. This is in contrast with the following cycles having zones without emitting any significant mount of radiation by combustion products, particularly near the squish area. The radiation in 3.8μm (Fig.5-(B)), which is expected to reveal radiation from soot indicating diffusion reactions, is also rather insignificant, which indicates possibilities either that the amount of liquid fuel layered over the surface was small or that the flame was too weak (due to low temperatures) to produce a strong diffusion reaction.

The flame propagations in the 2nd, 3rd and 4th cycles are more intense and exhibit a remarkable difference in strength, i.e., it is extremely intense in 2nd and comparably weak in 3rd and 4th cycles. (In some trials, the difference of intensity between these cycles was small.) The radiation intensity, however, does not seem to properly represent the heat release according to the corresponding p-t data. That is, in spite of the remarkable difference in radiation among these cycles, which is most notably strong in the 2nd cycle, their p-t data look about the same. While the intensities of the flame propagations (via 3.43μm band) are somewhat weak but yet continue to be similar to each other, the radiation via 3.8μm (from a high soot formation to reflect rich diffusion reactions) became strong in 4th cycle, which was followed by weak radiation in 5th cycle. Such a cyclically varying mode of diffusion reactions repeated in the remaining cycles in the over-rich operation. It is noted that in some cases, two consecutive cycles exhibited strong radiation, followed by weak radiation and so forth, and vice versa. During these early cycles, the local diffusion reactions started to grow after 15-20ATDC, which is at least a period of 20CA after the flame fronts started. This time interval appears to represent the heating period required for the liquid fuel layered over the surface to commence/support the local diffusion reactions, which continues in an increasing intensity even long after the flame fronts disappeared. The continuing local (diffusion) reactions in the absence of flame fronts is further discussed later.

The p-t data indicates that the combustion started to deteriorate after the 5th cycle, which also seems to be reflected by the imaging results. The p-t data from the 8th cycle is particularly suggestive of what has been mentioned earlier, i.e., the vapor formation becomes sufficient enough within several cycles, and thereafter the vapor-air mixture becomes too rich to burn. In order to confirm this observation, an additional experiment was performed: One image per cycle was obtained in each band at the same CA (i.e., 35ATDC) from 256 successive cycles, but those from the first 32 cycles are displayed here (Fig. 9). It is clear that beyond several cycles after the start, the over-rich operation was no longer useful in achieving satisfactory flame propagation. This supports a fuel injection strategy of switching off the over-rich mixture within a few or several cycles from the start. The results also suggest that it would be meaningless to obtain images from over-rich cycles other than those already included in Fig. 5. Also, there was a considerable amount of liquid fuel flowing down along the cylinder surface as the engine was operated by the extended over-rich fuel injection. This observation plus the weak radiation of both flame propagation and diffusion reactions seen from images of the very first firing cycle (Fig. 5) lead us to expect that some of fuel washes down along the cylinder liner.

Continuously changing diffusion reactions (Fig. 5-(B)) strongly suggest a possibility of accordingly varying amount of fuel layers over the chamber surface. Such a variation in the cylinder may be dictated by the amount of fuel accumulated in the intake port during this early period. That is, the amount of liquid fuel layered at the port would affect the activities in the cylinder in a similar way. On the other hand, changes in fuel vaporization may be another possible factor affecting the variation, which would be related to the thermal condition of the cylinder entity, including temperatures of back-flow and the residual gas. Reviewing the images, however, particularly when comparing those in the 5th through 8th cycles with each other, a strong diffusion flame is not necessarily found with correspondingly intense flame propagation. The observations suggest that the variation in vaporization could

of local diffusion reactions. That is, the varied amount of liquid fuel present in the cylinder seems to be the most probable factor in determining the subsequent in-cylinder reactions.

It is further noted that the activities exhibiting the local (diffusion) reactions started no earlier than 15ATDC (1-e in Fig. 7), which coincides with the time after the entire imaging view is covered by the flame fronts indicating near depletion of vapor-air mixtures (seen via 3.43μm band). This indicates that the liquid fuel layered over the (low-temperature) surface begins an active consumption only after the chamber temperature is elevated. Since the piston location becomes relatively far from the TDC thereafter, the reaction around the layers would be increasingly sluggish.

A few last observations to be mentioned about the images from the over-rich start are after the fuel vapor-air is consumed, some regions previously with no reaction front began to exhibit a new center of flame as observable in cycles 4, and 6, particularly in the squish area. The only possible explanation for this finding seems to be the slowly evaporating liquid fuel landed in those regions, which was not consumed by the flame fronts in the beginning, and the liquid layer upon receiving heat transfer produced enough vapor to support diffusion flames around. It is also noted that it is not unusual to find a cycle having flames similar to those in cycle-5, which has only small amounts of (diffusion) flames around the liquid layers. It seems most probable that such severe variations during those early cycles can be attributed to the intake-port condition dictating the fuel-air preparation in the cylinder. It is not conceivable that the in-cylinder thermal condition, which would affect the fuel vapor formation, changes so swiftly to cause such cyclic variations.

Images with Stoichiometric Mixture. Recall that immediately after the first batch of imaging was done with an over-rich fuel injection, the engine was fed with a near stoichiometric mixture for the next imaging (see Fig. 4). Since each batch of imaging contains results from eight consecutive cycles, it was attempted to choose a representative set of images in preparing Fig. 6.

In general, the radiation by gaseous mixture (as seen via 3.43μm band) gradually decreases with time particularly at the later stage of combustion, which may be seen by comparing those taken at 70ATDC with each other. This observation may be explained by the possibility of reducing postflame oxidation as the engine warms up. Since the early flame growths appear to be similar to each other (by looking at those obtained at 5ATDC, for example), the accelerating flame propagation before the piston goes away too far from the TDC may also explain the phenomena. As expected, the images captured in 3.8μm band show an increasing strength of radiation by the surface until the coolant temperature attained about 60°C (at about 20minutes under the present coolant system) and thereafter they seem not to vary considerably. Unlike the images taken right after the start, which show some parts of the chamber having almost no reaction (Fig. 5), those included in Fig. 6 indicate the flames propagating through out the entire reaction volume. According to the present experiment, once the engine ran for a few minutes from the start, the in-cylinder reactions become relatively predictable to expect a reasonable power output, except for a new finding as discussed below.

Although the difference in exposure period of imaging is taken into consideration, it was quite obvious that the amount of liquid fuel dramatically decreased within the period of about two minutes after the start. During the interval, there was a change in intake-port temperature from about 10 to 50°C. In general, the scale of the diffusion flame decreased with time. In turn, the temperature increase in the engine, most notably at the intake port (Fig. 4) and presumably over the chamber surface.

Let us review the sequential images in Fig. 6-(A) in reference to the imaging view (Fig. 3). For example examine those taken at 3.3 minutes after the start. There are intense local centers at the upper portion of the intake valve clearly visible starting from 35ATDC. (Note that in typical SI engines the flame fronts become no longer visible after about 30ATDC.) According to imaging results from the first eight cycles, the local reaction center started as early as 15ATDC, which was observable late in a warm engine. The reason for the difference was due to the radiation from combustion product masking that from the local centers over the surface. The dynamic nature of the local reaction is clearly observable when they are reviewed in a video animation display: It is restated that the centers stay as a stationary surface phenomena in the beginning, which become a moving volume reaction around.

The local centers continued to react even far after the flame propagation disappeared but in gradually decreasing intensity as the piston moves away from the TDC. According to observation by a video display, the diminishing image of the local centers seemed most likely due to the depletion of liquid fuel off the surface. Note also that imaging results obtained by a longer exposure period indicate that the local radiation continue to be remarkable even after the EVO. The weakening radiation may be also due to the lower piston location, which will cause the cylinder temperature to be low, resulting in both a low oxidation and low radiation. The above consideration brings up an expectation that the chamber surface is considerably cooled down during the non-combustion period before the next liquid fuel is delivered.

Without displaying a bulky volume of results, it is noted that the liquid layers producing such diffusion reaction centers showed remarkable cyclic variations. In some cycles, the local center was hardly observable, even when the engine was not at a high temperature, which can be seen in the sample results obtained at different times after the start (Fig. 6). For example, there were cycles exhibiting almost no local burning such as those captured at 8.25 minutes after the start, while the same obtained at 20.8 minutes (and also 25.6 minutes) indicated some remarkable local reactions. Again, it remains to be further studied that these reactions centers were often found in a rather remarkable strength even after the engine was relatively warmed, which observation was reported earlier [1].

Significance of Diffusion Reactions after Flames Disappeared. Regardless of the engine temperature, it is reasonable to expect that the continuing local reaction

centers would be a significant source of UHC emissions. As mentioned earlier, the local diffusion reactions started to grow after around 15ATDC and continued far after the flame fronts disappeared (e.g. after EVO). It is again noted that the flames here mean the reaction fronts of consuming fuel-vapor and air mixtures.

Since the slowly reacting local centers are considered to occur over the liquid layers, it is quite appropriate to analyze the nature of the reaction environment. Many issues come into consideration. They are: (1) the location of liquid layers; (2) the flow of the layer over the surface; (3) the reaction anchored over the layers, (4) the stability of reactions; and (4) deposit effects on the reaction centers. The formation of layers is dictated by various factors such as the geometric configurations, and thermal and fluid flow characteristics of the engine. In this experiment, the most significant layers are found over the surface which perpendicularly divides between the chamber cavity and the squish area, and the upper part of the intake valve (refer to images in Figs. 5 & 6 and photo in Fig. 3). The liquid layers formed over the surfaces would be mobile according to gas motions, gravitational force and other effects. Referring to images indicated by 2-a through 2-h in Fig. 5 such as those obtained in 3rd cycle, the layer appear to move downward. In order to gain some insight into what is happening there, let us picture a flame spreading over a flowing fuel on an inclined surface. Since the gas motions are not small and insignificant in the chamber, the reaction front many be blown off if the reactions are improperly anchored where the vapor is formed. Such a stability issue may partially explain the cyclic variations of local reaction centers during the over-rich operation (Fig. 5) as well as some in the stoichiometric combustion (Fig. 6).

Regarding the relationship of deposit layers to the local diffusion reaction centers, although it is difficult to state a conclusive remark at present, some tangible effects have been realized during the course of the present work: The deposit layer formed over the cylinder head surface was inadvertently cleaned in the middle of experiment, and the clean head surface seems to reveal a lower frequency of having local reaction centers than before. A permeable deposit layer holding a liquid fuel would produce different modes and reaction periods of diffusion reaction from those formed over a clean smooth surface covered with the same fuel.

Summary

An optical SI engine equipped with a conventional port injection fuel system was investigated during the cold start period as operated by unleaded regular gasoline. The results obtained in the study include high-speed multiple spectral infrared images from: (1) the very first firing cycle and next seven consecutive cycles; and (2) successive sets of the same images as the former as repeated during the warm-up period in an about two-minute interval. In the former imaging, the engine was operated with a over-rich fuel injection rate (equivalent to 3.5 the stoichiometric), and for the latter, it was run by a near stoichiometric fuel injection. The matching cylinder pressure-time data and temperatures at the intake port and others were obtained at the same time. The spark time was 6CA BTDC. Some of more significant findings are listed in the following.

(1) The very first firing cycle exhibited weak and low-rate flame propagations and insignificant reactions around the liquid fuel layers.

(2) The second, third and fourth cycles exhibited similar p-t results although their radiation intensities vastly varied both in times and locations with some remarkable cyclic variations.

(3) The flame propagations do not appear to be benefited by the over-rich fuel injection after a few or several cycles from the start.

(4) The reaction centers produce radiation after about 15ATDC, indicating the need of a time period for liquid fuel to be heated to support the local diffusion reactions.

(5) Some considerable amount of liquid fuel was flowing down along the cylinder during the over-rich start.

(6) The flame propagations and local diffusion reaction centers change quite dramatically within a few minutes from the start, producing more predictable flame and smaller amount of liquid fuel reactions over the surface.

(7) The reaction centers around the liquid fuel layer continued even (long) after the flame fronts disappeared.

(8) The liquid layers causing the local reactions did not appear in every cycle, and likewise the opposite was found after the engine was well warmed. Some cyclic variations in liquid layer formation is pronounced to exist in the engine cylinder.

(9) The deposit formation over the chamber surface appears to affect the formation-occurrence of local reaction centers around the liquid layers, which needs further study.

(10) The liquid fuel formed over the combustion chamber surface is considered to cause unburned hydrocarbon emissions from both cold and warm engines.

Acknowledgement

The present work has been performed under the sponsorship of the U.S. Army Research Office (Contract No. DAAH04-95-1-0430) and AASERT (DAAH04-94-G-0201), the U.S. Department of Energy (Contract No. ACC-4-14361-01, through National Renewable Energy Laboratory), Ethyl Corporation and Ford Motor Company.

References

1. Song, K., Clasen, E., Chang, C., Campbell, S., Rhee, K.T., "Post-flame Oxidation and Unburned Hydrocarbon in a Spark-ignition Engine," SAE Paper-952543, 1995.
2. Clasen, E., Campbell, S., and Rhee, K.T., "Spectral IR Images of Direct Injection Diesel Engine Combustion with High Pressure Fuel Injection," SAE Paper-950605, 1995
3. Jiang, H., Qian, Y. and Rhee, K.T., "High-Speed Dual-Spectra Infrared Imaging," Optical Engineering, 32 (6), pp. 1281-1289, 1993.

962066

Fuel Effects on Diesel Combustion Processes

Clasen, E., Song, K., Campbell, S. and Rhee, K.T.
Department of Mechanical and Aerospace Engineering
Rutgers, The State University of New Jersey
Piscataway, NJ 08855

Abstract

The crank angle locations for the *first occurrences* of several main combustion events in a Diesel engine were investigated for varied fuel parameters. The events studied include: preflame reactions; premixed flame propagation; start of pressure rise; maximum rate of pressure rise (dp/dt); and peak cylinder pressure. The fuels employed in the study were in two groups: (1) Base fuel-1 and derivatives prepared by mixing it with small doses of a cetane number (CN) enhancing additive; and (2) Base fuel-2 and those made by adding different amounts of bio-Diesel fuel.

The experiment was performed by using a single-cylinder direct-injection (DI) Diesel engine equipped with an electronically controlled high-pressure fuel injection unit. The in-cylinder processes during the periods of ignition delay and combustion reaction were measured by using a high-speed multispectral infrared (IR) imaging system developed at Rutgers University. The other events were found from the pressure-time history.

The purpose of using these fuels was to investigate: additive effects on the (invisible) preflame reaction and visible premixed flame development; flame behaviors of bio-Diesel fuels; CN effects on in-cylinder reactions; and others. There is some evidence that the formation of the visible flame kernels may not be directly related to the preflame reactions when the additive is used to increase CN. The reactions during the ignition delay of bio-Diesel fuels were rather unpredictable, therefore requiring additional investigation. Among the most indicative timelines for determining a fuel's CN were those of: the maximum dp/dt; the start of pressure rise; the first premixed flame; and the peak pressure. In particular, the timeline of maximum dp/dt seems to be most insensitive to the variation of injection timing. Some new findings are also reported in the paper.

Introduction

In addition to the physical processes, progressive invisible chemical reactions precede the abrupt flame propagation and rapid rise of pressure in a Diesel combustion chamber. These preceding reactions produce many different intermediate species presumably to play respective roles in the subsequent self-ignition and heat-releasing reactions. Much has been studied on these low-temperature kinetics-controlled elementary reactions for various simple fuels under similar reaction environments. However, because of the yet insufficient knowledge of the reaction mechanism of complex Diesel fuels (and the effects of physical events) in the spray during the ignition delay period, at present even the time when the chemical reactions actually commence during this period is not well understood. The reaction starting time, therefore, is not properly considered in the state-of-the-art computer models, which would be a key for implementing the formation kinetics of species in various applications, such as an accurate prediction of NOx and soot emissions. It is pointed out that since a great portion of modern Diesel engines are equipped with a high-pressure (electronically controlled) injection unit, the time period dictated by the physical processes may become insignificant for such systems.

This brief review illustrates the importance of determining the fuel's chemical tendency of initiating-propagating reactions in the compression-ignition (CI) environment. At present, the most widely accepted criterion for these fuel characteristics is cetane number (CN), a reference quantity evaluated based on the ignition delay, the time period from the start of injection to the first *visible* flame front or the start of *pressure rise*. Discussing the CN of a fuel, which is evaluated in reference to self-ignition characteristics of a mixture (of hexadecane and heptamethylnonane), some aberrant fuel formulations may not suit this traditional definition. Two such examples are brought up here, i.e., bio-Diesel fuels and fuels containing a CN-enhancing additives (CN booster).

While the molecular structure and bond energies of the fuel may help us understand how readily a fuel is decomposed to produce elementary species for preflame reactions, it remains debatable if the time period prior to

occurrence of the in-cylinder events is significantly affected by physical properties of fuel. It is particularly relevant when they are greatly modified, such as when a bio-derived fuel having unusually high-viscosity is mixed with the conventional Diesel fuel, which would modify the spray pattern and vaporization of the fuel. In other words, the addition of such a new fuel would not only changes the chemistry of reactions to affect the onset of the self-ignition (i.e., the crank angle degree, CA when the first visible self-igniton kernel appears, which is called hereafter as the *timeline* of visible flame) but also alters the physical processes within the plume, which would affect the timeline of the former. If this is the case, the injector characteristics affecting the physical processes will have to be considered in defining a fuel's CN. This may be further exemplified by the differences in spray formation via the conventional (low-pressure) injector and the new high-pressure injector. The next example involves the use of a fuel additive introduced to the base Diesel fuel in fractions of one percent in order to increase the CN. Since a small amount of additive will minimally modify physical characteristics of the mixture, this would rule out the physical effects on the CN. What is unknown, however, is whether the additive alters the overall chemical kinetics of hydrocarbon species of the base fuel, by hastening/multiplying most preflame elementary reactions, to cause an earlier visible flame, or if it simply produces abrupt explosive centers in the mixture, by "infusing" new complemental or separate reactions (in addition to those expected without the additive).

Additionally in the preflame reactions, unlike the flame initiation in spark ignition (SI) engines made directly on the fuel-air mixture by a single electric arc, the first visible flame kernel in the CI is a result of progressive thermo-chemical reactions occurring during the ignition delay. This kernel is not the sole center of the reaction propagation throughout the chamber, but there are numerous such reaction centers (within vaporized portions of the fuel spray) nearly equally "cooked" so as to be consumed almost simultaneously at the end of the ignition delay. The extent of preflame reactions, therefore, would dictate not only how early and explosively the premixed flame occurs but also the postflame products formation. These processes, therefore, affect the heat release characteristics dictating the thermal efficiency and the species formation determining the exhaust emissions.

However plausible the above argument as to the preflame reactions may sound, it was only within the recent year that the first tangible and illustrative evidence of the preflame reactions taking place in Diesel combustion were captured [1].* This study reported spectral images obtained from a direct injection (DI) CI engine with optical access by using Rutgers high-speed multispectral infrared (IR) digital imaging system. The method was to capture a set of four geometrically identical images in respective spectral bands at successive instants of time during both the periods of ignition delay and combustion reaction. The spectral bands in the study were chosen to capture radiations from different species formed in the fuel spray. They included one image

*Numbers in parentheses designate references at end of paper.

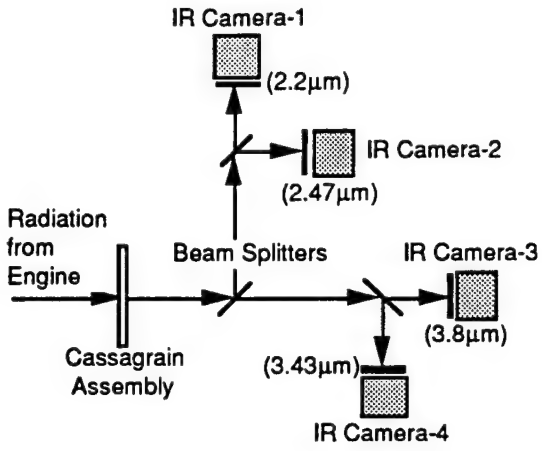

Fig. 1. Schematic Presentation of Rutgers SIS.

mainly exhibiting (visible) radiations from water vapor (and soot) and another showing (invisible) radiation from intermediate species. The "intermediate" precursors of the visible reaction products is pronounced here because their images were captured in a particular band during the ignition delay period, which discovery further motivated the present study. Note that images of similar preflame reactions were also observed via the same spectral band in an SI engine [2].

In the present study, in order to obtain a better understanding of the reactions during the ignition delay period, which is considered to be affected by both chemical characteristics and physical properties of the fuel, seven different fuels, including two different base fuels, were used. The first base fuel was mixed with small amounts of a CN booster and the second base fuel was blended with different amounts of bio-Diesel fuels.

Experiment

Since the present study was performed after obtaining the findings from the earlier work [1], the same apparatus were used. They include (1) high-speed multispectral IR imaging system and (2) Diesel engine with optical access, which will be only briefly described here. More details may be found elsewhere [1-4]. Note that the engine was equipped with an electronically-controlled high-pressure injection (HPI) system.

Multispectral IR Imaging System. This is a one-of-a-kind system newly designed and fabricated at Rutgers University [1-2,4], which is referred to as the Rutgers System or Super Imaging System (SIS). As shown in Fig. 1, this SIS has four units of high-speed IR digital cameras connected to a single optical unit. The radiation from the optical access of the engine is collected by a cassegrain assembly consisting of two concave mirrors, and the radiation is then relayed through three different spectral beam splitters. This arrangement produces four geometrically identical (pixel-to-pixel matching) images in respective spectral domains. A narrow band filter installed in front of each camera (indicated by the central wavelength

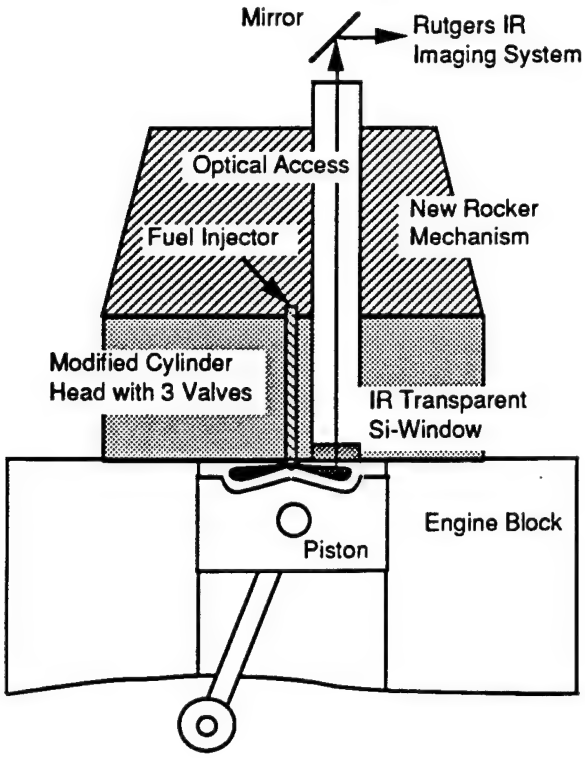

Fig. 2. Schematic Presentation of the Single Cylinder Engine Mounted by a Cummins 903 Cylinder Head with Optical Access for the SIS or Rutgers IR System.

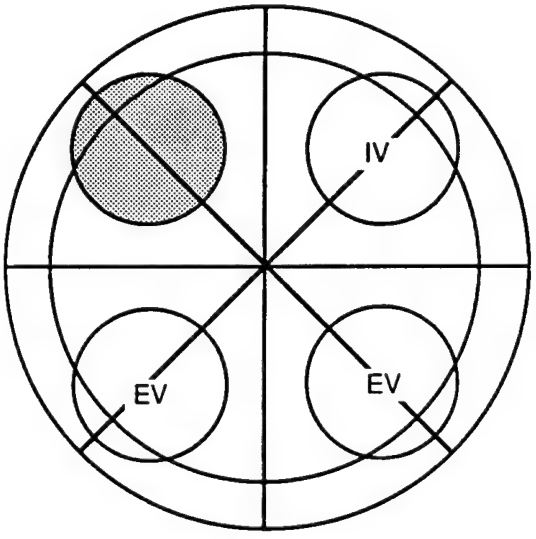

Fig. 3. Optical Access (shaded area) with respect to Spray Plume Axes.

in Fig. 1.) further specifies, within the corresponding domain, the spectral nature of the image upon the camera.

Among the performance features of the SIS having Pt-Si imagers (64x128 pixels each) in the camera are: imaging rate as high as 1,800frames/sec per camera; independently variable exposure period as short as 20μsec; spectral range of 1.5-5.5μm; and total 256 images to be captured (in each experiment) per camera. The cameras in the SIS are simultaneously operated according to the predetermined setting, including: the exposure period; the total number of images to be obtained per cycle; the start of imaging (in CA) with respect to a reference marker (here, top-dead-center, TDC); and the interval between successive images in CA.

Four spectral images simultaneously obtained by the SIS at successive instants of time implies that, when they are captured in spectrally discriminating manner, ideally as many as four difference pieces of information per corresponding pixels at the CA may be obtained. Upon properly processing the raw data, quantitative imaging may be achieved such as distributions of temperature, and concentrations of water vapor and soot. While new methods of such quantitative imaging are being developed in Rutgers, it is found that raw images produced by the SIS permit finding new pieces of in-cylinder information, which are difficult to obtain by using the conventional diagnostic devices.

Engine Apparatus. A single-cylinder DI-CI engine was constructed in collaboration with Power Energy International (Madison, WI) and BKM, Inc. (San Diego, CA), under a sponsorship of the U.S. Department of Defense University Research Initiative [3]. The engine body was constructed to accommodate components from a Cummins 903 engine. In this new single-cylinder arrangement, the engine (Fig. 2) uses a section of the 903 cylinder head to obtain representative characteristics of the DI-CI engine population.

Some modifications were made on the Cummins engine cylinder head for installing an IR optical window: conversion of one of the intake valves to make room for the optical access; a new rocker-arm mechanism, which provided a cylindrical space for the optical passage; a pressure transducer installed flush with the chamber wall; a measure to use either a Cummins (mechanical) PT unit injector or BKM's Servojet electronic-controlled HPI injector. The optical access (with viewing area of 37mm diameter) was made barely big enough to cover the projected view of a spray plume out of an eight-hole (0.15mm diameter) nozzle, which assumes all spray plumes to be identical to each other. Figure 3 shows the axes of plumes with respect to the (imaging) optical access, which will be referred to when the in-cylinder spectral IR images are discussed later. Additional engine information may be found elsewhere [1,3].

High-Pressure Injection. The electronically controlled HPI system which replaced the Cummins PT type injector in our 903 engine for the present study was basically a Servojet unit injector of the accumulator type [5]. Because of the crowded engine cylinder head due to new installation of an optical access and a pressure transducer (in addition to the existing components such as the valve train), the relatively bulky Servojet unit was not usable in the apparatus. Keeping the original system design features, an entirely new injector unit was fabricated in our laboratory:

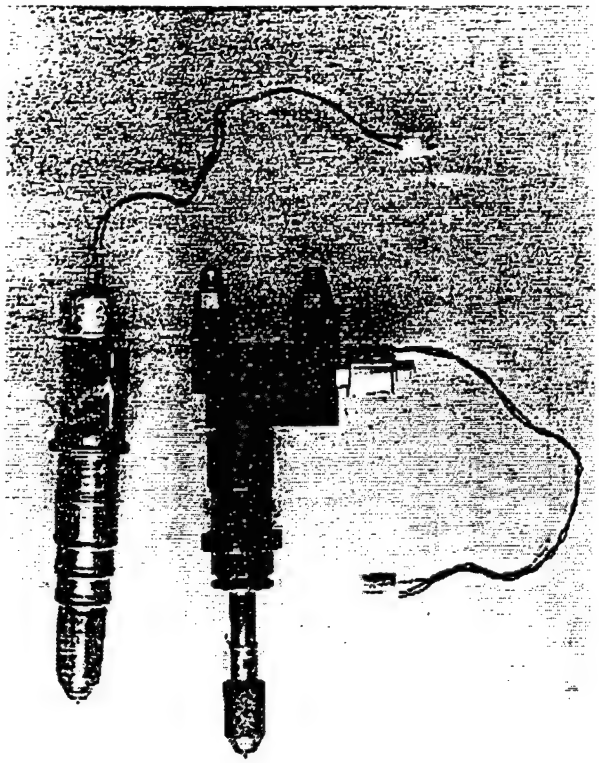

(A) (B)

Fig. 4. Electronic-controlled High-pressure Injectors: (A) Rutgers-built Unit and (B) Original BKM Unit.

Among the key considerations taken into account for this new unit was to use original injector tips of the Cummins PT nozzle, which was to provide technical and economic flexibility in choosing different injector tip geometries. The operation of the injector was performed by using the same electronic package given with the original Servojet unit. The high-pressure injection is achieved by an intensifier (1:16 ratio) in this HIP system to have as high as 165MPa (24,000psi, or 24Ksi)). The cut-off pressure of injection is approximately 10Ksi. Figure 4 shows the injectors: The original injector provided by BKM is on the right and the new unit built at Rutgers is on the left. Note the end portion of the new injector is from the Cummins PT nozzle.

An extensive bench-top characterization of this new injector package was performed prior to in-cylinder measurement. This was necessary to determine several important pieces of information about the new HPI, including the relationships of the actual start of fuel injection and the amount of fuel injected per cycle to the input control by the electronic signals, i.e., the pulse width and timing, and the accumulator pressure, respectively. It is pointed out that the time of injection was defined as the time when the fuel plume tip reached a sensor located about 10mm away from the injector nozzle hole. The injection (sac) pressure-time history was not measured in the present characterization, but is inferred to be the same as the original unit [5], which resembles a spike-shape that collapses rapidly to have a very short residual period of low injection pressure.

Fuels. Seven different fuels were used in the present work, as shown below (Table-I). The fuels in Group-1 were provided by Ethyl Corporation by mixing the base fuel-1 with respective amounts of an Ethyl additive known as Hess F9349 (boiling point, 153^{o}C) to obtain different CNs, as indicated in the table. Note that these fuels have different CNs with physical characteristics kept about the same. In the table, "Plot" indicates the presentation of data together on the same plane in figures shown later.

Table-1. Fuels Studied and Data Plots

Fuels	Contains (vol %)	Cetane No.	Plot
Fuel -1b	1.00 Hess F9349	70.8	
Fuel -1a	0.25 Hess F9349	60.1	
Fuel -1	0.0 (Base fuel-1)	51.6	(I)
Fuel -2	0.0 (Base fuel-2)	45.4	
Fuel -2a	20 Soy	Unknown	
Fuel -2b	40 Soy	Unknown	(II)
Fuel -2c	20 Soy & 20 Alkylate	Unknown	

The fuels in Group-2 were prepared at BDM (Bartlesville, OK) by mixing the base fuel-2 with respective amounts of an esterified soy oil (namely, bio-fuel) and alkylate, which is known to have CN of around 30. These fuels are expected to exhibit different behaviors in both the physical and chemical processes, particularly during the ignition delay period.

Results and Discussion

The core measurements in the present study include spectral IR images (in spectral bands of 2.2, 2.47, 3.43, and 3.8μm) simultaneously obtained at successive instants of time from a fuel spray plume during the ignition delay and combustion periods, and the pressure-time (p-t) data recorded at the same time. The measurement was performed with various injection times, namely 24.5, 18.5, 12.0, 9.0 and 6.0 bTDC. The engine was operated at 500rpm under a warmed condition throughout the entire experiment.

Nearly 1,000 sets of data were collected with some twenty cycles per condition in order to obtain a representative result for each. Since they were all gathered in digital form, this large amount of data was processed using several computer programs to determine important timelines of the Diesel combustion. They are periods from the start of injection to several consecutive events and a few new terms determined as some of the intervals:

(1) First (invisible) preflame image;
(2) First (visible) premixed flame image;
(3) Start of pressure rise;
(4) Maximum dp/dt;
(5) Peak pressure;
(6) First preflame image - first visible flame image;
(7) First visible flame - start of pressure rise, and
(8) Start of pressure rise - maximum dp/dt.

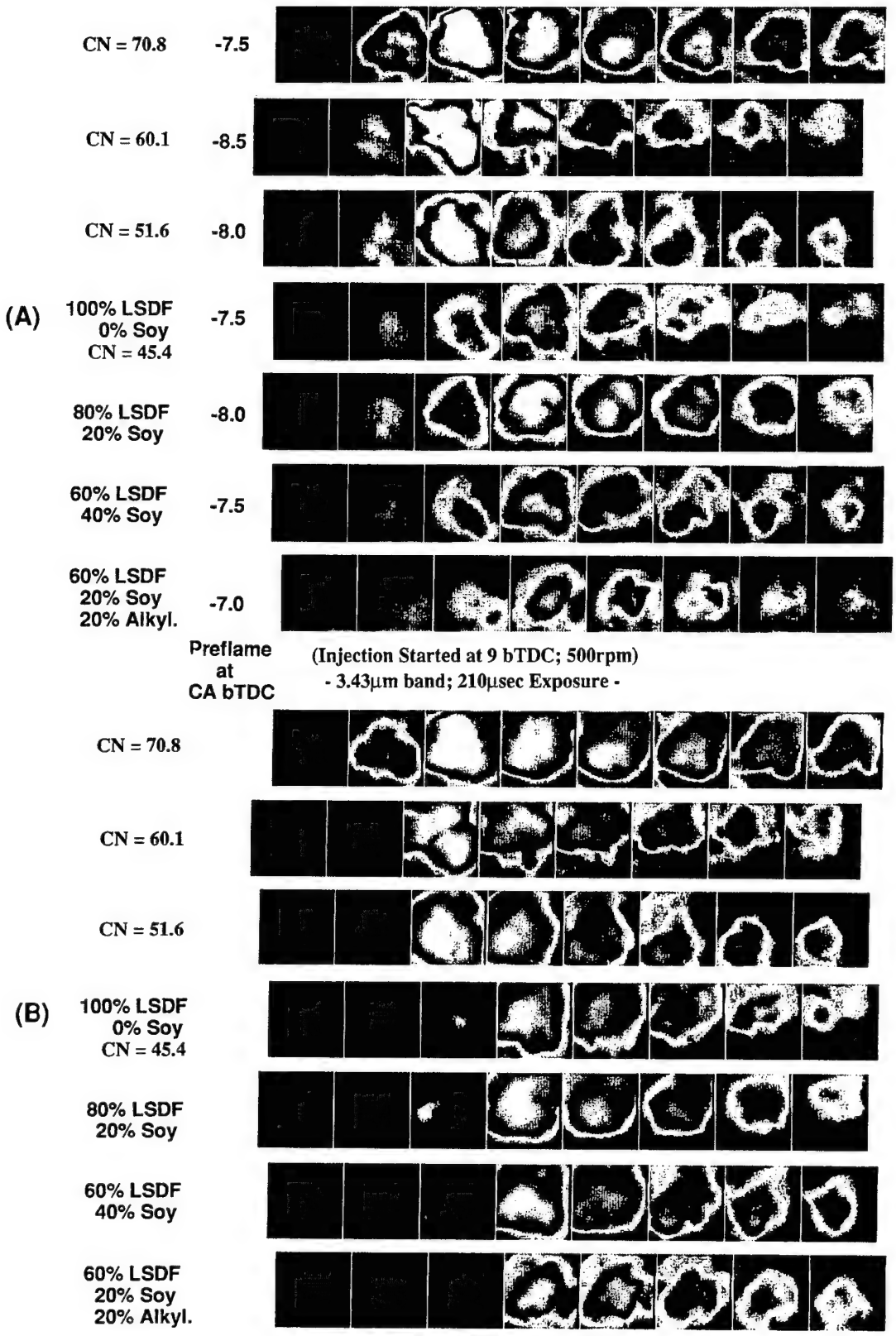

Fig. 5-(A). High-speed Spectral IR Images of Diesel Flame in 3.43μm.
(Starting with First Preflame Images for Individual Fuels)
-(B). High-speed Spectral IR Images of Diesel Flame in 2.2μm.
(Visible Flame Images Simultaneously obtained as 8-(A))

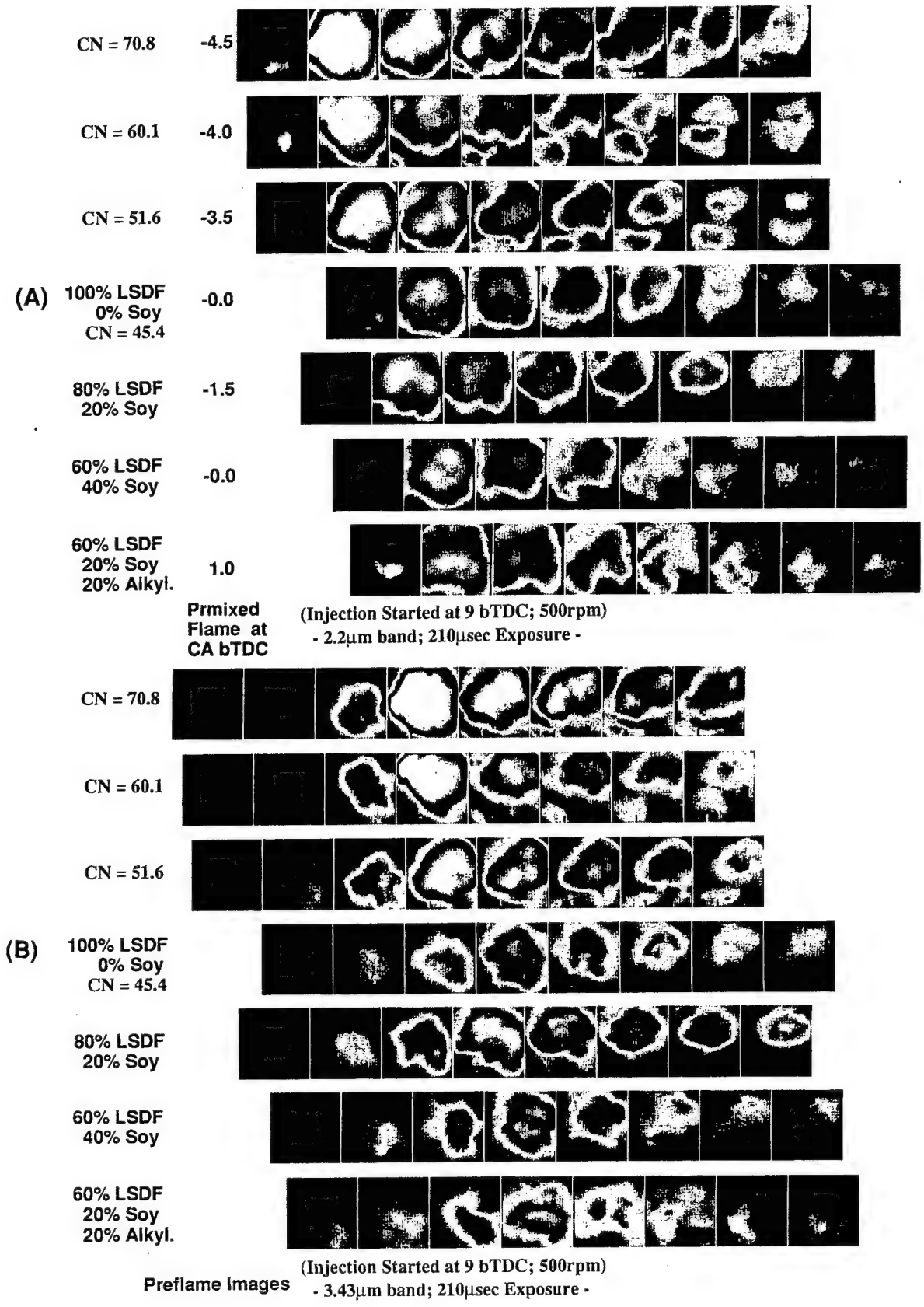

Fig. 6-(A). High-speed Spectral IR Images of Diesel Flame in 2.2μm. (Starting with First Visible Flame Images for Individual Fuels)
-(B). High-speed Spectral IR Images of Diesel Flame in 3.43μm. (Preflame Images Simultaneously obtained as 9-(A))

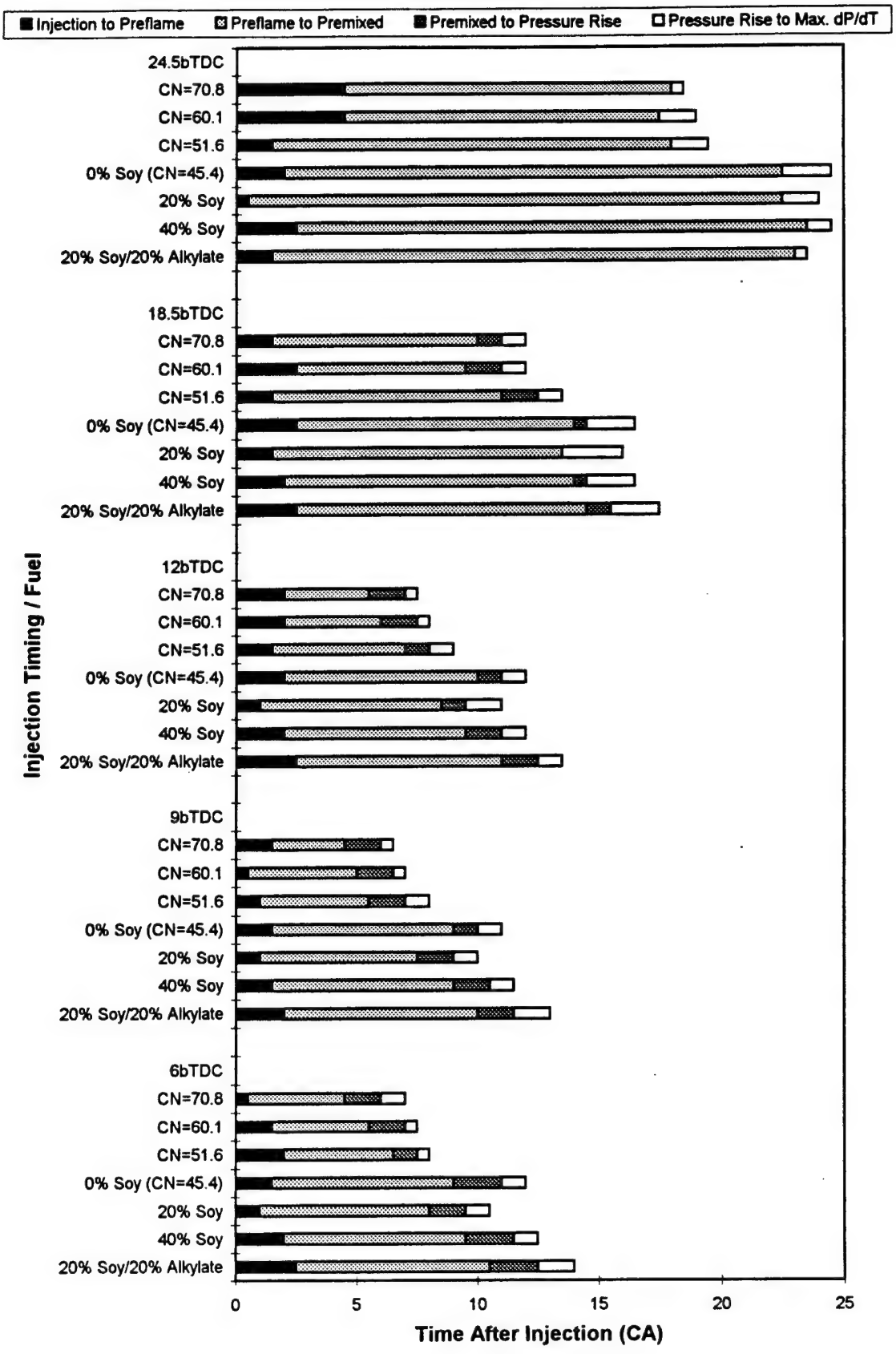

Fig. 7. Effects of Fuels on In-cylinder Reactions in a CI Engine Cylinder.

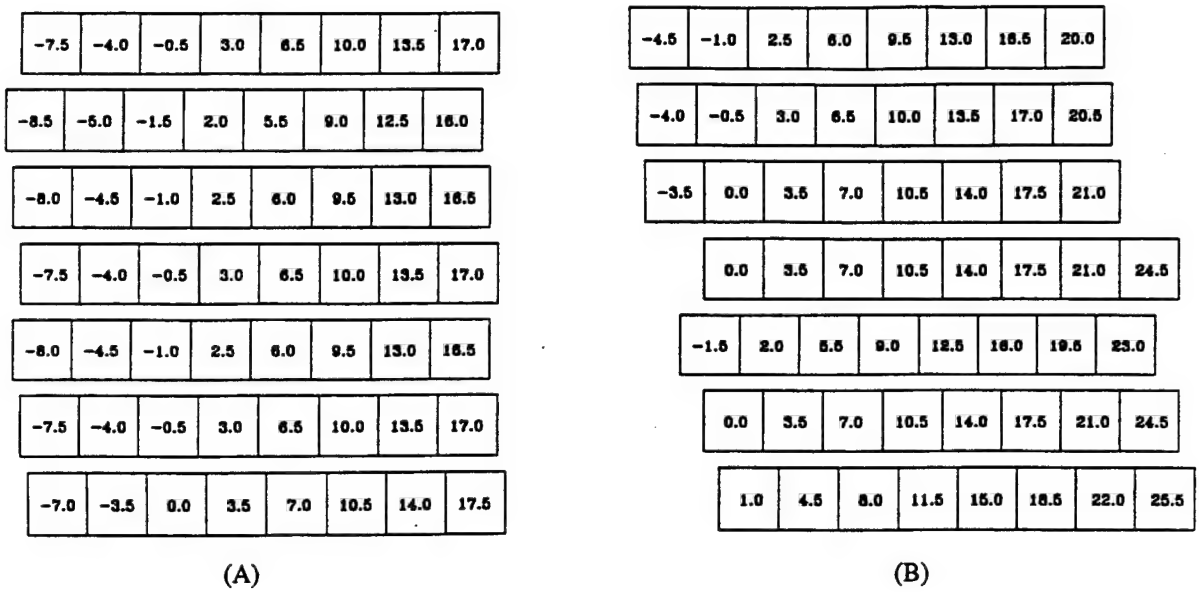

Fig. 8. Look-up Tables for High-speed Images to Indicate each Time of Imaging: (A) for Fig. 5 and (B) for Fig. 6.

The timelines of those events were measured with a temporal resolution as fine as a 0.5CA increment. Finding those of preflame and premixed flame, the feature of the SIS of varying the start of imaging (after a preset period, in temporal resolution of 0.5CA, from the reference marker, e.g TDC of the previous revolution) was utilized. After an engine condition was set forth, the start of imaging was varied back and forth until a barely detectable preflame image was found in the set of successive images, and the very CA when this image obtained was used for determining the timeline of preflame. The next images followed thereafter in every 3.5CA-interval in this experiment. Some sample results are displayed in Figs. 5 and 6. They are shown in pseudo-color in order to illustrate the local variations by displaying the digital results. Other events in p-t data were determined by using the computer programs as mentioned earlier, which is not elaborated here.

The overall results are summarized in Fig. 7. The timelines are illustrated in a relative scale representing CA periods in a self-explanatory manner. For example, the peak value in each column represent the period from the injection to the CA when the peak dp/dt occurred. Since this summary picture is highly crowded, individual timelines are separately plotted in Figs. 9-13.

In those plots, for an obvious reason of putting together results with varied CN as seen from Table-1, Plot-(I) includes those from the fuels of Group-1 and the base fuel from Group-2, as presented in the upper portion of each figure. Plot-(II) contains results from the fuels in Group-2 separately, as shown in the lower portion of the same figure.

Spectral IR Images. In order to determine the timelines of preflame and premixed flame, a set of spectral images was simultaneously obtained of both (invisible) preflame reactions (in 3.43μm band) and (visible) premixed flames (in 2.2μm band), plus those in 3.8 and 2.47μm bands. For example, looking at Fig. 5-(A), which was obtained with the injection starting at 9bTDC, the numbers in the second column indicate the CA when the first preflame was captured. A look-up table (LUT) for this figure is included for convenience of discussion in Fig. 8-(A). The rows of successive images for different fuels are arranged in a relative time-scale, with the far left indicating CA exhibiting the earliest preflame. Figure 5-(B) shows sets of (visible) premixed flame images simultaneously obtained at the corresponding CAs.

After completing this experiment, in order to determine the CA when the first premixed flame was captured, the same as above was performed, but at this time by finding the first visible image from the successive images in 2.2μm band, as shown in Fig. 6-(A). A matching LUT is included in Fig. 8-(B). At this time, the corresponding images via 3.43μm band was also obtained to investigate the development of the preflame under the same condition.

Comparing images at corresponding CA in Figs. 5 and 6, while there is strong radiation in 3.43μm band (with no radiation seen in 2.2μm band), no measurable change in p-t from that of a warm-engine motoring condition was found. This indicates that the observed preflame reactions make no impact on the heat budget. The preflame image, therefore, was suggested to be of chemiluminescence from some intermediate species including OH radical and aldehydes [1,2].

Fuels with Varied Amounts of Additives. First, figures labeled by (A) showing results from fuels with varied CN, the upper or right-side portion of each figure, is discussed. Note that those indicated by (B) with results on fuels mixed with varied amounts of bio-Diesel fuel is discussed later. The timelines of preflame and premixed flame are summarized in Fig. 9: Except for the very early starts of injection, i.e., 24.5 and 18.5bTDC, the ignition delay measurements (determined by the visible premixed flame) seem reasonable, the higher the CN, the shorter the

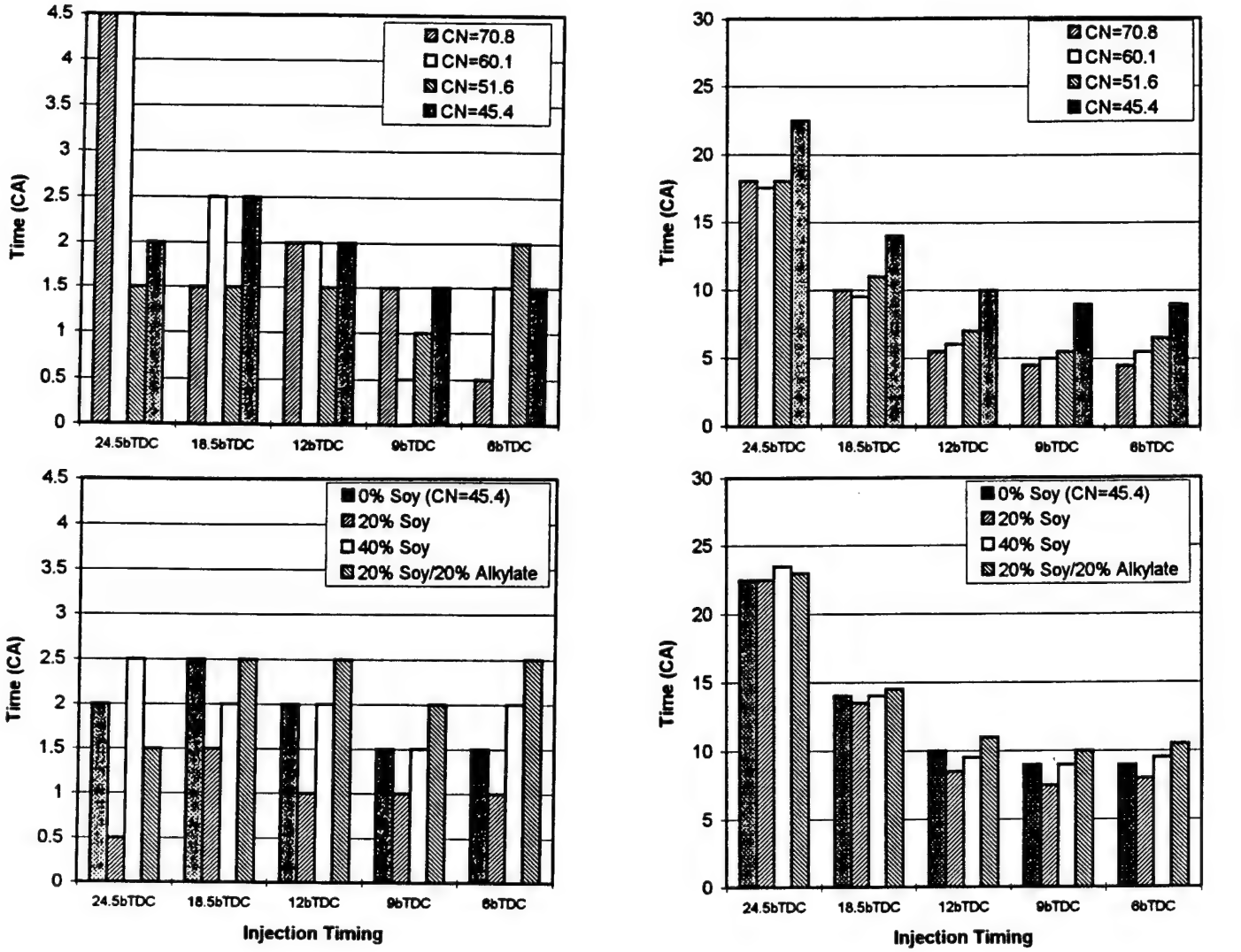

Fig. 9. Fuel Effects on Time from Injection: (A) to First Preflame Image, and (B) to First Visible Premixed Combustion.

ignition delay. This is similarly found from the timeline of the start of pressure rise obtained from p-t data as summarized in Fig. 10-(A). In addition, the timelines for the maximum dp/dt and the peak pressure are also included in Fig. 10-(B) and Fig. 11, respectively.

It is noteworthy from a comparison of Figs. 9, 10 and 11 to find that the timelines of maximum dp/dt and the start of pressure rise (preferably the former) may be the best indicator of all in determining the CN, because they appear to be *independent of the injection time*. In other words, these timelines may be most insensitive to variation of the reaction condition at the time of injection, and this warrants further study. If it is the case, the timeline of maximum dp/dt would be the more reliable indicator than the traditional defining method, particularly when the CN of fuels are determined by using a constant-volume bomb (instead of using the real-world engines). This is because a bench-top bomb apparatus may not exactly duplicate the same environment as in an actual Diesel engine cylinder at the end of compression.

Looking at Fig. 9, a couple of significant findings may be listed: They are: (1) the preflame reaction starts almost immediately after the start of fuel injection; and (2) there seems to be little difference in its timeline for fuels even with a wide variation of CN. Discussing the first, let's consider the CI environment. When the Diesel fuel containing components having self-ignition temperatures of lower than 500K is injected into compressed air at over 800K, it may not be difficult to expect some chemical reactions to occur without a significant (physical) delay. In particular, when the fuel is injected by an HPI of over 160MPa, the fuel plume will have finely disintegrated droplets vaporizing almost instantly to minimize any delay prior to commencing chemical reactions emitting chemiluminescent radiation.

Discussing the second finding, the change in the timeline of preflame is rather random and very small at best. Particularly, those for fuels with CN of 70.8, 60.1 and 51.6 are very small, which are results of mixing the base fuel with

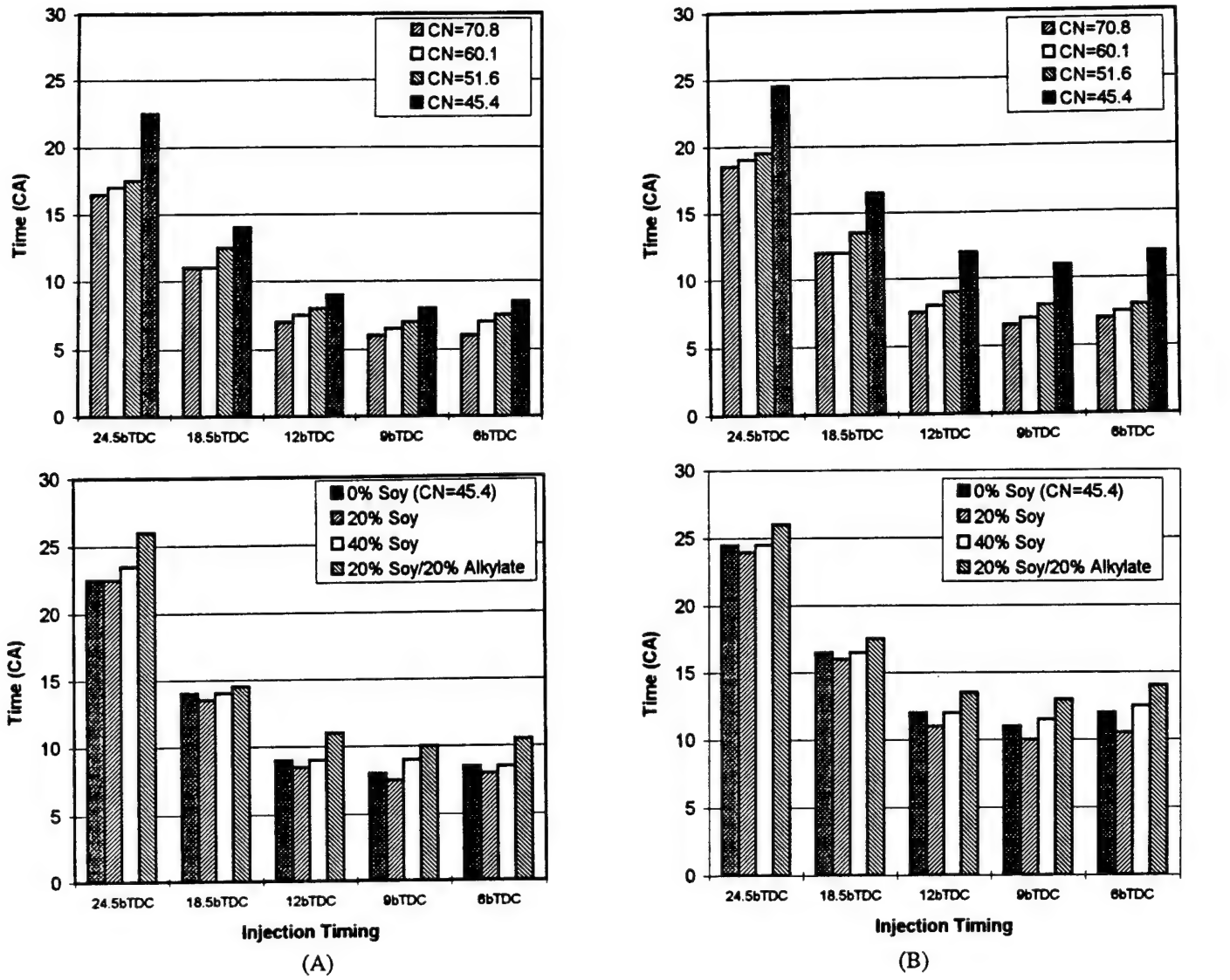

Fig. 10. Variation of Time from Injection: (A) to Rapid Pressure Rise and (B) to Maximum dP/dt.

small amounts of the additive, respectively. Except for the very late injection, the difference in the timelines of two base fuels (with CN of 51.6 and 45.4) appears to be more obvious and seemingly predictable than the above having bigger CN differences (achieved by an additive). It may be due to the fact that the difference in CN between these two base fuels was solely from the fuel characteristics, while the above was changed by mixing of an additive. The former observation suggests that the additive may not affect the preflame reactions, which seems to be reasonable in view of the consideration mentioned earlier. That is, since the amounts of the additives is so small that they are not expected to alter the formation of species as a result of the decomposition of the base fuel hydrocarbons as dictated via low-temperature kinetics. One the other hand, looking at Plot-(I) for the timeline of premixed flame shown in Fig. 9-(B), which is a traditional criterion determining CN, the additive resulted in what was expected. Recall that the onset of premixed flame accompanied by a rise of pressure is a result of thermal imbalance, when the high-temperature kinetics takes over the reaction routes. Putting these facts together, one may suspect that the role of the additive in the CI environment may be more to affect high-temperature kinetics, perhaps by infusing new exothermic reactions and or accelerating some key elementary reaction to such processes, which, without the CN booster, are not expected to occur to drive the mixture to a thermal imbalance stage sooner.

Fuels Containing Bio-Diesel Fuel. The lower or right-side portion of each figure, Plot-(II) contains results from fuels prepared by mixing the base fuel-2 with different amounts of bio-Diesel fuel. The timelines of both the preflame and premixed flame for fuels in Group-2 are rather unpredictable, compared with the same with those in Group-1. In general, addition of esterified soy (hereafter called, "soy") to a base fuel causes an increased CN, which seems reasonable when the base fuel and fuel containing 20% soy (Fig. 9) are compared with each other. What is quite

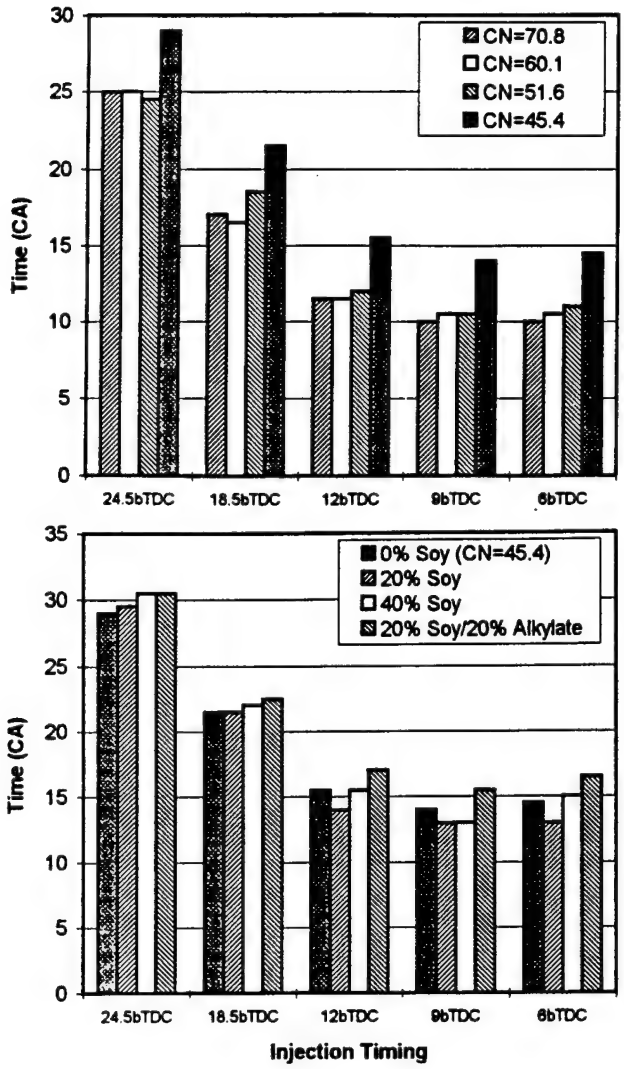

Fig. 11. Time from Injection to Peak Pressure Affected by Fuel.

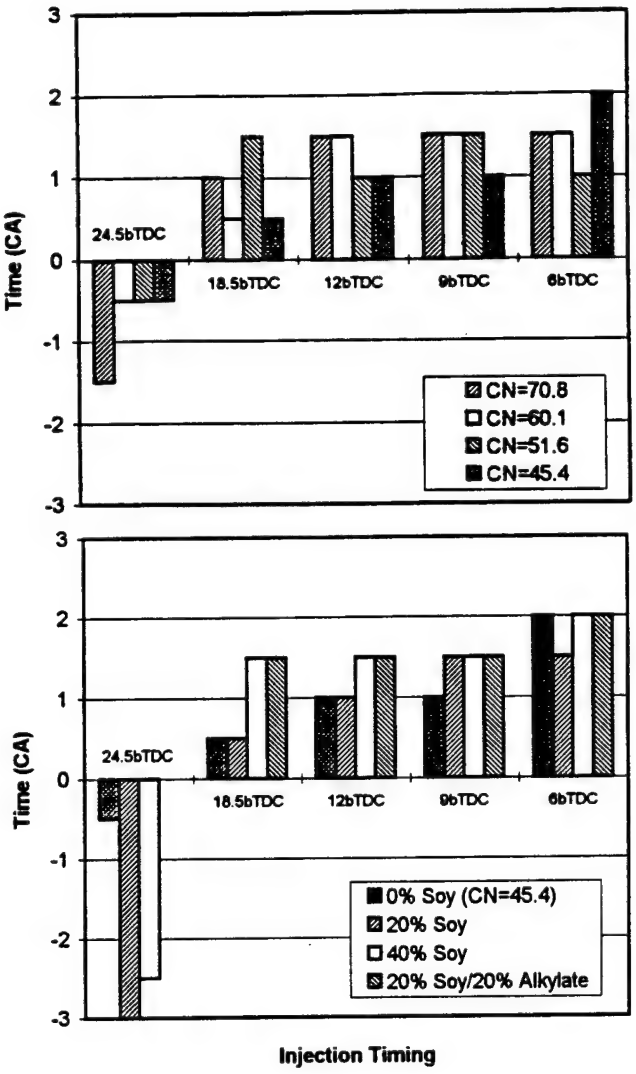

Fig. 12. Time Period from First Visible Premixed Combustion to Start of Rapid Pressure Rise.

unexpected is the fuel containing 40% soy, which behaved almost like the base fuel. Even radiation characteristics appear to be similar to each other (see Figs. 5 and 6). A possible reason for this unusual finding may be that the spray pattern is so greatly modified (by the physical role of viscous bio-fuel) to cause such a result, which is a marginally convincing interpretation at best calling for an additional study. Mentioning fuel-2c containing 20% soy and 20% alkylate, the trend was expected because the CN of this alkylate is around 30, which would lengthen the ignition delay. This suggests that the small effect of soy addition of shortening the ignition delay is offset by the alkylate's role of the opposite effect.

Ignition Delay and Combustion by Other Timelines. In addition to the timeline of premixed flame used for determining the ignition delay, those for the start of pressure rise, the maximum dp/dt, and the peak pressure are also considered (Figs. 10 and 11). Since the net energy release as the result of ignition is reflected by the start of pressure rise (compared with that of a warm-engine motoring operation), its timeline is also being used for evaluating CN. This timeline, however, does have some measurable differences from that of premixed flame as shown in Fig. 12, generally occurring later than the latter. This is considered to occur due to heat loss via several possible ways, including: the latent heat of liquid fuel vaporization, continuing endothermic chemical reactions in the plume, and heat transfer to the wall. There is an illustrative trend in both plots that the later the injection time, the longer the period from the first flame to the start of pressure rise, which seems to suggest the wall heat loss may not be a decisive possibility. A possible explanation is that the fuels having the same base fuel (even with big differences in CN) may have almost an identical difference between the timelines (for respective injection times).

When the fuel was injected very early, however, the trend was opposite, i.e., the visible flame was observed after the pressure rise was measured, which was most significant for fuel containing 40% soy, and that with 20% soy plus

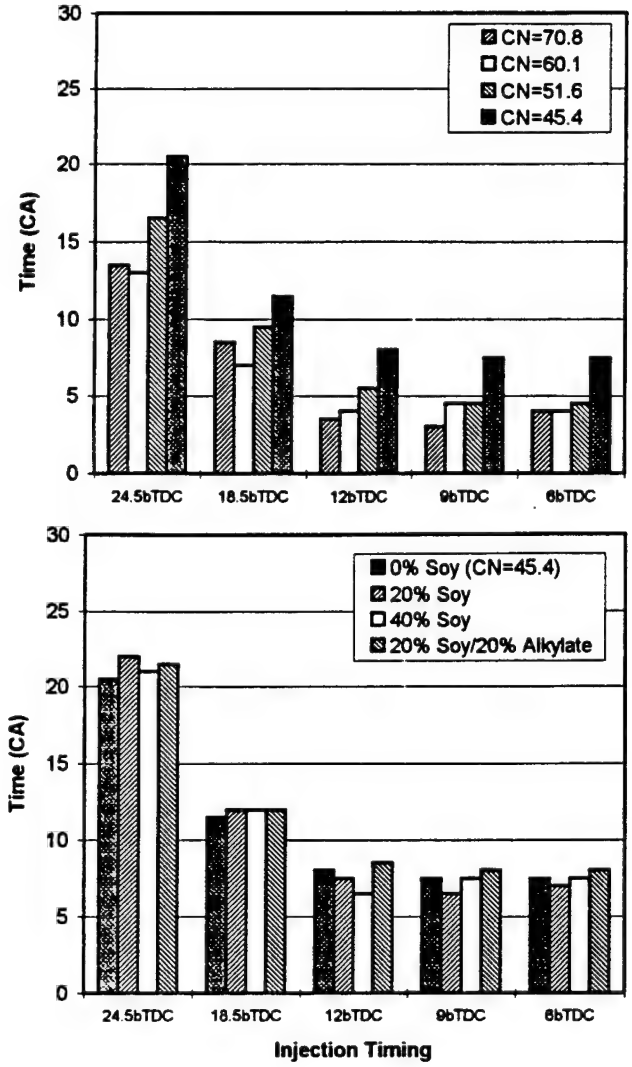

Fig. 13. Time Period from Preflame to Premixed Combustion.

20% alkylate. The only possible reason for this is that there were invisible exothermic reactions in the cylinder causing an early pressure rise. Without offering a convincing explanation, one may wonder if the unusual ignition behavior for fuel with 40% soy, as explained above, is related to this peculiar result. This seems to also support the argument on the probable limitations in using a constant-volume bomb to determine the fuel's CN, as discussed earlier.

Preflame Development. First, since the time period having preflame reactions prior to the premixed flame is expected to indicate how the intermediate species continue to build up prior to the onset of abrupt ignition, Fig. 13 is included here. Looking at Plot-(I), the result is quite similar to the timeline for the premixed flame (Fig. 9), which, therefore, may be a criterion to be used for determining ignition quality.

Let's consider what is happening during this period: Reviewing preflame images in Fig, 5-(A) compared with the onset of premixed flame images in Fig. 5-(B), particularly images obtained at 0.5bTDC for fuel-2 (see LUT at Fig. 8-(A)). When the small section exhibiting weak premixed flame (Fig. 5-(B)) is made to overlap the corresponding preflame image in Fig. 5-(A), one may find that the latter seems to contain both zones of the preflame reaction and premixed flame. A similar finding may be made when the same is attempted on images at 1.0bTDC for fuel 2a (containing 20% soy). This observation was similarly found when those in Fig. 6 are compared in the same way. Note that Fig. 6-(B) will have to be placed ahead, by a period 7CA, of (A) in order to compare with each other. In general, the longer the period between the two timelines (of preflame reaction and premixed flame), the stronger the reaction size of preflame zone. What seems to be intriguing is that the zone having the first premixed flame development is not necessarily where the strongest preflame radiation is found. For example, locating the first premixed flame in Fig. 6-(B) and matching it with the corresponding preflame image in (A), one could list such, particularly from fuel 1b; fuel 1a and fuel 2c. Although this trend appeared to occur more in those containing the CN enhancing additive, one could expect that the additive may produce separate chemical reactions leading to premixed flame (instead of increasing over all species formation of base fuel). Also, the mutual inconsistency between two images in respective reaction regimes (also in different times of occurrence) may be due to the gas motions in the cylinder. That is, the reaction volumes exhibiting preflame radiations are moved around prior to being matured to cause ignition kernels, which is captured as the first premixed flame propagation.

Why More NOx and Lower Particulate by Bio-Diesel Fuels? In general, vehicle fleet tests indicate that the higher the soy content the higher the NOx emission and the lower the soot measurement. At first, an observation with the bio-Diesel fuel experiment is mentioned. The soot deposit on the cylinder-side surface of the optical window was much less when the fuels containing soy were used, and instead, the surface was often covered with thin film of liquid layer, which was not the case when the conventional fuel was used to observe the formation of dry soot deposit. This may indirectly show a low soot formation with the bio-Diesel fuel. The in-cylinder images may give some insight into the reasons for such exhaust measurements also. In general the lower the CN, the lower the radiation intensity (Figs. 5 and 6) indicating the low soot formation.

Several observations may be listed regarding the increase of NOx formation with bio-Diesel fuel: In Fig. 5-A, there is some trend of having a greater activity in preflame reactions with bio-Diesel fuels. And the more active (and longer) the preflame reactions (and period), the less intense the premixed flame radiation, which indicate the portion of diffusion flame reaction is less, which is expected to produce more NOx. This consideration, however, does not seem reasonable when images (Fig. 5-(A)) with fuel-2 and those from fuel-2a are compared each other, which needs further study. At present, it is to be fair to indicate no conclusive interpretation can be offered from the bio-Diesel fuel results.

Summary

The timelines of main events in a direct injection Diesel engine equipped with a high-pressure (electronically controlled) injection unit were determined with a high-speed spectral IR imaging system and p-t history. The engine was operated by using seven different fuels including two base fuels: the first group of fuels was prepared by mixing a base fuel with different doses of CN enhancing additive (CN booster) and the second group was made by adding the other base fuel with different amounts of esterified soy (bio-Diesel fuel). The experiment was performed for four different injection times with the engine speed maintained at 500rpm under warmed engine condition.

The timeline, the crank angle when the first evidence is exhibited of a main event, with respect to the start of fuel injection, was determined for the following: (1) preflame reactions; (2) premixed flame; (3) start of pressure rise; (4) maximum pressure rise rate (dp/dt); and (5) peak pressure. New questions and issues came up as much as new findings were made in the study. Some are summarized in the following:

(1) The timeline of preflame reaction seem to be a useful indicator in determining CN of Diesel fuels while it is otherwise for fuels containing a CN booster. This may be explained by an expectation that an addition of the additive to a base fuel may infuse new chemical reactions in addition to the elementary (chain) initiating-propagating reactions controlled by low temperature chemical kinetics leading to the exothermic reactions sooner.

(2) The timelines of premixed flame, start of pressure rise, maximum dp/dt and peak pressure may be all used for determining CN of Diesel fuels, but the time of maximum dp/dt appears to be most indicative regardless of injection time.

(3) The base fuel containing bio-Diesel fuel yielded some predictable results while they were opposite when its content become very high, e.g. 40% of soy. This may be attributed by the physical change of spray pattern by the addition of the new fuel. It is clear further investigation is warranted.

(4) The timeline of premixed flame and that of the pressure rise did not occur at the same time although both are traditionally used for determining CN. The former preceded the later by as much as a few CA, for which the difference became even greater with retarded injection times.

(5) When the injection time was very early, e.g. 25bTDC, the behavior of in-cylinder events became rather unpredictable. This may indicate the limitations of using constant-volume bench-top reactors for determining CN of a fuel because its self-ignition environment may not be duplicated of a typical Diesel engine condition.

In order to resolve some unanswered questions, it is recommended that Diesel fuels having varied CN without containing a CN booster be compared with corresponding results from the matching Diesel fuels prepared by using the additive.

Acknowledgement

The present work has been performed under the sponsorship of the U.S. Army Research Office (Contract No. DAAH04-95-1-0430) and AASERT (DAAH04-94-G-0201), the U.S. Department of Energy (Contract No. ACC-4-14361-01, through National Renewable Energy Laboratory), and Ethyl Corporation.

References

1. Clasen, E., Campbell, S., and Rhee, K.T., "Spectral IR Images of Direct Injection Diesel Engine Combustion with High Pressure Fuel Injection," SAE Paper-950605, 1995.

2. Song, K., Clasen, E., Chang, C., Campbell, S., Rhee, K.T., "Post-flame Oxidation and Unburned Hydrocarbon in a Spark-ignition Engine," SAE Paper-952543, 1995.

3. Jeong, Y.I., Qian, Y., Campbell, S. and Rhee, K.T., "Investigation of a Direct Injection Diesel Engine by High-Speed Spectral IR Imaging and KIVA-II," SAE Paper-941732, 1994.

4. Jiang, H., Qian, Y. and Rhee, K.T., "High-Speed Dual-Spectra Infrared Imaging," Optical Engineering, 32 (6), pp. 1281-1289, 1993.

5. Abata, D., Stroia, B.J., Beck, N.J., and Roach, A.R., "Diesel Engine Flame Photographs with High Pressure Injection," SAE Paper-880298, 1988.

972973

Engine Performance and Exhaust Characteristics of Direct-injection Diesel Engine Operated with DME

S. Kajitani, Z. L. Chen, M. Konno
Ibaraki University
Hitachi, Japan

KT Rhee
Rutgers, The State University of New Jersey
Piscataway, New Jersey

ABSTRACT

Neat dimethyl ether (DME), as an alternative fuel candidate for Diesel engines, was investigated by measuring primarily engine performance and exhaust gas characteristics. In addition, other responses of the engine to the new fuel were also determined at the same time, including the injector needle lift and heat release. The engine measurements with this fuel were compared with those obtained by using conventional Diesel fuel.

Findings from the present work include: (1) It was necessary to add a small amount of lubricating additives to DME, if a conventional fuel injection system is employed. This was to achieve satisfactory injector performance and to minimize some excessive wear. (2) Engine performance for both fuels was basically comparable to each other, except for a better energy conversion efficiency with DME. (3) In the DME-operated engine, emissions of soot and unburned hydrocarbon (THC) were almost negligible, but NOx emission was about the same as in the Diesel oil operation. (4) The reduction of NOx emission by delaying the injection time was highly significant with DME.

INTRODUCTION

Since it is a derivative of methanol and also can be made from natural gas, both of which are known to be low-emission fuels in Diesel engines [1,2]*, DME was expected to deliver some similar emission characteristics. Importantly, the fuel has an advantage of better self-ignition characteristics, which has motivated recent interest in evaluating its wide use for Diesel engines.

In addition to oxygen contained in the molecule, the absence of a direct C-C bond in DME (CH_3-O-CH_3) is responsible for better spray combustion resulting in low soot emissions, which has been a formidable task to achieve in Diesel fuel operated compression-ignition engines. The emissions of other pollutants, however, are difficult to predict, but they were expected to be no worse than those with conventional Diesel fuel (or gas oil). Because of its low self-ignition temperature (235℃), DME was employed as an ignition improver when the use of methanol in Diesel engines was explored [3-5], which advantage lacks in such fuels that produce low soot emissions.

In spite of these seemingly favorable characteristics, other responses of direct-injection (DI) Diesel engines to this new fuel were examined for acceptability [6-9]. For example, in view of a high elastic modulus of DME compared with Diesel fuel, which is further discussed later, the needle lift of the conventional injector was expected to shift when it is operated by the new fuel. If it shifts even by a few crank angle degrees, the subsequent combustion processes will be remarkably altered, which will affect not only the engine performances but also the emissions. An in-depth understanding of such unpredictable engine behaviors is not only of academic interest but also a important precondition for a successful application of this new fuel in Diesel engines.

One of most serious problems faced in the use of DME in DI Diesel engines was that due to its low lubricity, when delivered via the conventional (Diesel oil) injection system, sever wears resulted to cause excessive leaks in the injection system [7]. Without a new injection system developed for using this alternative fuel, which is not a simple task to implement [10], it seemed to be more reasonable to modify the fuel by increasing the lubricity. This was taken into consideration in the present study.

Reviewing more the negative side of this fuel, it has a high vapor pressure under the normal operating

*Numbers in parentheses designate references at end of paper.

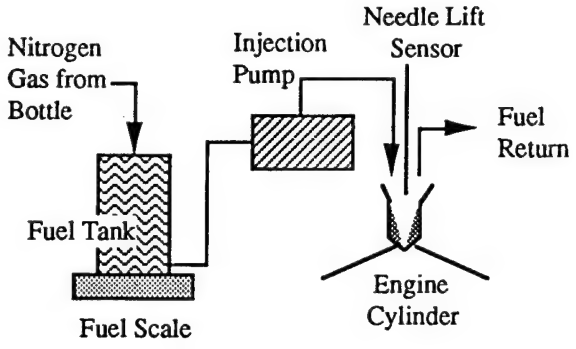

Fig. 1. Fuel System for Supplying DME to the Engine.

environment [11] so that it was necessary to take some special measures in the fuel handling and fuel delivery system of the engine. Even if this fuel in DI Diesel engines produces a satisfactory performance and low emissions, the problems associated with the high vapor pressure are expected to remain important to overcome when DME is used as an alternative fuel in Diesel engines. The relatively low fire hazard with the use of gas oil in Diesel engines, which is an important advantage in military and marine applications, is not likely to be expected when DME is widely used.

The low energy content of the fuel compared with gas oil may be a problem also, which would require about twice as frequent fuel fillings as compared with Diesel fuel for a comparable vehicle. Such problems, however, would not be more severe than those encountered in the use of methanol or natural gas, which have seriously been considered as an alternative fuel in Diesel engines, a measure investigated in order to achieve vehicles with ultra low emissions.

EXPERIMENT

Engine and Apparatus. Because it is important to investigate the responses of real-world engines when a new fuel is used in place of the conventional Diesel fuel, a commercial engine was directly used in the present study with a minimum modification. The engine employed in the study, therefore, was a DI Diesel engine manufactured by Yammer Diesel Corporation having dimensions as shown in Table-I. Since the engine is a typical DI unit with a Bosch-type fuel injector, for which specifications are also listed in Table-I, no additional elaboration of the engine is made here.

Table-I Engine Specifications

Bore x Stroke	92 x 96mm
Displacement	638cm^3
Compression Ratio	17.7
Rated Output	15.6kW/cylinder-2600rpm
Injection Pump, Plunger	8mm dia. (Bosch type)
Injector, Four-hole Nozzle	0.26mm hole dia.

As pointed out earlier, however, since the fuel has a high vapor pressure in the laboratory environment, the fuel system was pressurized by nitrogen gas (from a bottle) in order to prevent leaks and vapor-lock from occurring in the fuel system. Figure 1 shows a schematic presentation of this arrangement having a scale for determining fuel consumption during the engine operation.

The engine apparatus was instrumented sufficiently for implementing the objective of the study, including installation of a needle lift sensor (in the injector), a pressure transducer and interfacing the engine with emission measurement devices. Since these equipment are widely used in the field, no further discussion is added here.

The experiment was conducted for DME by obtaining engine performance and emission characteristics as well as monitoring other engine responses by comparing the same obtained by using (pump-grade) conventional Diesel fuel.

Upon reviewing various methods employed in previous studies [7-11], in most of the experiments in the present work, the fuel tank was pressurized at 3.43MPa (35kgf/ cm^2) when DME was used, which was therefore the inlet fuel pressure to the injection pump. In DME operations, the injection nozzle opening pressure was set at 8.82MPa (90kg/cm^2) when the engine ran at 960rpm, which was chosen about the same as a previous study [7], for a mutual comparison purpose. Note that the recommended opening pressure of the engine for Diesel fuel, on the other hand, was 20.1MPa (205kg/cm^2).

Fuel Additive. In the very beginning of the study, in order to investigate how serious negative impacts would occur to the engine, particularly in the injection system by the use of straight DME, the engine apparatus was operated without any change to the new fuel. The engine ran quite smoothly for a period of about 30 minutes from the start, but thereafter some unstable changes in speed and load were observed. This was soon followed by a severe stall leading to stop, and then it was no longer possible to start the engine. A careful inspection of the engine revealed serious wear on the needle of the injector nozzle, and a rather remarkable amount of scoring on the injector plunger as shown in Fig. 2.

From this initial engine testing with the new fuel, it became obvious that no meaningful study could be performed for straight DME in a Diesel engine unless some modification is made on the fuel. After some trial-and-error fuel-engine operation, it was found that an addition of Hitec560 (provided by Ethyl Japan Corp.) in portion of 100ppm to DME did not exhibit any detectable wear in the fuel system, at least for a period in completing the present experiment. Although this additive might have altered both the combustion and emission characteristics somewhat, it was a very minimum measure required to achieve an acceptable engine performance.

RESULTS AND DISCUSSION

The results from the work are presented in graphical form in Figs. 3-22, where the solid lines, in most

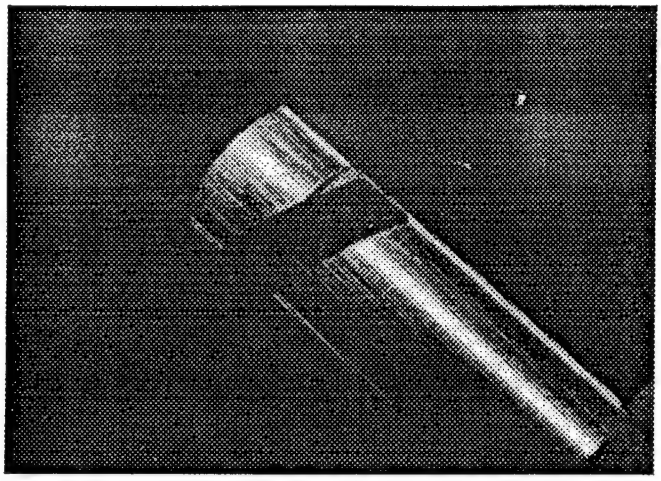

Fig. 2. Photograph of Injector Exhibiting Severe Wear after Used with DME.

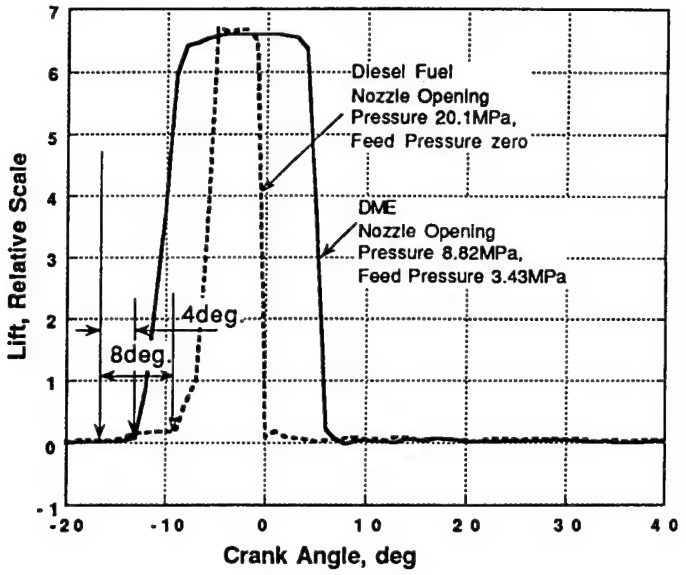

Fig. 3. Injector Needle Lift for DME and Gas Oil Operation.

cases, represent measurements with DME, and dotted lines indicate those with the conventional pump-grade Diesel oil. In spite of the increased lubricity of DME by the additive, in order to eliminate any possible artifact of injector wear on the spray formation, the nozzle needle was frequently replaced throughout the experiment.

Effect of Feed Pressure on Nozzle Opening. One of the key issues studied in the present work was to delineate some conflicting results of engine performance and emission as reported by others, which is further elaborated later. The key consideration taken for explaining the confusion was the fact that the DME application in Diesel engines involved differences not only in the fuels' physical properties, e.g. the elastic modulus of the two fuels (DME, 6.37×10^8 N/m^2; Diesel oil, 1.49×10^9 N/m^2) but also in the operating conditions including the fuel feed pressure, which ranged from 1.96 to 2.94MPa (20 to 30kgf/ cm^2) in other studies. These variations were expected to alter the nozzle opening time, which information lacks in previous studies.

In the first experiment, however, simply by following the engine manufacturer's recommendation, the nozzle opening pressure was adjusted for Diesel fuel at 20.1 MPa, with feed pressure at zero because there is no need for pressurizing the tank for this fuel. After obtaining measurements including the needle lift-tracing with this fuel, in a separate experiment, the fuel system was fed with DME at 3.43MPa, because it needs pressurization in the tank, as explained earlier. The nozzle opening pressure was set 8.82MPa at this time, which was the same as some of the other earlier studies. Note that the nozzle (static) opening pressure was controlled by adjusting the spring preload in the injector.

It is noted that this set of experiments varying both the feed pressure and nozzle opening pressure for the fuels may appear to be confusing in sorting out the individual effects on the needle lift. These initial experimental conditions were investigated, right after setting up the new

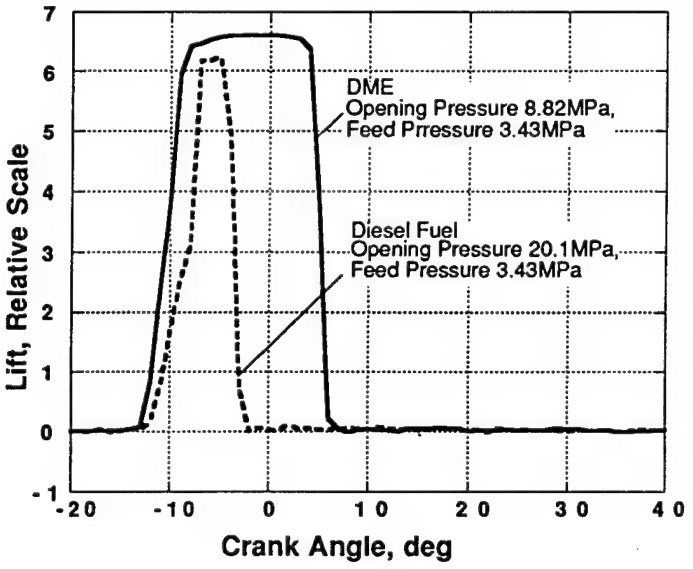

Fig. 4. Effect of Feed Pressure on Needle Lift.

apparatus, in order to duplicate a part of the previous studies in an attempt to explain some questions brought up by earlier studies as mentioned above.

Explaining the presetting of injection time and the engine's response, it was adjusted to occur at 17bTDC according to the recommendation by the engine manufacturer. As shown in Fig. 3, the actual start of injection indicated by the needle lift, however, was different from this (manual) preset timing: Under the setting, which was supposed to have the opening start at 17bTDC, the actual (dynamic) opening occurred at 13bTDC for DME and

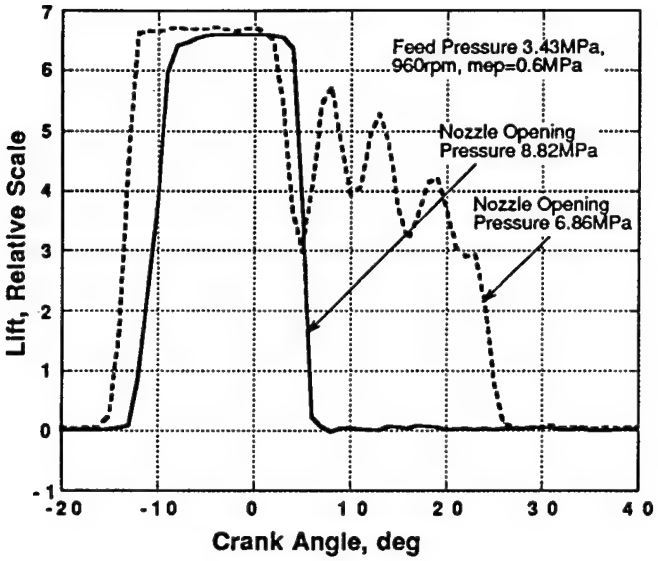

Fig. 5. Effect of Nozzle Opening Pressure on Needle Lift.

9bTDC for Diesel fuel, respectively. This exhibited that the opening with DME occurred earlier than gas oil by as much as by four crank angle degrees (CA). The results from these initial experiments seemed to offer some insight into the reasons for a significant difference in the start of pressure rise in a nearly matching experimental condition [7], which was not explained basically due to absence of the needle lift tracing.

This difference in the start of opening observed in the experiment was considered to occur by a combined effect of several variables, namely the feed pressure, the preset nozzle opening pressure, and the elastic modulus of the fuel. In order to sort out the multiple effects in this experiment, at this time the feed pressure was set the same, and new results (Fig. 4) were obtained to compare them with those shown in Fig. 3. Looking at the needle lift for Diesel fuel, the feed pressure was observed to be a strong factor affecting the nozzle opening time. That is, when the feed pressure was set the same, the opening pressure occurred at the about the identical time. The effect of the nozzle opening pressure on the start of injection, however, was not known from these experiments.

Effect of Opening Pressure on the Time of Nozzle Opening. An additional experiment with DME (Fig. 5), therefore, was performed by varying the opening pressure, i.e., 8.82MPa vs. 6.86MPa. With the low opening pressure, although it was about the same pressure as others employed, some considerable residual needle bouncing was observed, opposed to a relatively well-defined injection behavior with the higher opening pressure. The increased period of nozzle opening due to the bouncing, with the low nozzle opening pressure, was pronounced to be unusual and improper, as discussed more next. Note that there was a small amount of shift in the nozzle opening time when the opening pressure was varied. This effect seemed to be

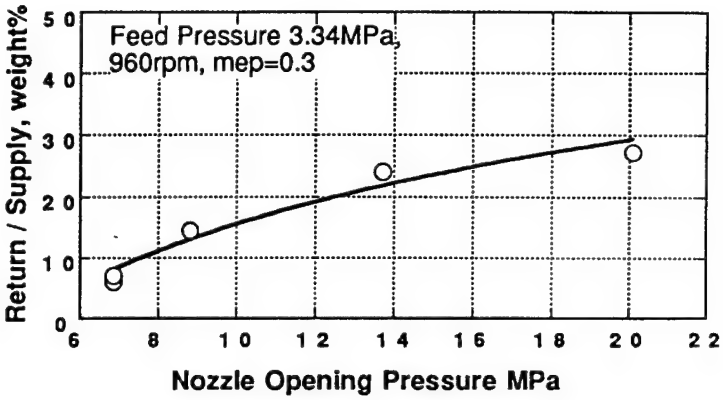

Fig. 6. Effect of Nozzle Opening Pressure on Fuel Return for DME.

measurable only when the opening pressures were low (refer to Fig. 4).

Regarding the suppressed residual bouncing by a high nozzle opening pressure, although there is no doubt that the increased spring preload on the nozzle needle would have played an important role, an additional factor may be considered, that is, the cooling of the injector. This consideration stemmed from the observation that when the opening pressure was set low (Fig. 5) the needle seemingly stayed almost afloat during the residual bouncing period, which is not a typical mode of needle bouncing in the Bosch type injector. This led to a new consideration that because of the elevated vapor pressure at high temperature with DME, the fuel at the nozzle tip might have been under a supercritical condition. If it is the case, it would have affected not only the plume formation characteristics but also the nozzle opening behavior. An indirect evidence for this consideration may be also seen from Fig. 6, which illustrates increased amounts of the fuel return for higher opening pressures. The high return was considered to increase the cooling of the injector nozzle to suppress the vapor pressure.

Effect of Injection Time. After evaluating the needle response to variation of several main parameters including those discussed above, the experiment was continued at this time by changing the start of injection time. (The change was not made in fine increments, since it required a considerable amount of engine modification, a conflicting measure to the original intent of performing the study with minimum engine change.) Two different injection times were studied, with settings of 17bTDC and 5bTDC (indicated by the manufacturer's manual), which had one tooth difference between the gears in the engine and injection pump. Note that the needle lift did not occur at the manual-indicated time, as explained earlier. In this experiment, the engine dynamometer was set at the speed of 960rpm and the load to deliver (brake) mean effective pressure (mep) of 0.3MPa (Fig. 7), and mep = 0.6MPa (Fig. 8), respectively.

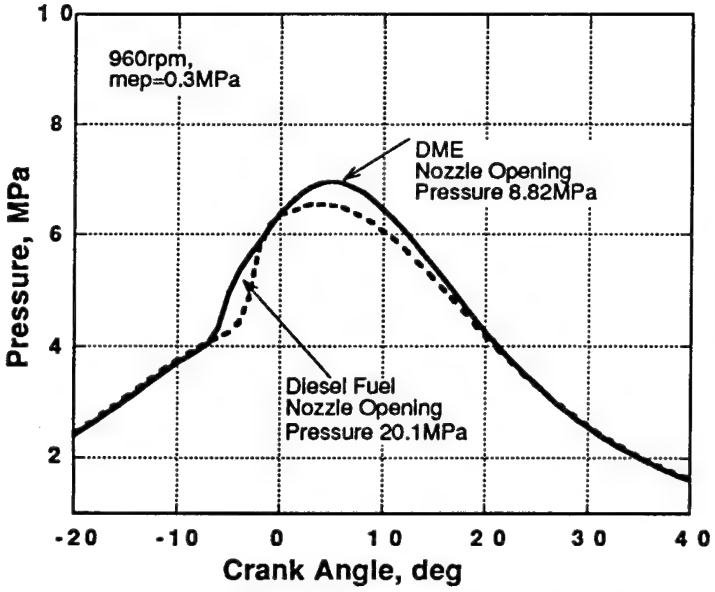

Fig. 7. Pressure-Time History for Pme = 0.3 MPa and 17bTDC Injection.

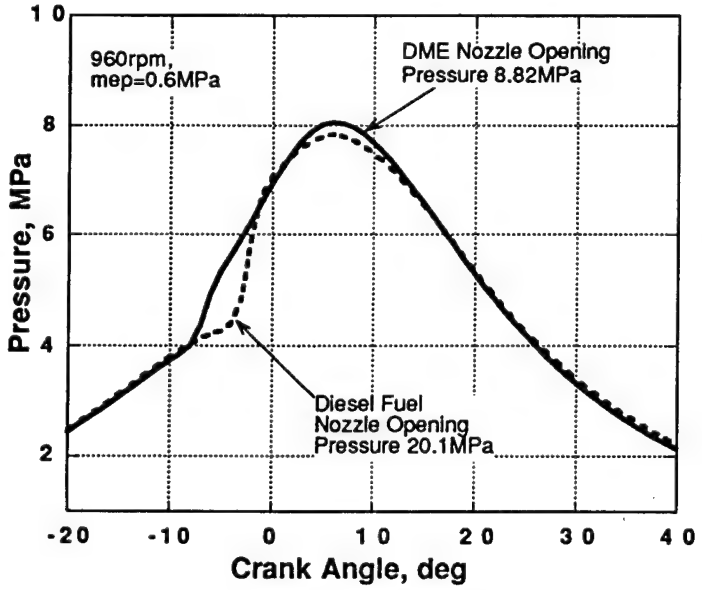

Fig. 8. Pressure-Time History for mep = 0.6 MPa and 17bTDC Injection.

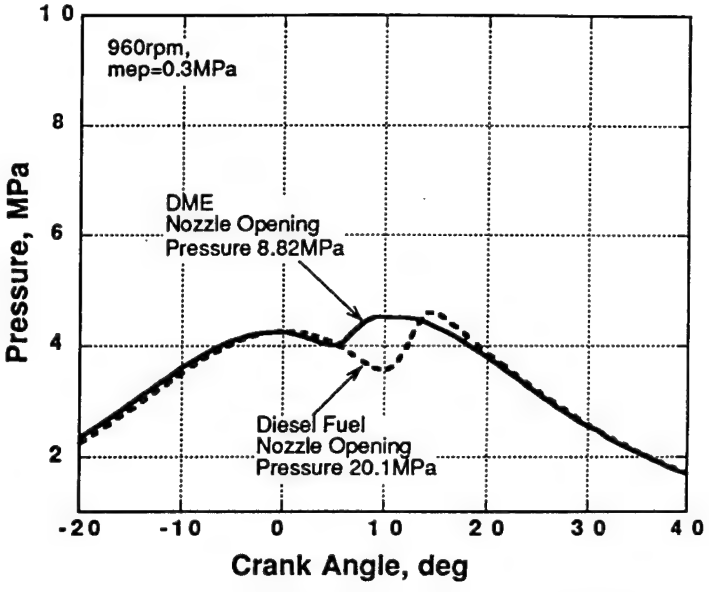

Fig. 9. Pressure-Time History for Pme = 0.3 MPa and 5bTDC Injection.

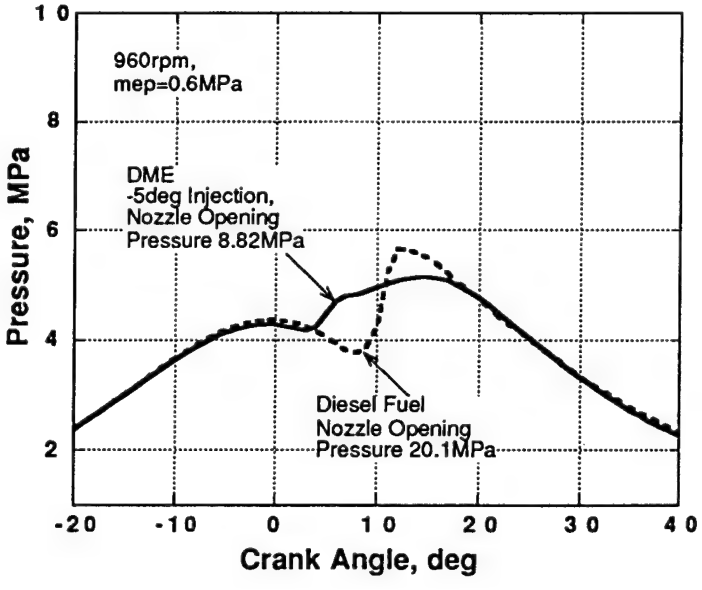

Fig. 10. Pressure-Time History for mep = 0.6 MPa and 5bTDC Injection.

Looking at the difference in the needle lift tracing as shown in Fig. 3, when the load was low (Fig. 7), the rapid pressure rise occurred earlier with DME than with gas oil by about the corresponding amount, although the peak pressure occurred almost at the same CA for both fuels. When the load was high (Fig. 8), the difference in start of pressure rise was even more obvious with DME compared with Diesel fuel. The earlier start of pressure rise in both experiments did not appear to occur due to an easy (chemical) ignition tendency of DME but more the differences in the start of nozzle lift. Recall that the early nozzle opening occurred due to the difference caused by the feed pressure and to a small extent by the nozzle opening pressure.

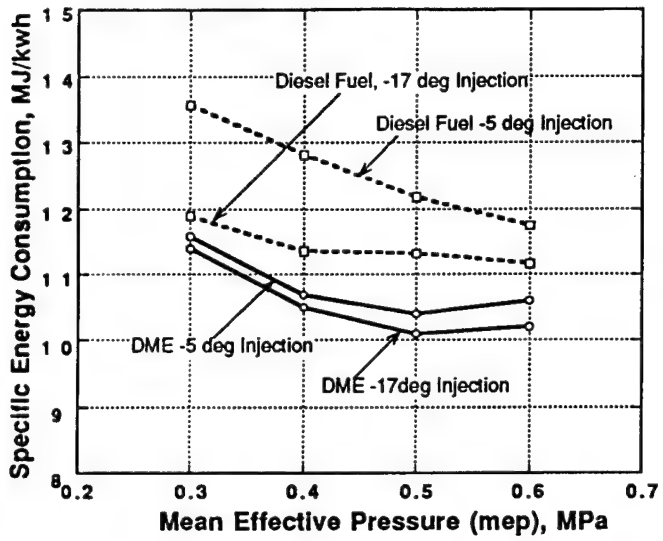

Fig. 11. Specific Energy Consumption.

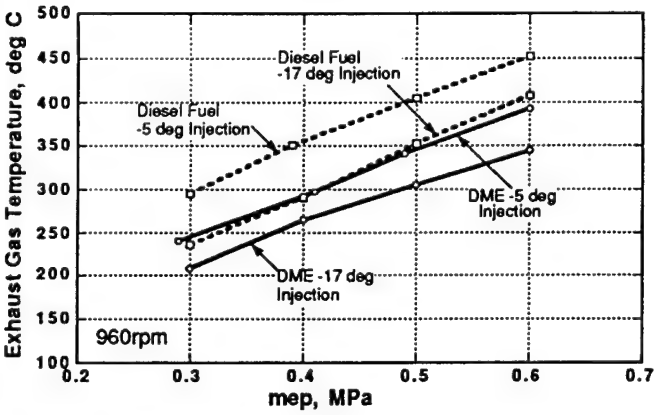

Fig. 12. Exhaust Gas Temperature.

This experiment is considered to clarify some unanswered issues brought up in previous studies, which were performed without knowing the shift in nozzle opening and the pressure-time data, for example. Such an early start of combustion with DME, compared with gas oil will no doubt result in increased NOx formation, as discussed more later.

Next, the same experiment was performed only with a change in injection time, i.e., from 17bTDC to 5bTDC, for both low and high loads as shown in Figs. 9 and 10, respectively. When the injection time was delayed, the effect of self-ignition tendency of DME seemed to play a predominant role resulting in a far earlier start of pressure rise compared with Diesel fuel operation. (This will be further discussed when Fig. 17 is presented.) That is, according to the needle lift tracing, the shift in the opening was about by four CA while the difference in the pressure rise is almost by seven CA, which was considered to occur due to the difference in the ignition delay dictated by various factors associated with not only the fuel characteristics but also cylinder conditions. Additional engine measurements are explained in support of the above discussion next.

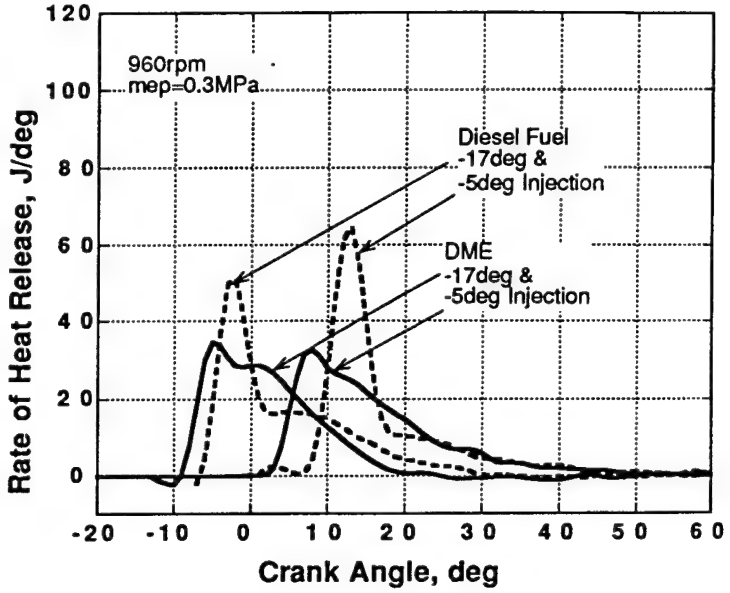

Fig. 13. Rate of Heat Release for mep = 0.3 MPa and 17bTDC and 5bTDC Injection.

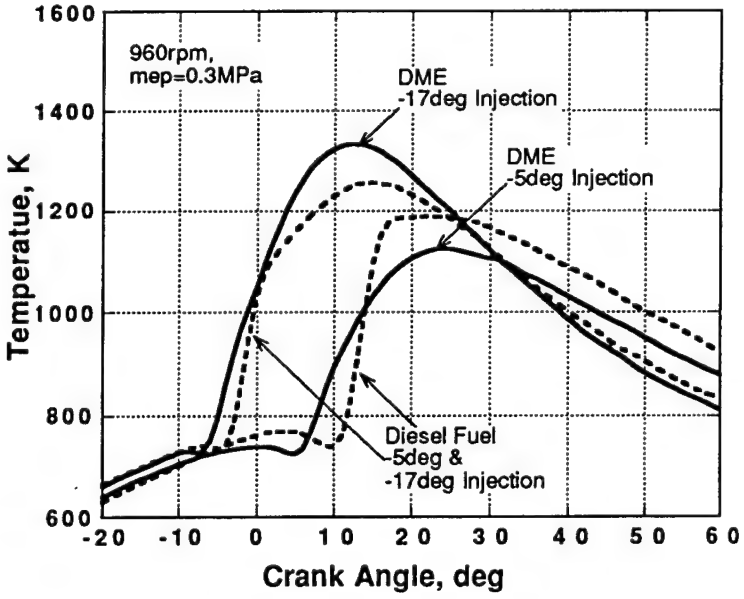

Fig. 14. Average Cylinder Temperature for mep=0.3MPa and 17bTDC & 5bTDC Injection.

Other Engine Measurements and Analysis. The specific energy consumption (SEC) in MJ/kwh (Fig. 11) and exhaust gas temperature (Fig. 12) were also measured in the experiments. Evidently, for both fuels, the late fuel injection, i.e., 5bTDC produced lower energy conversion efficiency than the injection started at 17bTDC. According to the present study, DME delivered a lower SEC than gas oil in a DI Diesel engine. The SFC measurements are the consistent with the exhaust gas temperature (EGT), namely

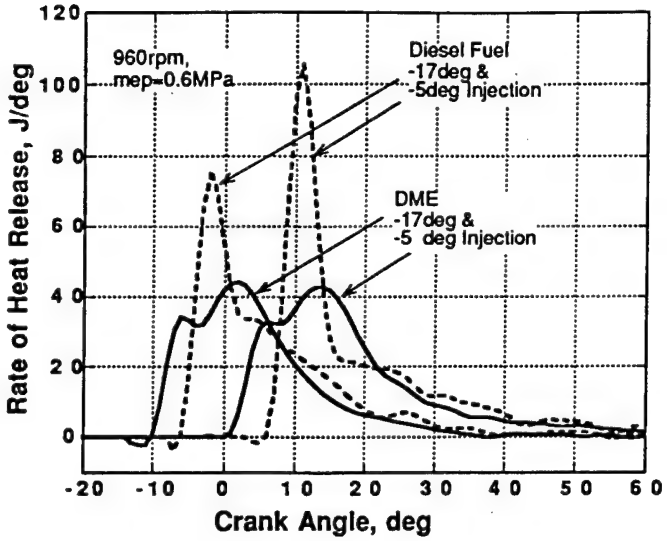

Fig. 15. Rate of Heat Release for mep = 0.6 MPa and 17bTDC and 5bTDC Injection.

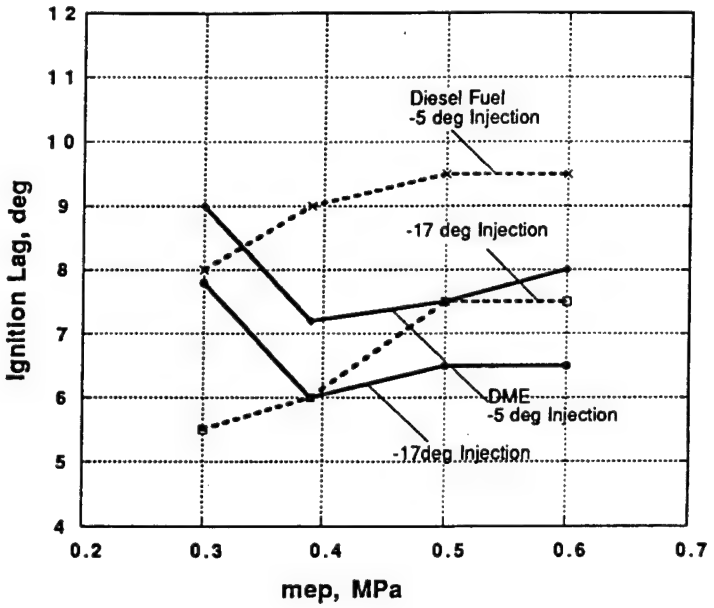

Fig. 17. Ignition Lag.

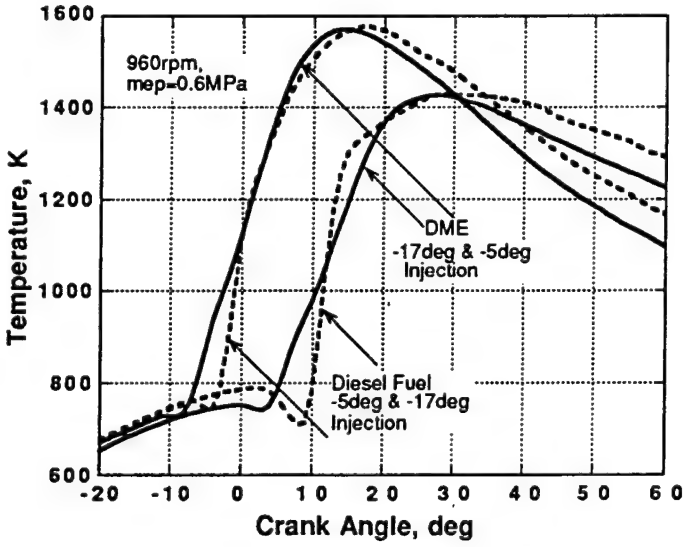

Fig. 16. Average Cylinder Temperature for mep = 0.6 MPa and 17bTDC & 5bTDC Injection.

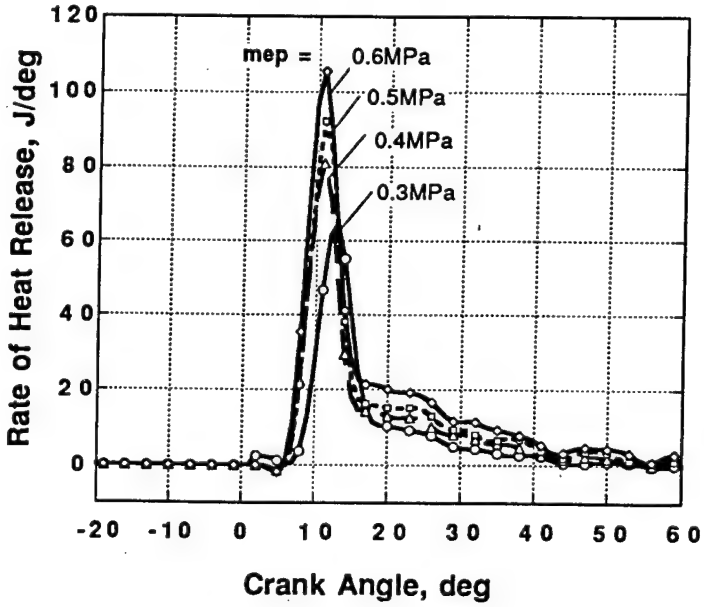

Fig. 18. Rate of Heat Release of Gas Oil Operation for 5bTDC Injection.

lower the SFC the lower the EGT. The difference in EGT for the two fuels was rather significant, as much as over 50°C, for example with mep = 0.6MPa. That is, the engine retrieved a greater portion of fuel energy as mechanical work before combustion products are wasted when operated with DME than with Diesel fuel. Among the reasons for the low SEC with DME seems to be that the combustion period is shorter with this fuel than its counter part, as explained when the heat release rate is discussed (Figs. 13, 15, 18, and 19).

It seems to be appropriate to discuss the heat release rate history (Figs. 13 and 15) at this time. When the load was low (mep = 0.3MPa) the combustion completed within a shorter period with DME than with Diesel fuel. When the load was high (mep = 0.6MPa) this trend was opposite, which will be discussed in terms of the period of fuel injection. By looking at these results, it became possible to explain why the engine with DME ran relatively quiet by observing that its premixed combustion stage was "milder" than that with the gas oil operation.

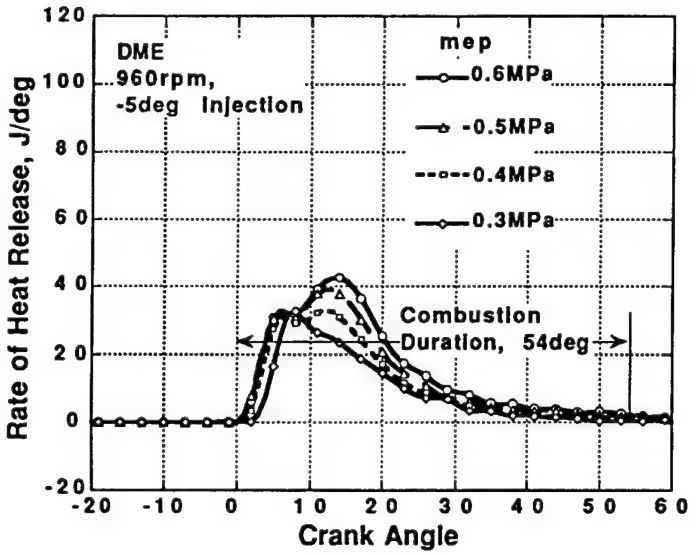

Fig. 19 Rate of Heat Release of DME Operation for 5bTDC Injection.

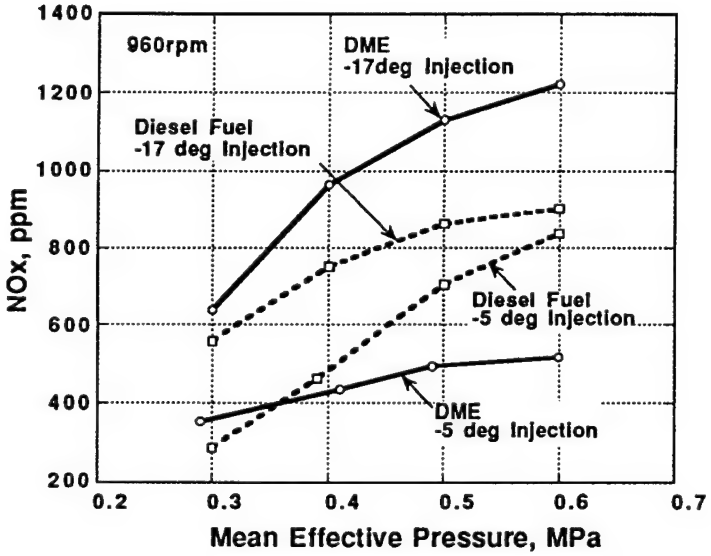

Fig. 20. NOx Emission.

Mentioning the mild premixed combustion with DME and its impacts, it is realized that the low soot emission with DME (as shown later in Fig. 22) is not due to a great amount of fuel consumption in its premixed combustion stage, which is the case in the typical gas oil operated Diesel engine producing a low soot emission. Recall also that in such engines, the shorter the ignition delay (Fig. 17), the milder the intensity of premixed combustion causing a quiet engine operation, which is consistent with the present DME fueled engine operations. However, a common observation of a short ignition delay in a Diesel engine to produce high soot emissions is no longer true in the DME operated engine.

It is worthy to discuss reasons for the mild premixed combustion in a DME fueled engine (Figs. 18 and 19). Since the energy content of DME is only about one half that of gas oil, under a similar injector operation and the same external load condition, DME has about twice as long a period of fuel injection than gas oil. While, as shown in Fig. 18, the injection of gas oil completed within a short period of time, particularly when the engine load is low, it continued even far after the onset of the premixed combustion stage for DME operation (Fig. 19). The continuing combustion for DME at a high load, therefore, is caused by the prolonged injection period. Under such a condition the DME spray plume is penetrated into the cloud of burned gas, which would have been a factor to produce a large amount of soot in typical gas oil operated Diesel engines, but it did not happen with DME. According to the present results, it seemed that the chemical aspect of fuel to produce low soot formation played a dictating role in producing low soot emissions. There are other physical aspects of the spray formation to produce low soot as discussed next. In spite of the longer injection periods with DME, its combustion completed sooner than with Diesel fuel (Figs. 18 and 19), which was considered to help achieve low SEC, as mentioned earlier.

In view of the long injection period and difference in other physical properties, including stoichiometric fuel/air, viscosity, surface tension and volatility, the spray formation of DME is expected to be quite different from that of Diesel fuel even under the same external load. As mentioned earlier, particularly if DME was under a supercritical condition in the nozzle, the fuel leaving the injection nozzle will be in or near a gaseous phase, which will result in formation of a wide (and short) spray plume. Note that Glensvig and Sorenson [12] suggested that a DME spray completes the evaporation within a very short period of time after injection. In addition, the high stoichiometric fuel/air ratio will have a greatly diluting effect in a DME spray. Also, the extended injection period means a greater momentum imparted on the DME spray, making it more dispersed. These all are expected help produce a lean local fuel/air ratio, that is, to have lean combustion compared with a Diesel fuel spray.

Exhaust Emissions. Three main emissions were measured for both fuels operated under mutually comparable conditions, namely NOx, unburned hydrocarbon (THC) and smoke. Considerably high NOx emission was observed when the engine was operated by DME under the engine-manufacturer recommended injection time for gas oil, i.e., injection at 17bTDC injection time (Fig. 20). It is noted that this observation is in contrast with low NOx emission reported by others [7]. One of the most probable reasons for the high emission is considered to be the unusually early start of combustion with DME (Figs. 8 and 15), as much as four CA. Recall that it was explained to occur due to the increased fuel feed pressure. The difference would have been somewhat smaller if the actual injector opening was the same for both fuel. Note that the dispersed fuel spray

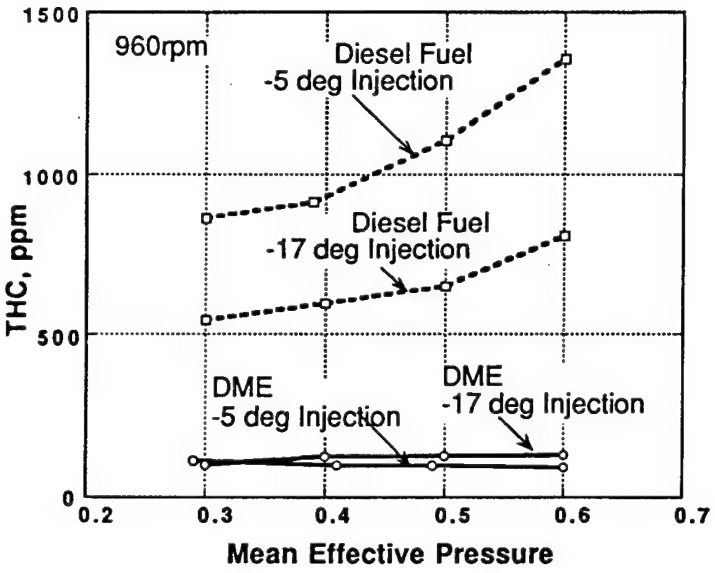

Fig. 21. Unreacted Hydrocarbon Emission.

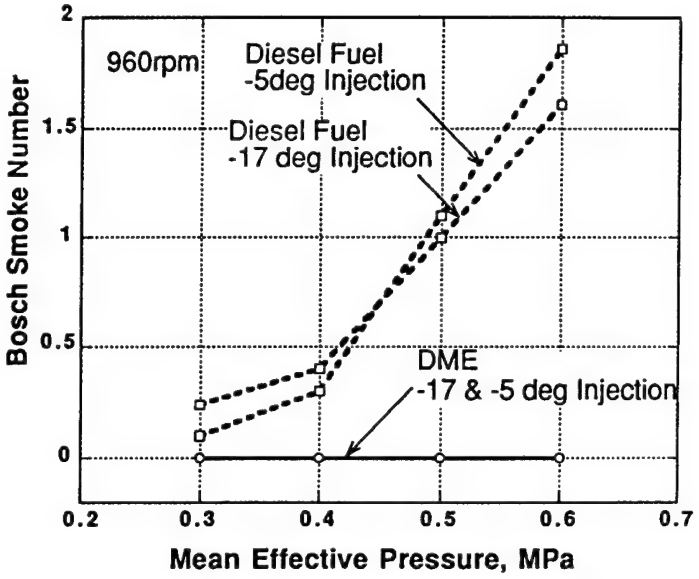

Fig. 22. Exhaust Smoke in Bosch Scale.

formation with DME would help produce low NOx emission.

When the injection time was delayed by changing from 17bTDC to 5bTDC, however, the NOx emission was much lower with DME. This finding is explained by the high rate fuel injection (mass of fuel/deg) with gas oil operation compared with its counter part (Fig. 15) producing high-temperature combustion products with the piston located still near the TDC. This is not expected to occur with DME due to a prolonged injection resulting in a continued combustion with the piston moving away from the TDC.

The emission of THC from the DME-operated engine was very low (Fig. 21), while THC was about the amount expected from a typical gas oil operated Diesel engine, regardless of injection time for a wide range of engine loads. This finding may be explained in terms of several parameters, including the average cylinder temperature (ACT), fuel-air ratio in the spray and chemical characteristics of the fuel. The low ACT (Figs. 14 and 16) and exhaust gas temperature (Fig. 12) with DME certainly do not seem to explain the finding. The dispersed locally lean fuel spray formation expected with DME, as explained earlier, may be a factor consuming the maximum amount of fuel before being wasted in the exhaust. This consideration, however, does not seem to be consistent with an expectation of having high-temperature pockets to explain the high NOx emission with DME. It leads to expect the chemical aspects of the fuel to rapidly consume the unreacted fuel before emission, that is the low self-ignition temperature of DME.

The emission of soot with DME operation was virtually zero (Fig. 22) under the entire experimental conditions investigated in the present study. The reasons for the low emission may be considered by listing various factors, including: the local fuel/air ratio, start of ignition, ACT, and fuel characteristics.

The absence of rich fuel pockets or any exposure of such mixtures to high-temperature combustion products is a precondition for low soot emission from conventional gas oil operated Diesel engines. The formation of a fuel-rich mixture may not be likely in DME spray plumes since the fuel is highly volatile, becoming a gaseous jet or attaining a high specific volume as soon as leaving the injector, which transfers a greater amount of momentum during a longer period of injection compared to the gas-oil injection (Figs. 13 and 15). Consider, however, this mode of fuel injection has a potential to produce large amount of soot: Since DME is self-ignited no later than gas-oil is, and since DME continues to flow into the cylinder even far after the onset of ignition, the direct exposure of fuel leaving the nozzle would be inevitable. This will cause dehydrogenation of the fuel molecules, which is a process known to increase the soot formation. The low soot formation observed with DME in a Diesel engine may then suggest that the DME spray formation may be sufficiently fuel lean as considered above, or even if it is not the case, the fuel itself has characteristics of resisting soot formation. As briefly mentioned earlier, since DME is an oxygenate like a methanol, which is known to produce low soot in Diesel engines, it may not be difficult to expect a low soot emission by the fuel. Therefore, it seems be reasonable to consider that the low soot with DME in Diesel engines is either or both the lean fuel/air spray structure and the fuel's intrinsic tendency of low soot formation in Diesel engines.

It may be added that the commonly known mutual exclusivity between the NOx formation and soot emission in Diesel combustion is no longer applicable in DME operated Diesel engines. Therefore, the control of NOx emission by retarding the injection time appears to be a plausible method without increasing soot emission. Furthermore, since the fuel does not produce soot, and it reveals high thermal efficiency, when new regenerative NOx absorbing devices being developed in the field are incorporated in DME

operated Diesel engines, some ultra-lean emission high-efficiency vehicle may be achieved.

SUMMARY

The use of neat dimethyl ether (DME) in a conventional direct injection (DI) Diesel engine was studied as an alternative fuel that produces a high-efficiency and low emissions. In order to obtain a better understanding of the engine's response to this new fuel, the present study was performed by using some additional engine measurement devices compared to others reported earlier. Particularly, the study was directed to closely monitoring the behaviors of the fuel injector, which was considered to help understand reasons for some conflicting results by others.

Some findings from the study may be listed as follows. DME can not be directly used in the conventional DI Diesel engine, so that either the fuel or the engine will have to be modified. This is mainly due to the fuel's incompatibility with the fuel delivery system resulting in excessive wear in the injector within a short period of the engine operation. A viable remedy proposed for this problem as employed in the study was to add a small amount of lubricant to DME, which did not appear to produce any noticeable negative engine performance and emissions. Note that the study was performed by obtaining measurements using both DME and conventional Diesel fuel under the comparable operating conditions for the purpose of mutual comparison.

The engine operated by DME exhibited remarkably high energy conversion efficiency, which was consistent with low exhaust gas temperatures. In addition to the high vapor pressure of the fuel, due to a low energy of DME causing the injection period to be much longer than its counter part, the spray formation was expected to be over all fuel lean and dispersed, which would affect the exhaust emissions.

The engine with DME produced very high NOx emissions when operated at the injection time recommended for the conventional Diesel fuel. The high NOx with DME (compared with gas oil) is considered to be caused by the remarkably early injector (needle lift) opening, which is attributed to the increased feed pressure, a necessary measure due to the high vapor pressure under the normal operational environment. This high NOx emission was considerably reversed when the injection time was delayed.

The emissions of unburned hydrocarbon and soot were negligible with DME. This was explained in terms of physical aspects of spray formation and chemical characteristics of fuel including the fuel's low self-ignition temperature and tendency of producing low soot. There is no doubt that some in-cylinder visualization of the reaction processes would have helped understand some of unanswered questions.

ACKNOWLEDGMENT

Messrs. Hideyuki Machida, Sumitaka Minegishi and Osamu Sukagawa assisted the experiment. Ethyl Japan Corporation provided Hitec560. The US Army Research Office supported one of the authors (KTR) under Contract No. DAAH04-95-1-0430.

REFERENCES

1. Hansen, J.B., "A Large Scale Manufacturing of Dimethyl Ether- A New Alternative Diesel Fuel from Natural Gas," SAE Paper 950063, 1995.

2. Karpuk, M.E. and Rowley, S.W., "On-board Dimethyl Ether Generation to Assist Methanol Engine Cold Starting, SAE Paper 881678, 1988.

3. Galvin, M.P., "Aspirated Ether Ignition System for Methanol Fueled Diesel Engines", 8th ISAF, p.601,1988.

4. Karpuk, M.E., Wright, J.D., Dippo, J.L, and Jantzen, D.E., "Dimethyl Ether as an Ignition Enhancer for Methanol Fueled Diesel Engines," SAE Paper 912420, 1991.

5. Murayama, T., Chikahisa, T., Guo, J. and Miyano, M., "A Study of a Compression Ignition Methanol Engine with converted Dimethyl Ether as Ignition Improver," SAE Paper 922212, 1992.

6. Cipolat, D. "Methanol/ Dimethyl Ether Fueling of a Compression Ignition Engine," 11th ISAF, p.411, 1991.

7. Sorenson, S.C., Mikkelsen, S.E., "Performance and Emissions of a 0.273 Litter Direct Injection Diesel Engine Fueled with Neat Dimethyl Ether," SAE Paper 950064, 1995.

8. Fleish.T., MacCarthy, C., Basu, A., Udovich, C.C., Charbonneau, P., Slodowske, W., Mikkelsen, S. and McCandless, J., "A New Clean Diesel Technology: Demonstration of UL-EV Emissions on a 1994 Model Diesel Engine Using Dimethyl Ether," SAE Paper 950061,1995.

9. Kapus, M.E., Cartellieri, W.P., "ULEV potential of DI/TCI Diesel Passenger car engine operated on Dimethyl Ether," SAE Paper 952754, 1995.

10. Kapus, P., Ofner, H., "Development of Injection Equipment and Combustion System for DI Diesels Operated on Dimethyl Ether," SAE Paper 950062, 1995.

11. Holidorff, H. and Knapp, H., "Vapor Pressure of N-Butane, Dimethyl Ether, Methyl Chloride, Methanol and Vapor-Liquid Equilibrium of Dimethyl Ether-Methanol," Fluid Phase Equilibria, 40, p. 113, 1988.

12. Glansvig, M. and Sorenson, S.C., High Pressure Injection of Dimethyl Ether, ASME ICE Fall Technical Conference, vol 3, p. 57, 1996.

970872

Quantitative Imaging of In-Cylinder Processes by Multispectral Methods

C. Chang, E. Clasen, K. Song, S. Campbell, and K. T. Rhee
Rutgers University

H. Jiang
Detroit Diesel Corporation

ABSTRACT

With the objective of achieving better investigation of engines-fuels by obtaining instantaneous quantitative imaging of in-cylinder processes, several steps have been taken for some years at Rutgers University. They are: (1) Construction of a new multispectral high-speed infrared (IR) digital imaging system; (2) Development of spectrometric analysis methods; (3) Application of the above to real-world in-cylinder engine environments and simple flames. This paper reports some of results from these studies.

The one-of-a-kind Rutgers IR imaging system was developed in order to simultaneously capture four geometrically (pixel-to-pixel) identical images in respective spectral bands of IR radiation issued from a combustion chamber at successive instants of time and high frame rates.

In order to process the raw data gathered by this Rutgers system, three new spectrometric methods have been developed to date: (1) dual-band mapping method; (2) new band-ratio method; and (3) three-band iteration method. The former two methods were developed to obtain instantaneous distributions of temperature and water vapor concentrations, and the latter method is to simultaneously find those of temperature, water vapor and soot in gaseous mixtures, i.e., to achieve quantitative imaging.

Applications of these techniques were made to both SI and CI engine combustion processes as well as bench-top burner flames. Discussion is made on the methods and new results.

INTRODUCTION

BACKGROUND. Investigating how design-operation and fuel variables affect in-cylinder events, a question may arise: What in-cylinder information would be most desirable when experimentally studying the reaction processes?

A plausible answer to this question, which is perhaps as old as the advent of the internal combustion engines (ICE), is considered here. That is, in order to improve our understanding of the reactions, it would be desirable to obtain instantaneous distributions of temperature and species within the combustion chamber at successive instants of time. Such pieces of information may be referred to as "quantitative images." When they are made available, there is no doubt that a better understanding about the engine can be achieved, including the thermal budget, knock and even emissions. This goal, in fact, has been sought after by many auto-engineers using various methods such as different probes and electro-optical diagnostic methods in the past. While their measurement were made mostly at a limited number of points at a time, (visible-ray) photos obtained of combustion processes at high rates have helped in gaining a global understanding of the in-cylinder phenomena.

Realizing powerful advances in modern sensors and data processing technologies, a new approach of ICE-research was initiated at Rutgers University some years ago in order to achieve the goal of quantitative imaging as extensive as possible. This approach is, in a sense, an attempt of gaining multiple effects expected when both methodologies of point measurements and cinematography are combined together. This paper reports the new research methods and some of recent results obtained from the work.

PREVIOUS STUDIES. Several earlier studies relevant to the present work are discussed at first. They are summarized in Fig. 1 along with new methods to be discussed here. It was 1947 when Uyehara and Myers [1]* first reported a laboratory-built two-color (emission spectrometry) measurement system applied to determination of the instantaneous flame temperature in a Diesel engine

*Numbers in parentheses designate references at end of paper.

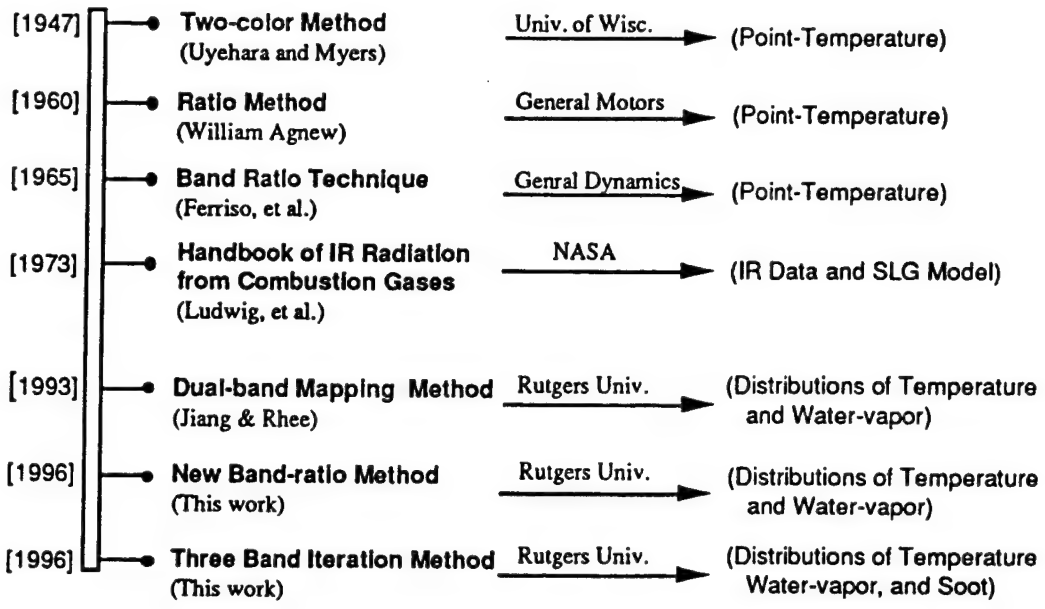

Figure 1. Multiple-band Spectrometric Methods for Temperature and Species Measurement in Flames.

combustion chamber. The basic concept of this new technique was the ratio of spectral radiation intensities of soot was directly related to the flame temperature, which assumed that soot was a gray-body and that radiation from gaseous species was negligible via two bands they employed. Note that a similar methodology was employed by others in later years [2]. They continued to develop new two-color (absorption spectrometry) methods for in-cylinder temperature measurement by employing sodium vapor [3] and water vapor [4] as radiatively participating species.

The concept of the ratio method was also introduced in 1960 by William Agnew [5] to determine temperatures of the end gas in an SI engine (near the peak). In this emission spectrometry method, he indicated that two readings from detectors receiving respective spectral radiations by water vapor in a laboratory flame was related to the mixture temperature. The ratio method was explained by using the Plank's equation,

$$E = C_1 / \lambda^5 \, [\exp (C_2/\lambda T)-1] \qquad (1)$$

where, C_1 and C_2 are constants. The concept of the method, again, was that the ratio of the emissive powers at two wavelengths, E_1/E_2 was a function of temperature only, which in his method was experimentally determined for a working relationship,

$$E_1/E_2 = [D_1/D_2] \, (K_2/K_1) \, [\varepsilon_2/\varepsilon_1] \qquad (2)$$

where, D is the output of the detector and K is the relative sensitivity of the detector system via each wave band of λ. In the above equations, K_2/K_1 and $\varepsilon_2/\varepsilon_1$ were determined by calibration using a bench-top burner apparatus, and D_1/D_2 was the experimental measurement relating to temperature of the mixture. Two wavelengths employed in his method were those for receiving radiation from water vapor, 1.89μm and 2.55μm. Note that his calibration was done to relate the ratio of detector readings to temperature closer to the peak value along the line of sight in the flame.

In 1965, Ferriso, et al. [6] introduced a so-called band-ratio technique (BRT), which was similar to the ratio method by Uyehara and Myers, and Agnew. They, however, employed measurements of radiation via rather wide band filters, namely: (A) 2.63-3.3μm; (B) 2.3-2.63μm; (C) 1.7-2.3μm; and (D) 1.3-1.7μm. They experimentally demonstrated that ratios of detector signal output (i.e., $\theta_{C/B}$, $\theta_{D/C}$, and $\theta_{D/B}$) were related to the exhaust gas temperature from a rocket motor. What is to be mentioned here is that since the band widths were so wide, their measurements involved radiation from more than one species in the combustion products. This may be one of the reasons why the relationships of θ vs. T were relatively crude [6], which is further discussed later.

Thanks to NASA Handbook (SP-3080) of infrared (IR) radiation (of gaseous mixtures) provided by Ludwig, et al. [7] in 1973, which contains the spectral absorption coefficients of individual gaseous species at varied temperatures and pressures, more meaningful work became possible. Agnew in 1960 probably did not have access to such data when he conceived his ratio method so that he resorted to experimental means in order to obtain the working calibration curve for his system.

After developing a new high-speed two-color IR imaging system at Rutgers [8, 9], which was to simultaneously capture two geometrically identical images in respective spectral bands, results from the NASA IR data and single-line-group (SLG) model [7] were employed in order to develop a new dual-band mapping method (DBMM). In an earlier paper [10], without giving a detailed

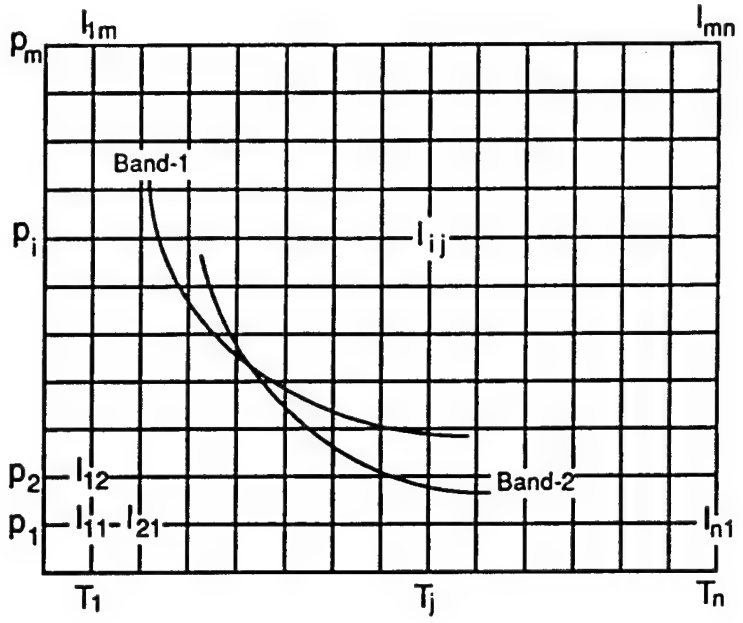

Figure 2. Algorithm for Dual-band Mapping Method (DBMM).

elaboration of the method, distributions of temperature and water vapor concentration obtained by this method were reported. In the following, the DBMM is discussed in comparison with other methods developed during the course of the present work.

RUTGERS SPECTROMETRIC METHODS AND RESULTS

DUAL-BAND MAPPING METHOD (DBMM). When a volume of uniform gaseous mixture in a known concentration of source (target) species having a given physical thickness is at a specified temperature and pressure, it is possible to calculate the spectral radiation intensities of the mixture. The core of the DBMM is to find temperature and species concentration in such a mixture when two spectral intensities are given, a reverse process of the former.

In order to achieve this goal, a new algorithm was developed as discussed by using a spectral intensity matrix (I_{ij}) of the mixture (Fig. 2), which covers, for a given wave band (Band-1), in a range of varied partial pressure of water vapor (p_i) and temperature (T_j). Then, an iso-intensity line is traced over this matrix according to the spectral intensity measured from the experiment. Then the same is made for the intensity matrix for another band (Band-2), and overlap these two matrixes with each other in order to find the crossing point of both iso-intensity lines. This is like finding two unknowns from two simultaneous equations.

In spite of the straight-forward concept of this method, error in the final result is likely to be high due to the two somewhat mutually paralleling lines as seen from Fig. 2. Even a small uncertainty in measurement would lead to a rather large error in the results. Furthermore, since the physical length of individual optical paths through a real-world flame is difficult to determine, the error could increase more. It is noted again, in spite of such limitations stemming from probable imperfect measurements, the results obtained by this method are unique. A sample result is shown when a new band-ratio method is explained later.

RUTGERS FOUR-COLOR IMAGING SYSTEM. Prior to discussing other spectrometric methods, the Rutgers high-speed four-band IR digital imaging system (referred to as the Rutgers System or Super Imaging System, SIS) is explained. While the abovementioned two-color system continued to be used for flame and engine studies [8-11], and also for implementation of the DBMM [10], an entirely new system was developed as schematically shown in Fig. 3. Since this SIS was described earlier [12-14], it is only briefly explained here.

Referring to Fig. 3, the radiation from an object is collected by the cassegrain assembly (152mm diameter), which is spectrally split to place four spectral images over respective high-speed digital imaging units. The SIS, therefore, can be used to simultaneously obtain four separate sets of 64x64 digital image in corresponding spectral bands. Ideally, images of four different pieces of information can be obtained at successive crank angles (CA).

While the spectrometric techniques were being developed for achieving quantitative imaging by processing the digital data captured using the SIS, the main topic of the present paper, the raw results alone have been useful in finding some new observations. They include: preflame reactions [11-14]; liquid-fuel layers over the cylinder head surface; and postflame oxidation [12,13], which were not reported earlier by others.

NEW BAND RATIO METHOD. The computer program developed for the abovementioned DBMM, which contained spectral absorption coefficient data under varied temperatures and total pressures, and incorporated with the SLG model, was further improved. The SLG model from

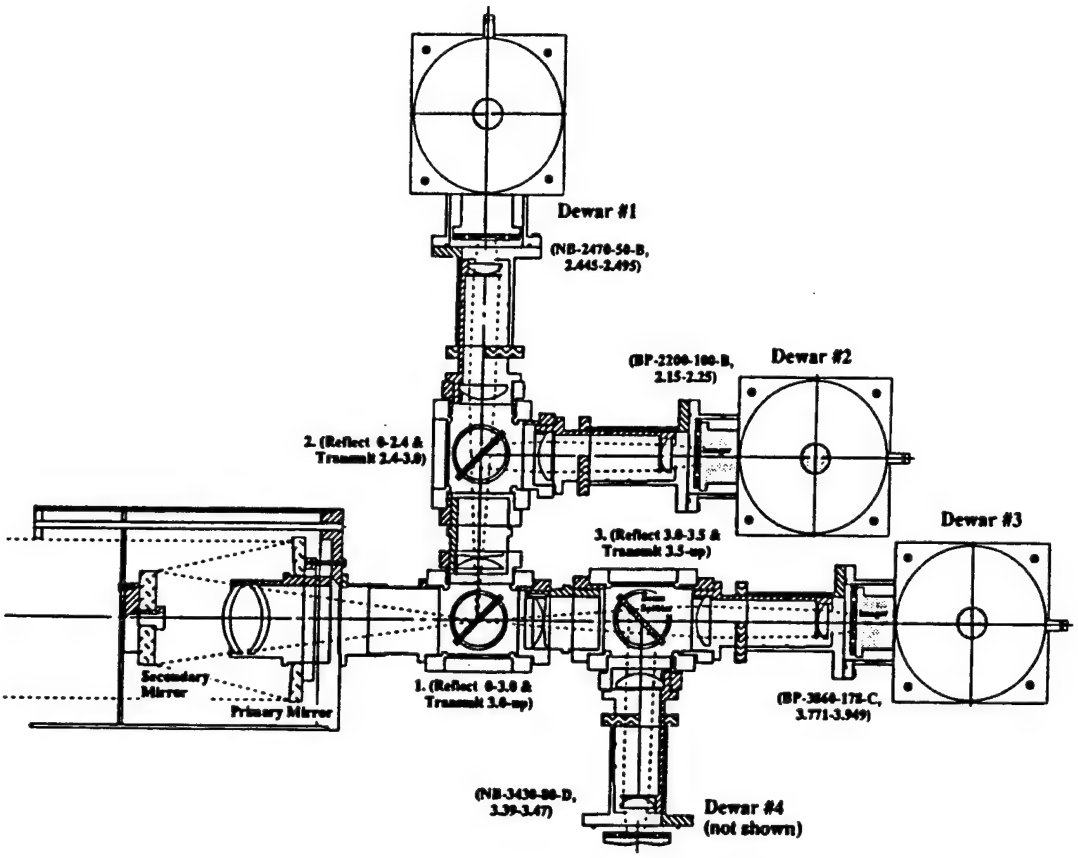

Figure 3. Schematic Presentation of Optical Portion of Rutgers SIS.

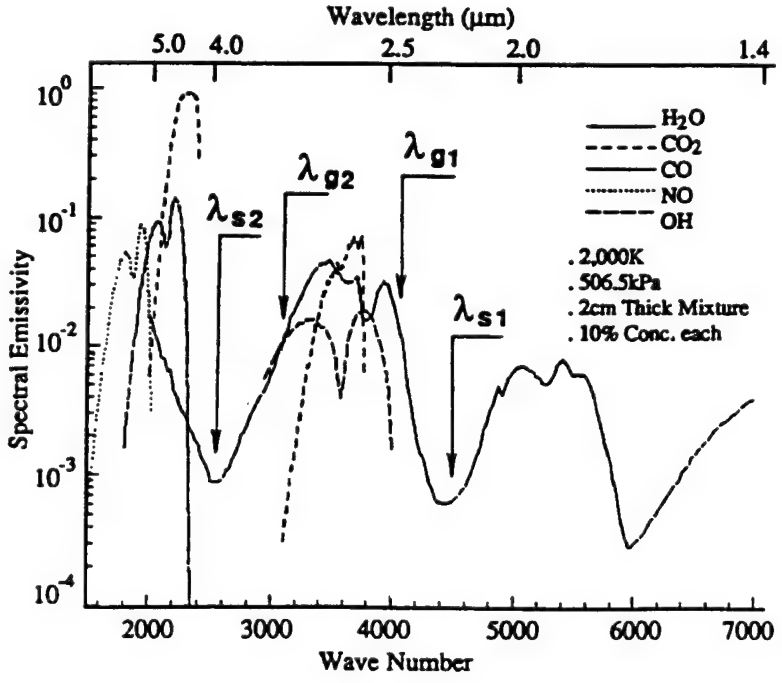

Figure 4. Spectrogram Constructed by using Rutgers DBCP for a Gaseous Mixture.

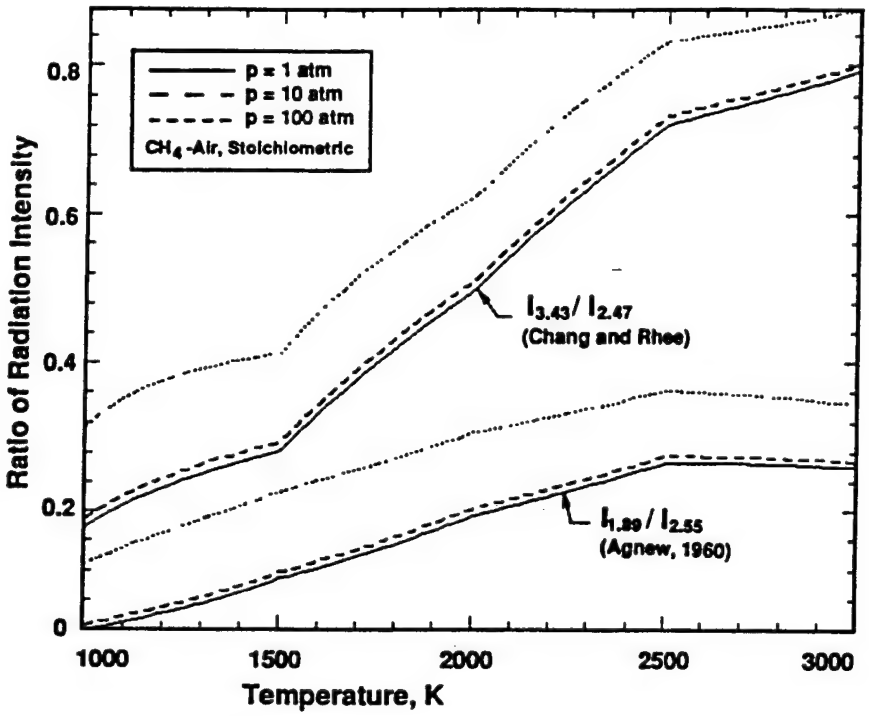

Figure 5. New Band Ratio Method (NBRM) to Determine Temperature in Gaseous Mixtures.

NASA's IR handbook [7] was to facilitate utilization of those absorption coefficients given for each wavenumber, such as for calculation of the spectral radiation intensity and emissivity of a specified gaseous mixture. For example, Fig. 4 was prepared by using this data-based computer program (DBCP). This was done for a sample gaseous mixture (thickness 2cm) composed of H_2O, CO_2, CO, NO, and OH with concentration C=0.1 in mole fraction each under pressure, P=10atm. The figure suggests that bands at 2.47μm and 3.43μm have strong radiation by water vapor, which are employed in the following spectrometric method. Development of this DBCP paved the way to the analysis of spectral characteristics of radiating species in the present IR domain to come up with the new band-ratio method (NBRM), as shown in Fig. 5.

The figure is self-explanatory and it indeed supports Agnew's earlier experimental work and Ferriso's BRT measurement method. It is noted that this result was constructed by the abovementioned DBCP to relate the ratio of spectral intensities from mixture containing a target species to temperature of the mixture under a specified total pressure. No experimental factor is involved in the result.

There are several new features in the NBRM: (1) It includes the pressure effects on the relationship, which neither Agnew nor Ferriso, et al. considered in their methods; (2) The method employs a single radiatively participating species; (3) Its band widths are narrow to improve the accuracy; (4) The analysis permits identification of a pair of desirable bands for achieving more accurate temperature determination; and (5) The relationship is universally applicable unlike the detection system-dependent curves generated via experiment [5,6].

Regarding the pressure effect on the NBRM, Fig. 5 indicates how significant it may be when reactions under varying pressure are considered such as in an engine cylinder. The NBRM was applied to two wave bands employed by Agnew [5] as shown by the solid-line, which is compared with dotted curves for high pressures in the same figure. This illustrates the NBRM's need for incorporating the effect of reaction pressure in order to obtain accurate temperature results. In selecting bands (i.e., filters in experiment) for the NBRM, it is desirable for them to pass radiation from only a single source species. For example, when this method is applied to a hydrogen-air flame, not only the selection of bands will be simple but also the measurement accuracy will be high because there is only water vapor emitting IR radiation in the product. When bands which permit some strong radiation by additional species (e.g. carbon dioxide an/or soot) to pass together with radiation from the target species (here, water vapor) were employed by the NBRM, the relationship in Fig. 5 was not unique indicating errors to be made in measurements. Recall that, since wide bands tend to include radiations from more species, those employed for the Ferriso's BRT were considered to be inappropriate.

In typical hydrocarbon-air flames, many species including intermediate species are formed and also consumed, which radiate more or less in the IR band domain. They can not be considered all in a simple spectrodiagram shown in Fig. 4. Even a narrow band rarely passes radiation by only a single species without interference by others. If such interference is not negligible, the accuracy will suffer. Note that the accuracy will be enhanced, however, when additional bands (for corresponding species, otherwise

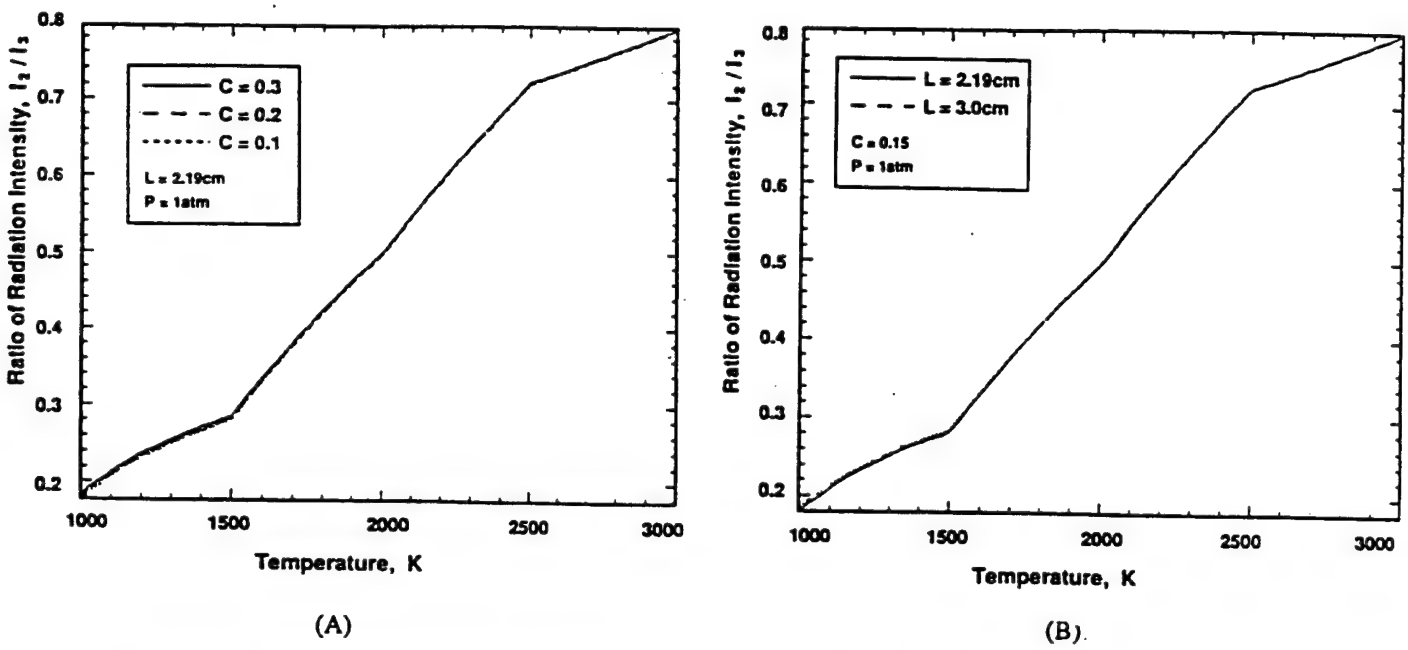

Figure 6. Characteristics of New Band Ratio Method Indicating Minimum Dependency of: (A) Species Concentration and (B) Path Length.

causing interference) are employed, which is demonstrated by the new method as discussed later.

When two solid lines in Fig. 5 are compared with each other, the measurement accuracy is expected to be higher for a steeper curve, which suggests the selection of a proper pair of bands to be important in the NBRM. The last statement is reiterated because unlike the voltage measurements out of the sensors employed by others in the past, the present method is to find temperature from intensities of the mixture, which is independent of the system response, e.g. values of K in Eq. (2).

Additional analyses revealed that the relationship (Fig. 5) was found to be quite independent of the species concentration and physical length of the optical depth, as shown in Fig. 6. These characteristics are very important in applying the NBRM in the typical combustion environment where concentration and flame thickness vary greatly along the line of sight. These results illustrate that $\varepsilon_2/\varepsilon_1$ in EQ (2) is not affected by the variation of concentration and optical length, L. It becomes reasonable if the optical thickness is relatively small as seen from the Beer's law, $\varepsilon = 1 - \exp(-\kappa L)$. That is, when κL is very small, $\varepsilon \sim \kappa L$. Note that κL is indeed small in many combustion environments, which is optically thin, except for soot-laden flames whose solution is considered by another method later.

CALIBRATION. At this time, the method of the system calibration for determining spectral intensities from the difital images is explained. The purpose of this calibration is to accurately measure, for individual pixels, the radiation intensity of a (target) mixture (either in a bench-top flame or engine cylinder). Note that the ratio relationship to temperature (Fig. 5) needs no calibration. For this, the imaging system is placed at exactly the same geometric orientation with respect to the target as in the actual (engine) experiment. Then, the digital output from pixels are compared with those obtained when the target is replaced by a blackbody at a known temperature. The conversion matrixes of the system-response permit the construction of spectral intensity distribution at the target using the raw data, i.e.,

$$I_{ij} = a_{ij}\, v_{ij} + b_{ij}\,, \qquad (3)$$

where, v is digital output in voltage. Note that the system response in Eq. (3) includes the combined effects of: (1) optical window in the engine; (2) optical elements in Fig. 3; (3) individual pixels; (4) the location of pixel with respect to the axis of the path; and (5) electronic components. Since the need for such characterization is well known, no further elaboration is made here.

In addition, effects of deposit formation over the optical window on the measurement is discussed. While in visible range imaging, even a small amount of window deposit degrades the image quality, which occurs within a short period of engine operation, imaging in the present IR domain is found to be lightly affected by the deposit. For example, the quality of in-cylinder image obtained of a gasoline-operated SI engine, after more than 20 minutes of continuous operation (without cleaning the IR window) from the (cold) start, still appeared to be reasonably good [13]. Similar insensitivity was also found in imaging of a reacting spray plume of a direct injection CI engine [11,14]. Such a high transmission of IR radiation through the deposit-layered window, however, does not necessarily guarantee accurate quantitative imaging. On the other hand, the ratio method of

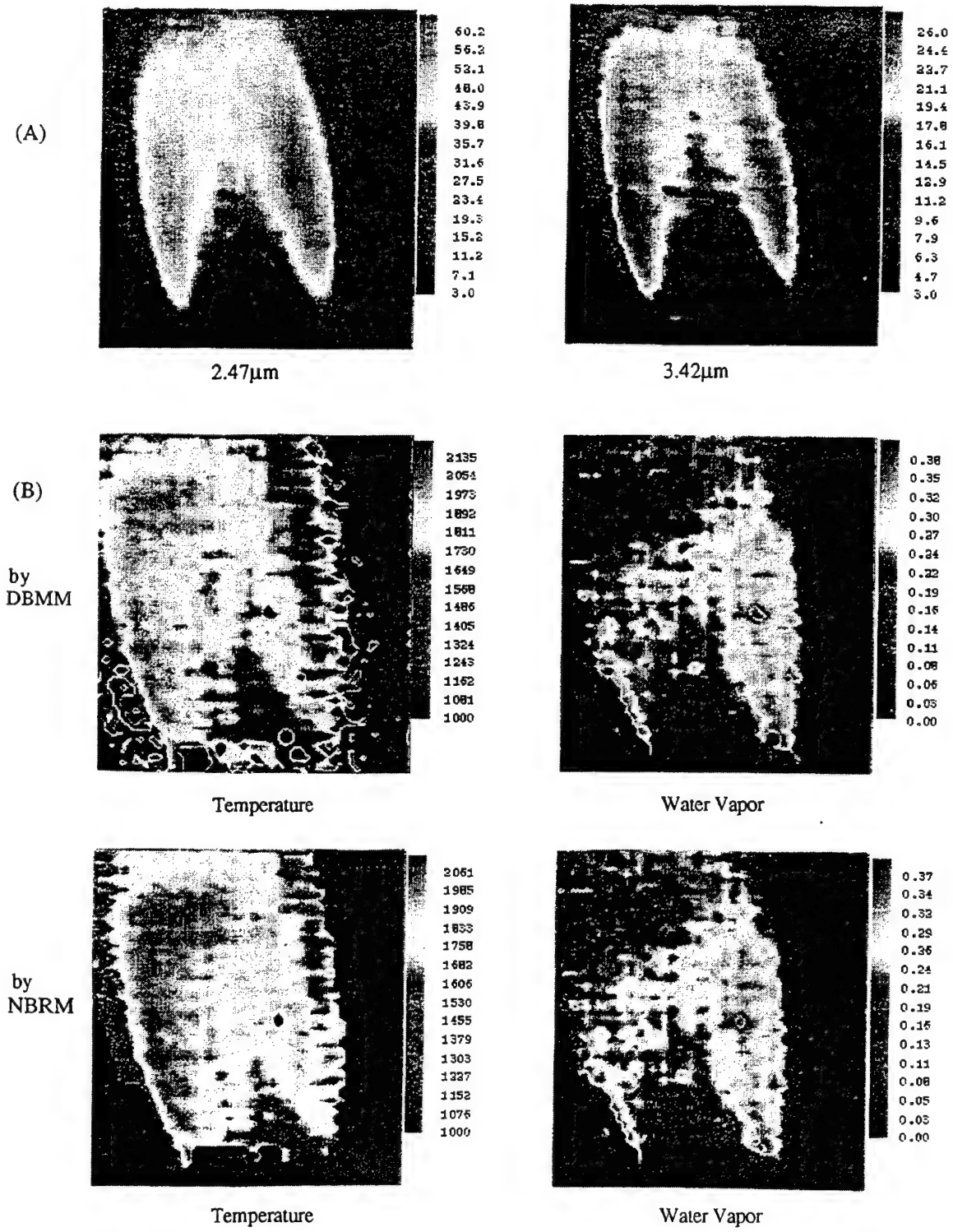

Fig. 7. (A) Spectrometric Intensity Images of a Hydrogen-air Flame in 2.47μm and 3.42μm, and (B) Distributions of Temperature (K) and Water Vapor (atm-cm) by DBMM and NBRM.

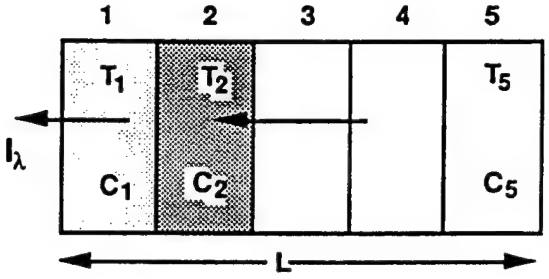

Figure 8. A Case Analyses of a Flame with Designated Temperature and Water Vapor Concentration.

processing spectral IR data has advantages over others such as single-band imaging, because effects due to either absorption or emission (by the deposit) on both band measurements would tend to cancel each other minimizing the error.

SAMPLE RESULTS BY NEW SPECTROMETRIC METHODS. A set of results obtained by using the DBMM and NBRM is shown in Fig. 7. The spectral IR radiation images of a hydrogen-air diffusion flame in bands of 2.47 μm and 3.43μm were obtained (Fig. 7-(A)) from a setup, which is a duplicate of a laminar-flow burner employed by Lewis and von Elbe [10,15]. The raw data was processed to construct intensity images by using system response matrix (Eq. 3) in order to achieve quantitative imaging by the methods. Shown in Fig. 7-(B) are the temperature distribution (TD) in K, and water vapor distribution (WVD) in atm-cm determined by using the DBMM and the NBRM, respectively. Once the TD is determined, since the emissivity is calculated using the Plank's equation, the WVD is found using the Rutgers DBCP mentioned earlier. The presentation is made in pseudo-color in order to display more local variations.

It is pointed out that the distributions are two-dimensional as seen by the imaging system, and that each point measurement, within the matrix, represents that of the corresponding line of sight in the direction perpendicular to the image plane. The two methods produce mutually comparable results except for the border zones where the DBMM overestimates the temperature. This is found to occur due to an assumption of the identical flame thickness throughout the flame in DBMM, which is not realistic because it is small around the border.

In spite of differences between flames by the present DBMM / NBRM experiment and Lewis and von Elbe [15], (For example, one was an instantaneous measurement and the other was an time-averaged local measurement using the sodium-line reversal method, and also fuel) the results are mutually comparable each other. The absence of a similar result in literature, however, did not facilitate any further evaluation of the WVD.

WHAT TEMPERATURE? When the target mixture is uniformly mixed, the temperature determined by using the present ratio method would be the same at any point over the mixture. The temperature along the line of sight, however,

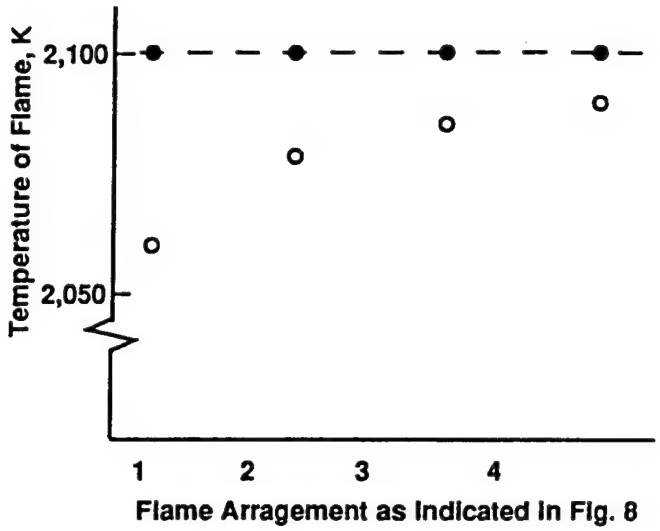

Figure 9. Temperature Determination by NBRM for various Flame Configurations.

varies in most combustion products so that the nature of measurements obtained by the method needs a discussion. A question comes to mind as to whether it is either close to the average temperature, or the highest temperature of the mixture somewhere along the line of sight, or other values. The same issue was also addressed in earlier studies [3,4].

In order to resolve the above question, the temperature determined by the NBRM was evaluated by using a simplified flame configurations as described in Fig. 8. The flame is assumed to consist five equal-thickness segments within the total thickness L having respective uniform temperatures (T_i) and water-vapor concentrations (C_i). Spectral radiation intensity at one side of the flame, I_λ will be a result of emission-transmission of individual segments as determined by

$$I_\lambda = I_{\lambda_1} + \tau_{\lambda_1} I_{\lambda_2} + \tau_{\lambda_1}\tau_{\lambda_2} I_{\lambda_3} + \cdots$$
$$= \sum_{i}^{n} \left(\prod_{m}^{i-1} \tau_{\lambda_m} I_{\lambda_i} \right) \qquad (4)$$

Note that, in the radiative participation by these mixtures, the absorption of radiation by a segment, as issued from others, is included to affect its thermal budget, as specified at each segment. In this analysis, for the sake of simplicity the temperature considered in each segment is assumed to be the result of various processes including such absorption.

In this evaluation, two spectral intensities (via wave bands of 2.47μm and 3.43μm) are determined by using Eq. (4) and the Rutgers DBCP. The ratio of these two, then, are used for finding temperature by the NBRM for several cases as considered next. Note that the flame thickness L = 2cm and the total pressure p = 1atm.

Results are shown in Fig. 9 for the following flame configurations: "1" in flame arrangement indicates a mixture of combustion product when segment-2 is occupied by a mixture at 2,100K with water vapor concentration C =0.12 and other segments are with radiatively transparent species;

"2" means when segments-2 and-3 are are filled with the same mixture; and so forth. For these cases, the NBRM determines exactly the same temperature, as indicated by the filled-in dots, which proves that the method is valid at least for such a uniform mixture.

On the other hand, since the flame is not uniform in general, other cases were considered, including those as same as the above but having segment-1 filled with a mixture at 1,100K and C=0.06. Results for these cases are indicated by open-dots in the figure. Important characteristics of temperature by the NBRM deduced from this analysis may be listed: (1) The temperature determined by the method is quite close to the peak temperature; (2) When the water vapor concentration is high in the segment with the peak temperature, the determination is closer to the peak value; and (3) The effect of low-temperature mixtures in a flame (e.g. segment-1) on the measured temperature may be significant in some cases.

THREE-BAND ITERATION METHOD (TBIM). The NBRM can be applied to relatively "clean" flames with minimum soot formation. There are many flames, however, containing significant amounts of soot emitting strong radiation, which defeats the application of the NBRM. A new three-band iteration method (TBIM) was developed for such cases. This method permits simultaneous determination of distributions of temperature, water-vapor and soot in combustion products as explained next.

Figure 10 is introduced in order to discuss the basic concept of the TBIM, which is similar to Fig. 5 and assumes to have only water vapor and carbon dioxide in the mixture. The lowest curve in the figure indicates the spectral intensity of combustion products from a hydrocarbon (H/C=2)-air mixture to produce a water vapor concentration, C=0.10 (for 2,000K and 1 atm), which was constructed by using the DBCP. Other upper curves represent the radiation from the same mixture containing soot as specified by given volume fractions, f_v . In this method, in addition to two unknowns as considered earlier by the NBRM, one more affecting the emissivity of a mixture is determined, which is to find the absorption coefficient of the soot using the Rayleigh-limit expression [16,17],

$$\kappa_{s\lambda} = \frac{36n^2k\,(\pi/\lambda)\,f_v}{[n^2(1-k^2)+2]^2+4n^4k^2} \qquad (5)$$

where, n, nk are complex refraction indices of soot determined by the dispersion equation [18].

The governing equations for the problems, therefore, are established Beer's Law for three spectral bands, namely 3.8μm, 2.47μm, and 3.42μm as:

$$\varepsilon_{380T} = 1-\exp(-\chi_{380S}-\chi_{380H})$$
$$\varepsilon_{247T} = 1-\exp(-\chi_{247S}-\chi_{247H}) \qquad (6)$$
$$\varepsilon_{342T} = 1-\exp(-\chi_{342S}-\chi_{342H})$$

where,

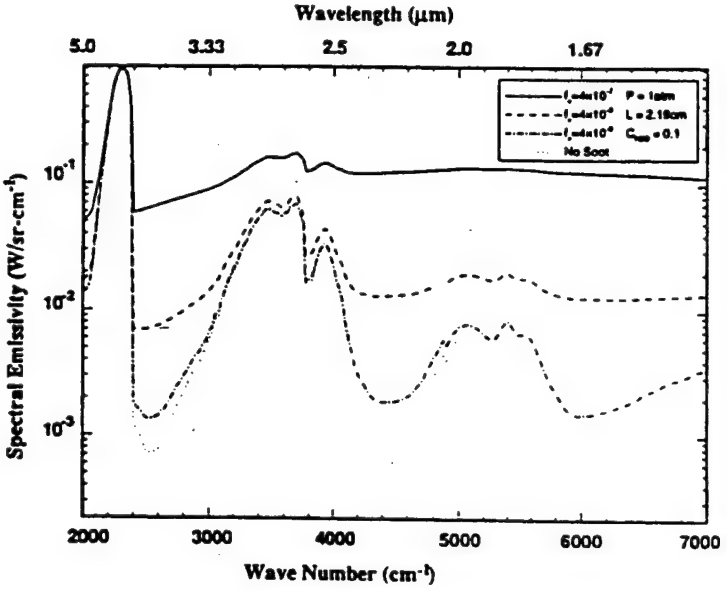

Figure 10. Spectrodiagram of Combustion Products of a Hydrocarbon-air Flame with Soot.

$$\chi_{380S} = \kappa_\lambda L/3.80^{\alpha}$$
$$\chi_{247S} = \kappa_\lambda L/2.47^{\alpha}$$
$$\chi_{342S} = \kappa_\lambda L/3.42^{\alpha}$$

and α=0.95-1.0 [19]. Note that the final results are found to be insensitive to the value of semiempirical constant, α. Here, χ for water vapor (at different temperatures and pressures) is determined from the DBCP. In the equation, the roles by soot and water vapor are denoted by subcharacters, S and H, respectively.

Mentioning the iteration method for finding the solution, Fig. 11 is offered here. Although the radiation from water vapor is small in 3.8μm band in low pressure reactions, the effect is, nevertheless, included in the present TBIM in order to minimize the error particularly in high pressures. In the calculation, at first, measurements via 3.42μm and 2.47μm are assumed to be free of soot radiation to use the NBRM for determining the initial value of flame temperature. Next, the extinction coefficient, χ by water vapor is calculated, which is reflected on determination of κL on 3.8μm band. The κL effect is then subtracted from χ for the two bands used for the initial estimation of temperature. The new temperature calculation by the NBRM for the two band, then, becomes more accurate than the initial estimate. The next steps are for improving the accuracy by going back to calculation of the extinction coefficient of water vapor for 3.8μm band. The iteration process is continued until a converging temperature value is found.

RESULTS OBTAINED BY TBIM. This new method was applied to the measurement of a bench-top burner and in-cylinder mixtures of a (cold) gasoline SI engine and a Diesel oil (D-2) operated direct injection (DI) CI engine.

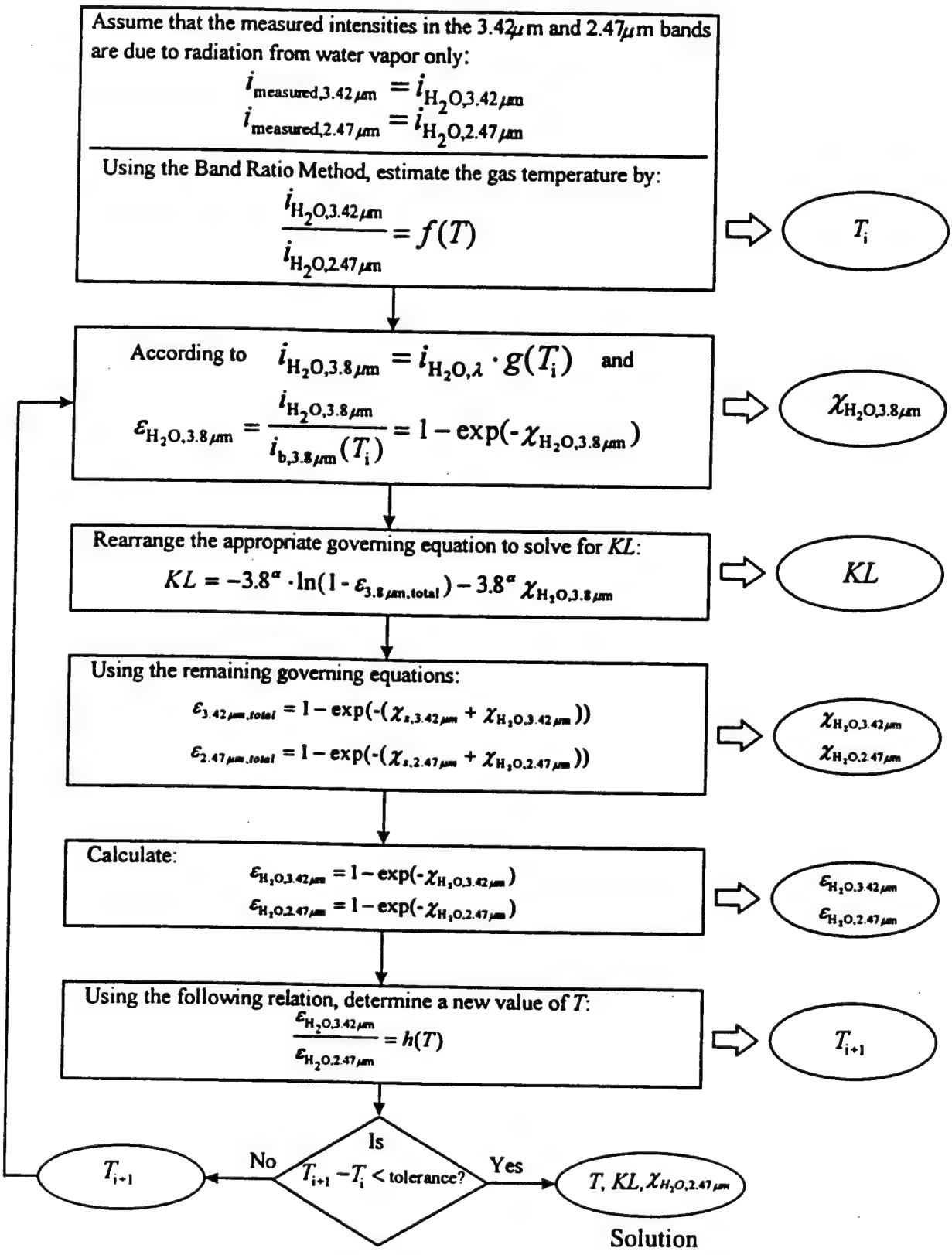

Figure 11. Flow-chart for the TBIM applied to Soot-laden Hydrocarbon-air flame.

Prior to presenting some results from the CI study, a short description of the experimental apparatus is made here. More details may be found elsewhere [11,14]. A single-cylinder DI-CI engine was mated with a section of Cummins 903 four-valve cylinder head where a high-pressure electronically-controlled injection system was installed. For imaging, one of the intake valves was replaced by an optical access (37mm diameter), which is barely big enough to observe one of eight sprays made through nozzle holes with 0.15mm diameter. The high-pressure injection system used in this experiment is basically a BKM's Servo-jet type [20]. In order to achieve versatility of the system, however, almost the entire unit was newly fabricated at Rutgers [11,14] to operate at pressures over 165MPa. The imaging, therefore, was made through the cylinder head to look down the spray from the top. In addition to gathering of raw spectral digital images by the SIS, other engine data were also collected, including the matching pressure-time data as required by the NBRM, which is a part of the TBIM.

The raw data matrixes were converted to corresponding spectral intensity distributions by using the calibration method as explained earlier. Figure 12-(A) shows these intensity images of a spray plume at successive CA with injection starting at 9CA before the top-dead-center (bTDC) as indicated by a look-up-table (LUT) shown in Fig. 13. The spray is directed diagonally as indicated by the arrow mark shown in box for 5.5CA bTDC. They are in bands of 2.47μm, 3.42μm and 3.80μm, which were to capture radiation from water vapor and soot assuming interference from other species is negligible (refer to spectrodiagrams shown in Figs. 4 and 5).

Discussing the spectral intensity images, the first image of spray was captured *immediately* after the fuel injection via 3.42μm band, which was reported earlier [11,14]. This new observation was explained by chemiluminescent radiation issued by some unknown species, which may include OH, CH, C_2, aldehydes, and others expected in preflame reactions during the ignition delay period. The new finding seems to be reasonable because the fuel-air mixture undergoes many elementary reactions prior to exhibiting explosive (visible) premixed flame reactions, and because the early mixture formation occurs at injection. The first images obtained via other bands, i.e., at 2.2μm, 2.47μm and 3.80μm were all found at the same CA, which was captured in this case at 5.5CA bTDC. (This is far after finding the first preflame image in 3.42μm band around 9CA bTDC.) They represent the onset of the premixed combustion stage. In a great amount of results, where the first preflame zones were observed in the spray, there also the first premixed reaction center appeared. In some cases, however, the two zones do not necessarily match each other, which warrants further investigation.

In general, the spectral intensity distributions are somewhat different from each other particularly in the early stage of combustion, which is until around 1.5 after TDC. Thereafter the images in 2.47μm and 3.42μm are similar each other, which differs from that in 3.8μm. The similarity of images representing radiation by water vapor in the later stage of combustion is explained by the negligible amount of radiation by other species expected then, which is opposite in the early stage of combustion indicating many different species presenting to issue individual radiations.

Fig. 13. Look-up-Table for Fig 12.

The TBIM was employed to obtain distributions of temperature (K), water vapor (atm-cm) and soot (κL) by processing the abovementioned spectral intensity data, as shown in Fig. 12-(B). In order to construct the quantitative images, digital results were plotted according to corresponding color strips, for which several observations may be listed: (1) The numbers quantifying the characteristics of Diesel spray-plume combustion by high-pressure injection seem to be reasonable; (2) The local variation is continuous without abrupt changes except for those in the early stage of combustion; (3) The progress of reactions with time are smooth and gradual; and (4) No solution was obtainable for those in the early stage of combustion.

In addition to the absence of complexity in calibration, well-established governing equations and spectral absorption data from the handbook, as employed in the TBIM, the above observations seem to help trust the validity of the results. The quantitative images (e.g. distributions of temperature, κL and water vapor) are within values reported by others, except for low κL in the present measurement compared with those by mechanical injectors, which may be explained by the low-soot formation characteristics by the high-pressure injection system. The absence of abrupt local variation over the same quantitative image is expected in the continuum flow in the later stage of combustion. Similarly, the smooth changes in the distributions with time are expected in a progressively reacting spray. The inability of finding solutions in the early stage of combustion by the TBIM is also reasonable and compatible with the other observations. This is because the many intermediate species produced in the stage (recall the preflame images via 3.42μm band, for example) are expected to emit radiations added to those by water vapor and soot. Misrepresentation of spectral intensity measurements due to such interferences drove the iteration process of solution out of convergence, as indicated by the black zones in the results. (It is reminded that measurements of combined radiation from multiple species will cause erroneous results unless they are all included via additional governing equations, and corresponding spectral image data). These observations are not sufficient conditions for confirming the full validity of results, but certainly required conditions.

Reviewing the direction of spray (Fig. 13), the results in Fig. 12 indicate the region along the axis of spray is at low temperature, which was similarly found in combustion of spray by a mechanical injector [21]. The low-temperature

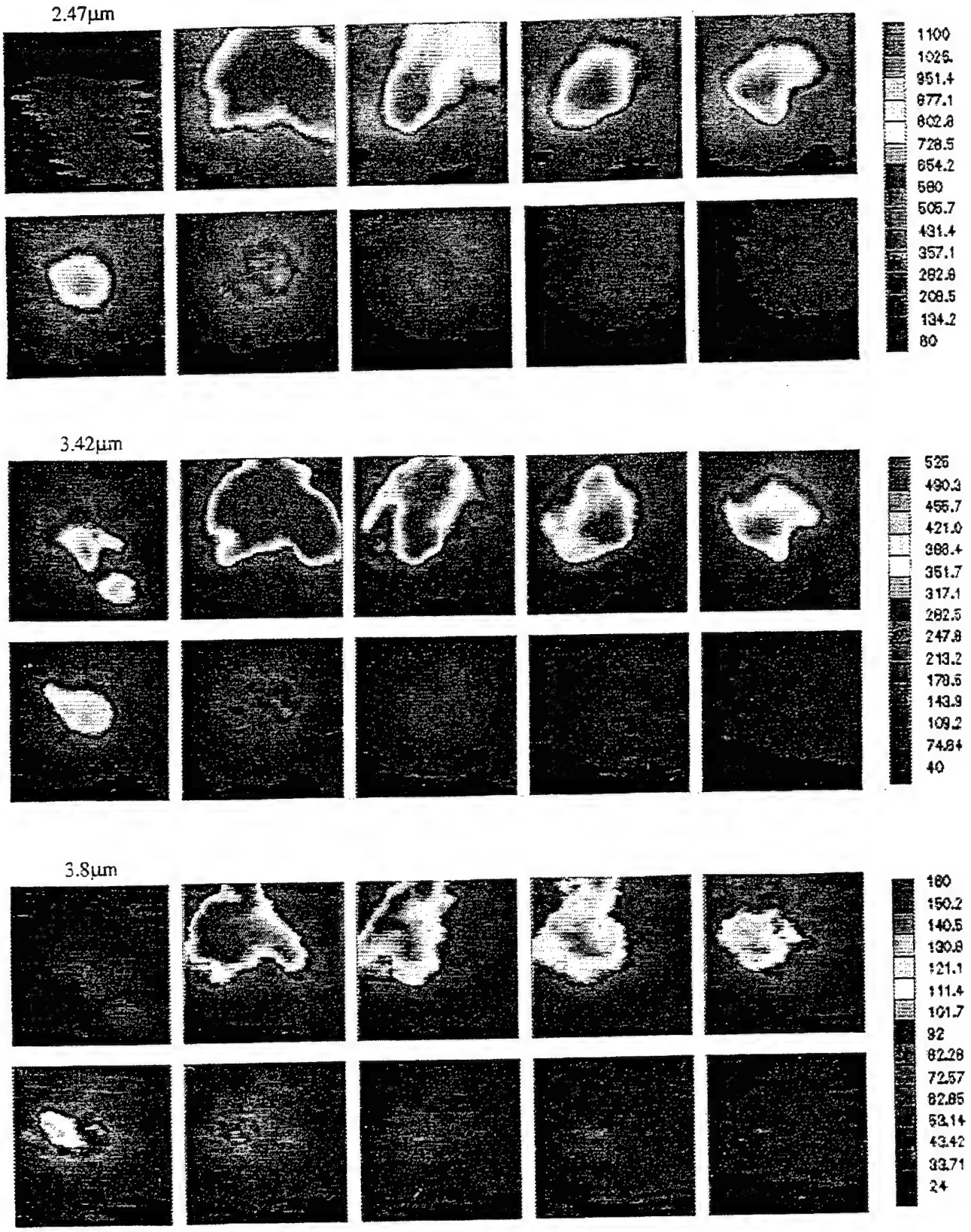

Figure 12. (A) Spectrometric Intensity Image of a Spray-plume in a DI-CI Engine at Successive Crank Angles.

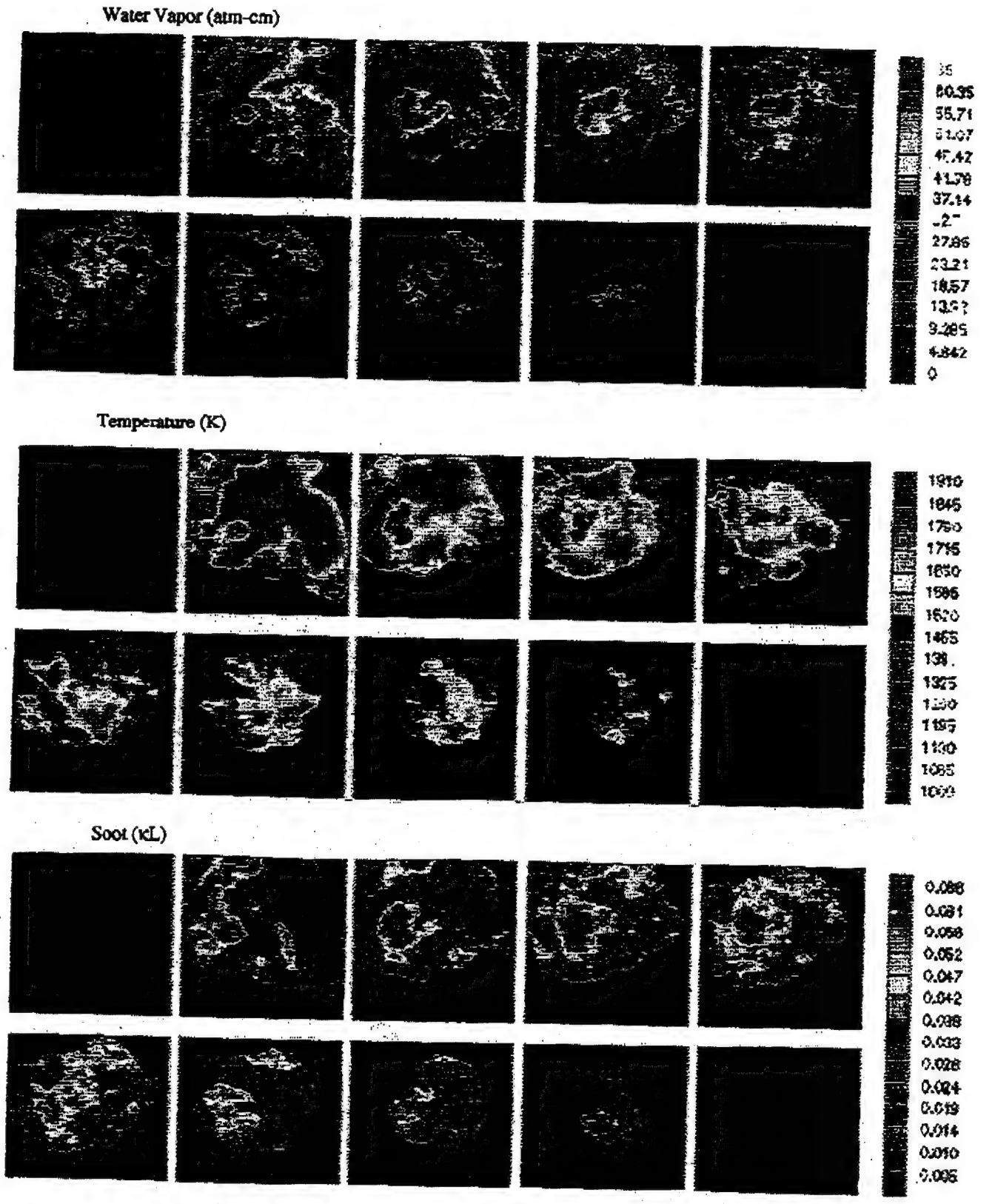

Figure. 12. (B) Distributions of Water Vapor (atm-cm), Temperature (K) and Soot (κL).

regions were interpreted to occur due to the continuous air entrainment expected along the spray axis [21]. Regarding the distributions of water vapor and κL, notably the concentrations are found to be high in the low-temperature zones.

The low κL in those zones may indicate more rapid consumption of soot there, which, however, does not seem to be consistent with the following observation. Since the high temperature zones most probably represent combustion products formed from mixtures with near stoichiometric fuel-air ratios, the water vapor concentration in the corresponding zones should have been also high, which is not the case in the present measurements. The most plausible interpretation of the distributions appears to be a physical factor, which is the high temperature effect on the specific volume of products. Inspecting the data again, when the temperature varies by a factor of two, the concentration inversely changes by about the same value. This finding is most obvious in the later stage of combustion to suggest insignificant impacts by the chemical reactions on the species distributions then.

SUMMARY

Instantaneous distributions of temperature, water vapor and soot were determined in flames by using the Rutgers Super Imaging System (SIS) and new spectrometric methods. Such information may be viewed as "quantitative images."

The SIS permits simultaneous measurement of IR digital images (matrixes) in the same geometrical configuration but in separate spectral bands at successive crank angles at high rates. The spectrometric methods are for processing this raw data to obtain the distributions. These techniques were applied to the investigation of bench-top flames and in-cylinder reactions of both SI and CI engines.

Three new spectrometric methods were presented in this paper: Dual-band mapping method (DBMM); New band-ratio method (NBRM) and Three-band iteration method (TBIM). These methods all employ a new data-based computer program (DBCP) constructed by employing experimental IR data for gaseous species and single-line-group (SLG) model from NASA Handbook (SP-3080).

The concept of DBMM is to find distributions of water vapor and temperature from a mixture when two spectral IR intensity matrices of the mixture are given, which is a reverse process of a common problem of finding the latter when the former are given. Solutions by the method are unique, but errors can be high.

The NBRM is consistent with a few earlier experimental methods employed for temperature measurement in gaseous mixtures. Its concept was conceived during the process of analyzing IR data in the NASA Handbook using the DBCP that the ratio of two spectral intensity of a radiating species in a gaseous mixture is uniquely related to the mixture temperature. Other important characteristics of the method (e.g. pressure effect) were also discovered.

The governing equations of TBIM are basically the Beer's law expressions for three separate species. The three simultaneous equations included absorption coefficients of gaseous species (from DBCP) and those for soot calculated by the Rayleigh-limit expression plus dispersion equation. Because of the implicit nature of the problem, determination of the final results for each pixel was performed by an iteration method.

Instantaneous spectral intensities of a hydrogen-air flame were processed by both DBMM and NBRM. The results are mutually comparable with each other except for some expected errors by the DBMM. They are also consistent with time-averaged measurements obtained from the similar flame using the sodium-line reversal method as found in literature.

The simultaneous determination of distributions of temperature, water vapor and soot formation was achieved by the TBIM. This was made by processing high-speed spectral IR digital images of a reacting spray plume in a direct-injection CI engine equipped with a high-pressure injection system as operated by Diesel oil (D-2). The results appear to be reasonable in view that any indirect evidence does not challenge the validity and that they are comparable with results by others. The new quantitative images as well as the raw data offer some new insight into the reactions in the cylinder.

ACKNOWLEDGEMENT

The present work has been performed under the sponsorship of the U.S. Army Research Office (Contract No. DAAH04-95-1-0430) and AASERT (DAAH04-94-G-0201), Ethyl Corporation and Ford Motor Company.

REFERENCES

1. Uyehara, O.A. and Myers, P.S., "Flame Temperature Measurements-Electronic Solution of the Temperature Equations," SAE Quarterly Transactions, vol. 1, No. 4, 1947.

2. Matsui, Y., Kamimoto, T., Matusuoka, S., "A Study on the Application of the To-color Method to the Measurement of Flame Temperature and Soot Concentration in Diesel Engines," SAE Paper-800970, 1980.

3. El Wakil, M.M., Myers, P.S., and Uyehara, O.A., "An Instantaneous and Continuous Sodium-line Reversal Pyrometer," ASME Transactions, Paper No. 50-A-94, 1950.

4. Myers, P.S. and Uyehara, O.A., "Accuracy of and Representative Results Obtained with an Infrared Pyrometer Measuring Compression Temperatures," Inst. of Mechanical Engineers, pp. 64-75, 1965.

5. Agnew, W.G., "Two-wavelength Infrared Radiation Method Measures end gas Temperatures near their Peaks," SAE Journal, October 1960.

6. Ferriso, C.C., Ludwig, C.B., and Boynton, F.P., "A Band-ratio Technique for Determining Temperatures and Concentrations of Hot Combustion Gases from Infrared-emission Spectra," 10th Symp. (Int'l) on Combustion, 161, The Combustion Institute, 1965.

7. Ludwig, C.B., Malkmus, W., Reardon, J.E., Thomson, J.A.L., Handbook of Infrared Radiation from Combustion Gases," NASA SP-3080, 1973.

8. Jiang, H., McComiskey, T., Qian, Y., Jeong, Y.I., Rhee, K.T., and J.C. Kent,"A New High-Speed Spectral Infrared Imaging Device Applied for Imaging Gaseous Mixtures from Combustion Devices," Combustion Science and Technology, 90, 5-6, p. 341, 1993.

9. McComiskey, T., Jiang, H., Qian, Y., Rhee, K.T., and Kent, J.C., "High-Speed Spectral Infrared Imaging of Spark Ignition Engine Combustion," SAE Paper-930865, 1993.

10. Jiang, H., Qian, Y. and Rhee, K.T., "High-Speed Dual-Spectra Infrared Imaging," Optical Engineering, 32 (6), pp. 1281-1289, 1993.

11. Clasen, E., Campbell, S., and Rhee, K.T., "Spectral IR Images of Direct Injection Diesel Engine Combustion with High Pressure Fuel Injection," SAE Paper-950605, 1995.

12. Song, K., Clasen, E., Chang, C., Campbell, S., Rhee, K.T., "Post-flame Oxidation and Unburned Hydrocarbon in a Spark-ignition Engine," SAE Paper-952543, 1995.

13. Campbell, S., Clasen, E., Chang, C., ad Rhee, K.T., "Flames and Liquid Fuel in an SI Engine during Cold Start," SAE Paper-961153, 1996.

14. Clasen, E., Song, K., Campbell, S., and Rhee, K.T., "Fuel Effects on Diesel Combustion Processes," SAE Paper-962066, 1996.

15. Lewis, B. and von Elbe, G., *Combustion, Flames and Explosions of Gases*, p. 281, Academic Press Inc, 1961.

16. Chang, S.L. and Rhee, K.T., "Computation of Radiation Heat Transfer in Diesel Combustion," SAE Paper-831332, 1983.

17. Bard, S. and Pagni, P.J., Carbon Particles in Small Pool Fire Flame," J. of Heat Transfer, vol 103, pp 357-362, 1981.

18. Dalzel, W.H. and Sarofim, A.F., "Optical Constants of Soot and their Application to Heat Flus Calculation," ASME Trans. vol. 9, p. 100, 1969.

19. Hottel, H.G., Broughton, F.P., "Determination of True Temperature and Total Radiation from Luminous Flames," Industry and Energy Chemistry, 4-2, p. 166, 1932.

20. Abata, D., Stroia, B.J., Beck, N.J., and Roach, A.R., "Diesel Engine Flame Photographs with High Pressure Injection," SAE Paper-880298, 1988.

21. Jeong, Y.I., Qian, Y., Campbell, S. and Rhee, K.T., "Investigation of a Direct Injection Diesel Engine by High-Speed Spectral IR Imaging and KIVA-II," SAE Paper-941732, 1994.

Diesel Engine Response to High Fuel-Injection Pressures

T. Themel, M. Jansons, S. Campbell, and KT Rhee
Rutgers, The State University of New Jersey
Piscataway, New Jersey

ABSTRACT

A single-cylinder direct-injection (DI) Diesel engine (Cummins 903) equipped with a new laboratory-built electronically controlled high injection pressure fuel unit (HIP) was studied in order to evaluate design strategies for achieving a high power density (HPD) compression ignition (CI) engine.

In performing the present parametric study of engine response to design changes, the HIP was designed to deliver injection pressures variable to over 210 MPa (30,625psi).

Among other parameters investigated for the analysis of the HPD DI-CI engine with an HIP were the air/fuel ratio ranging from 18 to 36, and intake air temperature as high as 205°C (400°F). The high temperatures in the latter were considered in order to evaluate combustion reactions expected in an uncooled (or low-heat-rejection) engine for a HPD, which operates without cooling the cylinder.

Engine measurements from the study include: indicated mean effective pressure, fuel consumption, and smoke emissions.

It was found that a Diesel engine incorporated with an HIP under varied operational conditions, including those encountered in uncooled engine design needs variation of injection parameters, namely the start of injection and the rate shape. When the engine operating condition shifts, the rapid variation of those parameters are needed in order to optimize the engine power delivery and fuel consumption as well as to minimize smoke emissions.

Other engine responses to the varied parameters in this high-pressure Diesel engine are also reported in the paper.

INTRODUCTION

The Diesel engine, or compression ignition (CI) engine has several advantages over the spark-ignition (SI) engine. It is more efficient, reliable, fire-safe, and environmentally-friendly than the SI engine, and therefore is almost exclusively employed in long-haul heavy-duty trucks and buses, basically the entire US military fleet (safer fuel and less vulnerable), and merchant marine (lower insurance premium). The engines being used in mining galleries are all CI systems.

A great portion of passenger cars in countries which are trading with the US (in particular Europe and Japan) are powered by CI engines. Since the CI engine is more efficient, it emits less greenhouse gas (CO_2) than a comparable SI engine, a contribution towards the world-wide efforts of minimizing global warming.

The CI engine will be more widely used if it achieves a higher power-density (HPD, horsepower per displacement or weight), cleaner emissions, and quieter operation, goals which have become more sought after and attainable in recent years. For example, consider the two former goals: Better air utilization for a HPD will increase the exhaust gas temperature, which facilitates development of an efficient catalytic converter. Also high air utilization, which has been limited by the smoke emission, has become more feasible through the use of modern electronically-controlled high injection pressure fuel systems (HIP). In addition, the HIP offers a potential for increasing the engine speed, another approach to an HPD.

In developing an HPD CI engine mated with an HIP, however, many design problems will have to be overcome, including a greatly increased engine block temperature (therefore temperatures of intake air, fuel and lubricating oil). The increase will undoubtedly affect processes of CI combustion, notably the preflame reactions and onset of self-ignition, as well as the subsequent heat release and pollutant formation. The impacts on the processes would be more unpredictable when operated at high speeds.

When the methodology of the uncooled CI engine is incorporated in a HPD, which eliminates parasitic components (e.g. the water pump and radiator) as well as the water jacket, the engine power density will further increase. However, the many problems including those mentioned above will undoubtedly become more difficult to solve. In spite of such difficulties, development of an uncooled HPD CI with an HIP operated at high speeds is a great challenge worthy to strive for because it offers a new dimension of opportunity for engine technology advancements and usefulness.

Realizing the need for analysis of the engine response to an HIP, which is expected to alter various in-cylinder reactions as mentioned above, a new study was initiated towards a goal of HPD by the uncooled direct injection (DI) CI engine methodology. Since no such HPD engine is widely used at present, a more reasonable approach was to employ an experimental apparatus representing a real-world DI-CI mated with an HIP operated under varied thermal conditions. This was because the existing DI-CI reciprocating engine is considered to be the system basis employed for the goal of the new HPD engine. Results from the study, thus, were expected to help construct a more useful road-map to the development of an HPD CI engine. The study was also directed to assessing the new engine concept and whether it would satisfy regulatory as well as user requirements.

EXPERIMENTAL

When a DI-CI engine with an HIP is operated at high speeds in order to achieve a HPD, the heat release per displacement will become closer to that in a typical SI engine. This will greatly increase the overall engine temperature, which will affect the in-cylinder reactions to become presumably very different from those in the conventional DI-CI engine. In order to closely investigate the processes, the engine apparatus was constructed to offer engine combustion environments representing as closely as possible those in an HPD DI-CI engine, which is discussed next.

Engine. A Cummins 903 engine (V-8) was utilized to make a unit of V-2 apparatus, a saw-off of a quarter of the original engine, which then was modified to operate only one cylinder and to have the remaining cylinder-piston reciprocate without compression in order to help achieve dynamic balancing. The engine has a bore-stroke of 140-121 mm (displacement of 1.85 liters) and compression ratio of 13.5 to 1. Since the same family of 903 engine has been widely used in the past, no additional discussion on the engine dimensions is made here.

This single-cylinder engine was installed with a new intake-air (electric) heating unit which can increase the air temperature as high as 205°C (400°F) at high speeds, because such a high intake air temperature was expected in an uncooled engine whose combustion reactions were to be also studied. The air was supplied from the building via a pressure controller (maintained at 30.9 KPa or 4.5 psi and higher depending upon the intake air temperature as explained later) and a flow metering unit. The engine cooling was done by using a closed-flow unit (with glycol as coolant) connected to a water-cooled heat exchanger for temperature control. The unit was designed to accommodate a coolant temperature as high as 149°C or 300°F.

The apparatus lined up with an electric dynamometer was sufficiently instrumented in order to implement the objective of the study, including an in-cylinder pressure transducer, temperature probes, and a smoke meter.

High Injection Pressure Fuel System (HIP). Since high utilization of the intake air is an important precondition for achieving an HPD DI-CI engine, which is facilitated by an HIP, a considerable amount of design and development work on a new HIP was a logical step taken in the present study. Note that for earlier studies, a laboratory-built HIP which delivered an injection pressure of up to 165 MPa (24,000psi) was employed [1-3]*, which offered the basic expertise toward the new design-construction of an improved HIP, which is explained in the following.

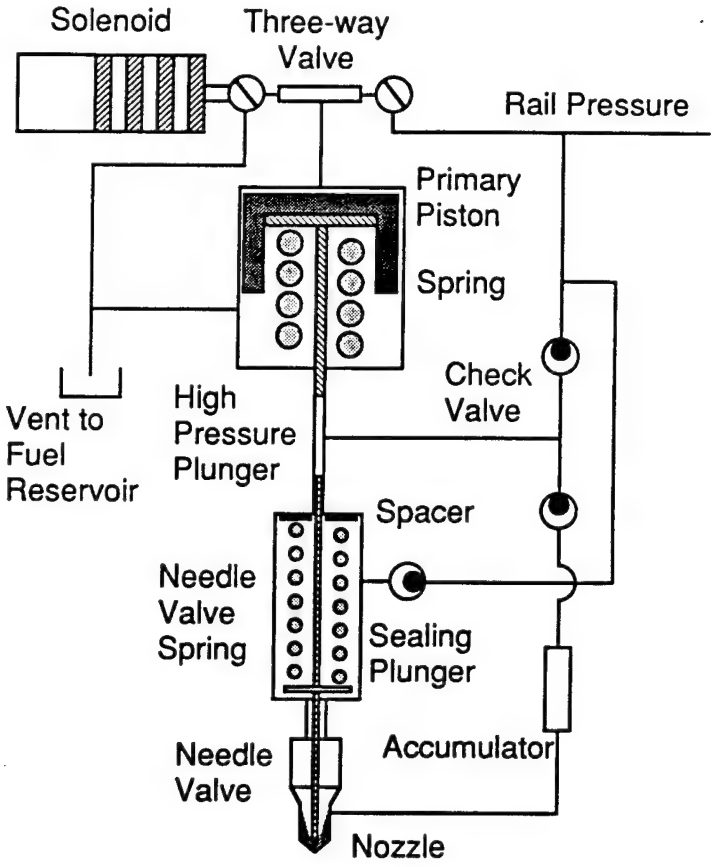

Fig. 1. Laboratory-built Electronically Controlled High Injection Pressure (HIP) Fuel Unit.

In developing and characterizing an HIP unit, one of the more uncertain issues associated with the system performance is the actual injection pressure that a unit can deliver. For example, in a common-rail type HIP, the pressure at the accumulator does not represent the injection pressure at the nozzle tip due to pressure drop expected to occur between the two locations. The pressure intensifier type HIP to be discussed next, however, is considered to be more apprehensive on the issue, that is it generates the injection pressure closer to the nominal value.

A schematic drawing of our new HIP is shown in Fig. 1, and was basically the same design as BKM's Servo-jet type [4]. It is a "pressure intensifier type" having a primary piston where a variable low pressure fuel (as high as 12 MPa or 1,750 psi in this) is connected via a three-way

*Numbers in parentheses designate references at end of paper.

valve at a position as shown in the drawing. The fuel trapped in the lower side of the primary piston and accumulator is compressed by the factor of the area ratio (17.5 for the present design) between the piston and plunger. Since the needle valve is under the same high pressure, no fuel escapes through the nozzle at this time. When the injection is to be made, the three-way valve is switched to a valve position 90 degrees clock-wise from that shown in the figure. This will abruptly relieve the pressure on the upper portion of the primary piston by draining the fluid to the vent reservoir. The subsequent pressure imbalance across the sealing plunger, then, lifts the needle to spill the fuel at a high pressure into the combustion chamber.

The present unit was designed/fabricated in such a way as to directly engage it with the low-pressure fuel supply port in the Cummins 908 engine cylinder head, which was not possible in the factory-delivered Servo-jet unit. That is, the original stock PT-type injector in the engine was simply replaced by the newly designed unit with no additional modification of the head. This resulted in a unit with the same external dimensions as the PT injector. This consideration suggested a direct use of, in the new unit, both a nozzle tip holder and the nozzle tip as well as the o-ring from the PT injector.

By taking the high pressure fuel injection into consideration, which will produce high injection rates, a stock nozzle tip having the smallest nozzle hole diameter (0.15mm) available to us was incorporated in the new unit. (This measure was also meaningful for flexibility and economic reasons.) In designing the new unit, however, a computational analysis indicated that the nozzle tip holder in the existing PT-nozzle was not made sufficiently strong to withstand the high-pressure generated by the present intensifier. Consequently, all of the components in the unit were newly fabricated in our laboratory except for the three-way solenoid valve and the abovementioned nozzle-tip.

Regarding the pressure at the nozzle tip before the injection, recall the dead-weight type calibration-device for testing pressure gages, which utilizes a similar concept as the present unit does. Except for the dynamic and transient nature of the performance in the present unit, the injection pressure at the opening of the nozzle, thus, is considered to closely represent the nominal pressure determined by the (low) rail pressure and the area ratio mentioned above. Although the physical concept of the dead-weight device employed in the unit is perceptive, it would be desirable if the pressure-time history at the tip would have been determined for backing up this expectation, however.

The control of the injection pressure, therefore, was made by adjusting the fuel rail pressure from a gear-pump. On the other hand, the amount of fuel injected by the new unit was controlled by the thickness of a spacer placed at the upper end of the needle valve spring. The purpose of using the spacer was to vary the cut-off pressure of fuel injection. That is, the thicker the spacer, the stronger the preload of the spring and the earlier closing of the needle valve. Note that the cut-off pressure without any spacer was adjusted at approximately 61 MPa (10,000 psi). For varied amounts of fuel injection, the unit opens the needle valve at the same time, but closes it sooner for a smaller amount of fuel injected but at a higher cut-off pressure.

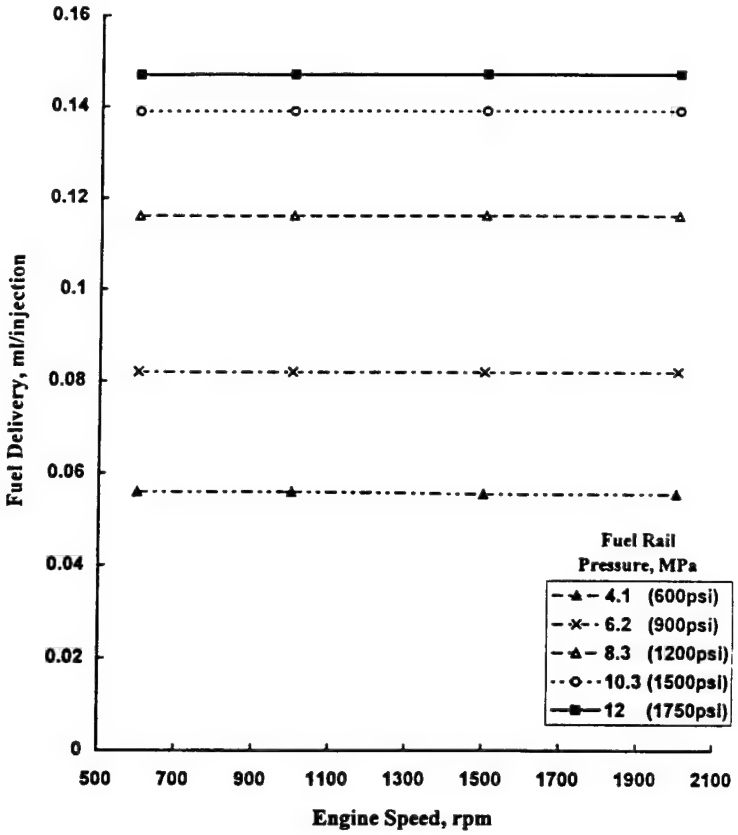

Fig. 2. Relationship of Fuel Delivery to Engine Speed and Fuel Rail Pressure (Spacer thickness, 0.76 mm).

Characterization of HIP. After completing construction of the new unit, an extensive system characterization was performed using a bench-top test device. The injection time was determined by placing a pressure transducer at a location approximately 10 mm away from the nozzle hole while the period of energizing the three-way valve was varied. This determines the period of connection between the rail pressure and the primary piston. The timing of the pressure transducer signal was compared with the end of the energizer period when the needle was expected to rapidly lift up.

Figure 2 shows the relationship of the amount of fuel delivery to the engine speed for varied rail pressure. The result exhibits a predictable performance of the new unit, a trend which was the same for all spacer thicknesses employed in the experiment. Note that the rail pressure represents the injection pressure determined by the intensifier (area) ratio, that is 17.5. For example, the rail pressure of 12 MPa corresponds to an injection pressure of 210 MPa (30,625 psi) at the nozzle opening.

Results obtained using all of the spacers were combined to plot Fig. 3, which facilitated determination of the amount of fuel delivery. As expected for a given spacer thickness, the higher the rail pressure the greater the amount of fuel delivered. The results shown in the figure for variation of spacer thickness and rail pressure were employed for the range of the present parametric study of the

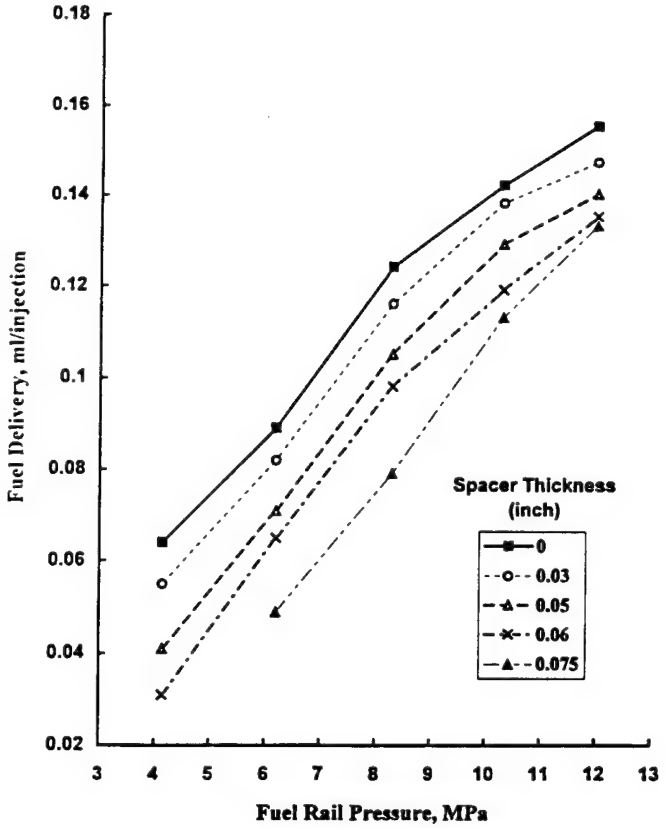

Fig. 3. Fuel Delivery Affected by Rail Pressure and Spacer Thickness.

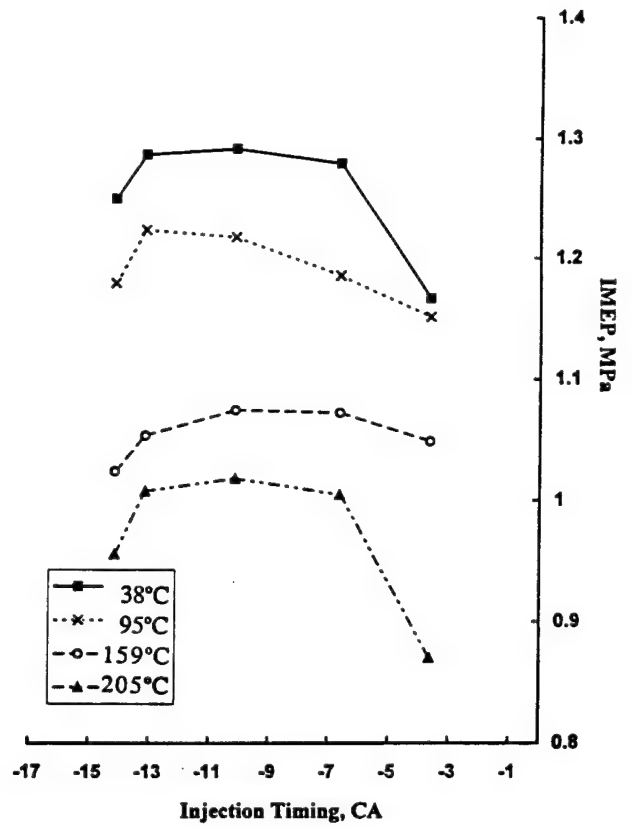

Fig. 4. IMEP for Varied Injection Timing and Intake Air Temperature (1000rpm, Rail Pressure 12Mpa).

HPD CI-DI engine with HPI. For example, the mass of air flow into the engine was compared with the fuel delivery from this plot in order to determine the overall air-fuel ratio for each engine running condition.

RESULTS AND DISCUSSION

The experiment was conducted in two steps. At first, the engine equipped with the new HIP was operated by varying injection time for different intake air temperatures as listed in Fig. 4. This was done at 1,000 rpm speed and 210 MPa injection pressure (by having rail pressure of 12 MPa). Measurements shown in Fig. 4 suggested that the start of injection at 10 degrees of crank angle (CA) before the top-dead-center (bTDC) was proper for the experiment. Therefore, the first part of the experiment was performed at this fixed injection time.

The analysis of the large amount of engine measurements accumulated in the above experiment, however, indicated that the fixed injection timing for a wide range of engine variation was improper as explained later. Consequently, the same engine experiment was performed at varied injection times producing the best-torque under the respective operating conditions, the second step of the experiment which was not planned in the beginning.

Explaining the results, the indicated mean effective pressure (IMEP) determined from the pressure-time data are shown in Fig. 5 for varied engine conditions as noted by individual symbols. The family of curves obtained for fuel injection pressures in MPa of 210 (30,625 psi), 180 (26,250 psi), and 144 (21,000 psi) is included, respectively. The overall results exhibit a trend as expected, which is the lower the air/fuel ratio, the higher the IMEP. The engine speed did not appear to significantly affect the results for the range of investigation in the study, which is further discussed below. Most notably, it was possible to run the engine as rich as 18 to 1 air/fuel ratio while the smoke emission was no worse than that observed with the conventional PT injector operated at leaner overall ratios of 35 to 1.

The increase of IMEP achieved in the present CI-HIP engine by better utilization of the trapped air, which increased by a factor of almost two compared with the conventional engine, is highly promising in paving the way to designing an HPD engine. It is pointed out that the generation of high injection pressures requires an increased consumption of the power from the host engine, which will deteriorate the specific fuel consumption, as further discussed later. Nevertheless, the present results by the use of an HIP seemed to shed some strong light into a possibility of operating a CI engine at richer air/fuel ratios, which are more closer to the stoichiometric.

Although no attempt was made to measure engine noise in the study, it is pointed out that noise became higher when the engine was operated overall rich, i.e., as it came closer to the stoichiometric. Expecting that the elimination

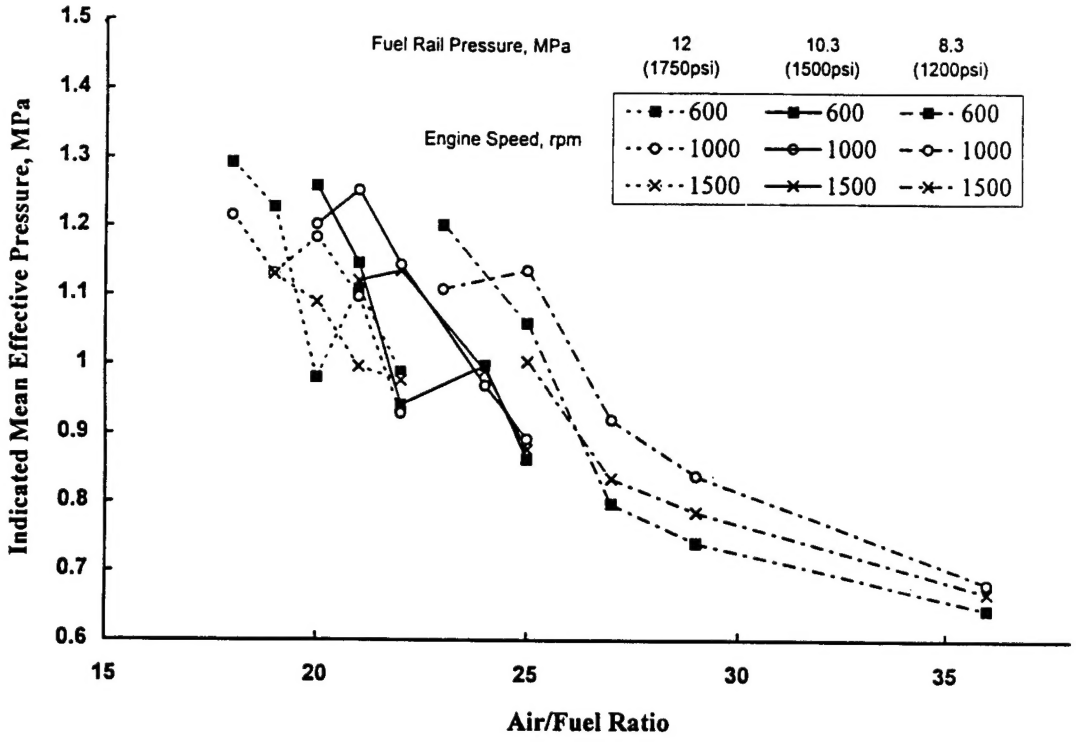

Fig. 5. Indicated Mean Effective Pressure (IMEP) as a Function of Air/fuel Ratio (all engine speeds at Intake Air Temperature 38℃ and Injection Timing of 10 BTDC.

of exhaust NOx emission by a catalytic converter would be facilitated when the exhaust gas temperature greatly increases via a high air utilization, no attempt was made to measure its emissions. To support this consideration, it is noted that the exhaust temperature ranged between 360-416° C (680-780° F) when the engine ran at air/fuel ratios of 30-20 to 1.

Recalling Fig. 3, since for a given thickness of the spacer, the higher the rail pressure (thus the injection pressure) the greater the amount of fuel flow through the nozzle, the IMEP increased with the rail pressure (Fig. 6). This trend was similarly found for other intake air temperatures. As briefly mentioned above, the speed effect on the measurement was small except that it appeared to peak at 1000 rpm, the same speed employed for determining the (optimum) injection time (Fig. 4). An additional discussion is made later on the need for varied injection time as related to this observation.

Intake Air Temperature. The measurements explained above were obtained for intake air temperatures (°C) at 38, 95, 150, and 205, respectively. Figures 7-10 were plotted for comparison purpose of intake temperature effects on IMEP for varied overall air/fuel ratios and injection pressures. Although the observation of a higher IMEP by a richer air/fuel ratio was expected, its great deterioration at higher intake air temperature was a surprise. Since the fuel system was adjusted to deliver a fixed amount of fuel according to the bench-top calibration (Fig. 3), the intake pressure was increased to compensate the deterioration of volumetric efficiency with increase of the air temperature. It is reminded that the measurements were obtained for high

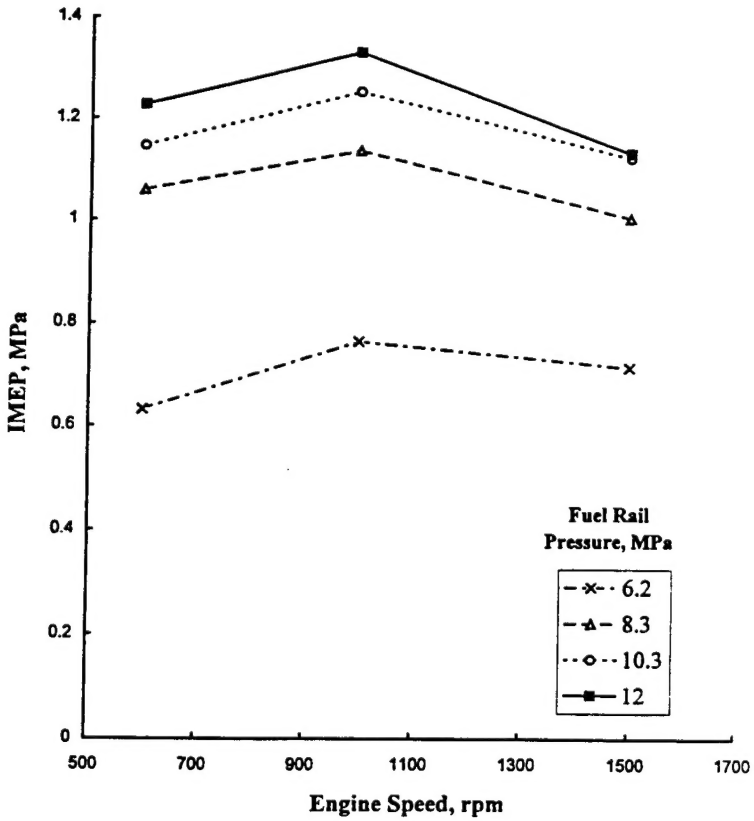

Fig. 6. IMEP as a Function of Injection Pressure (Spacer, 0.76mm). Intake Air Temperature, 38°C.

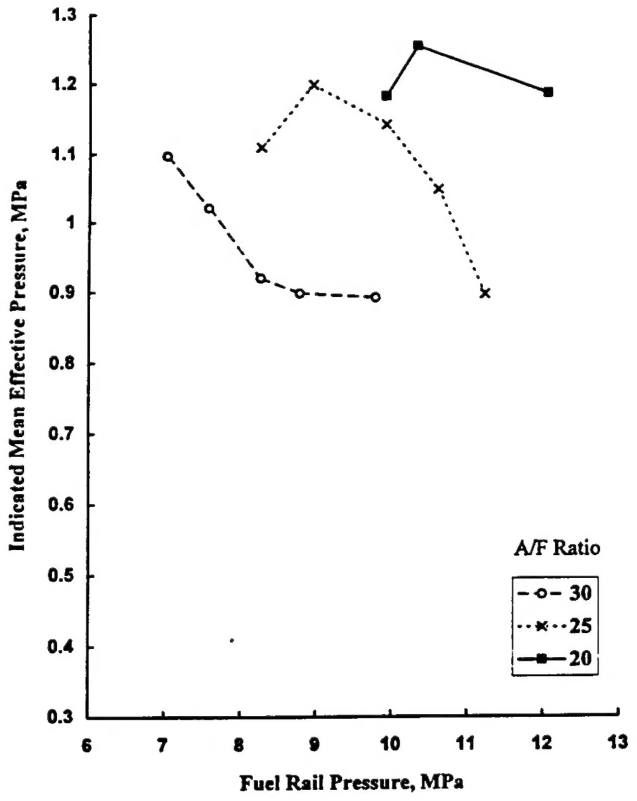

Fig. 7

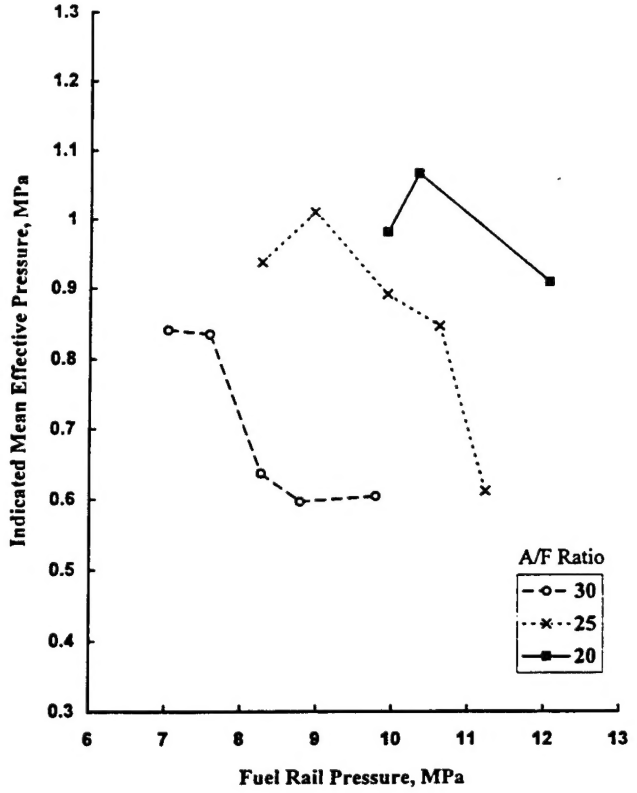

Fig. 9

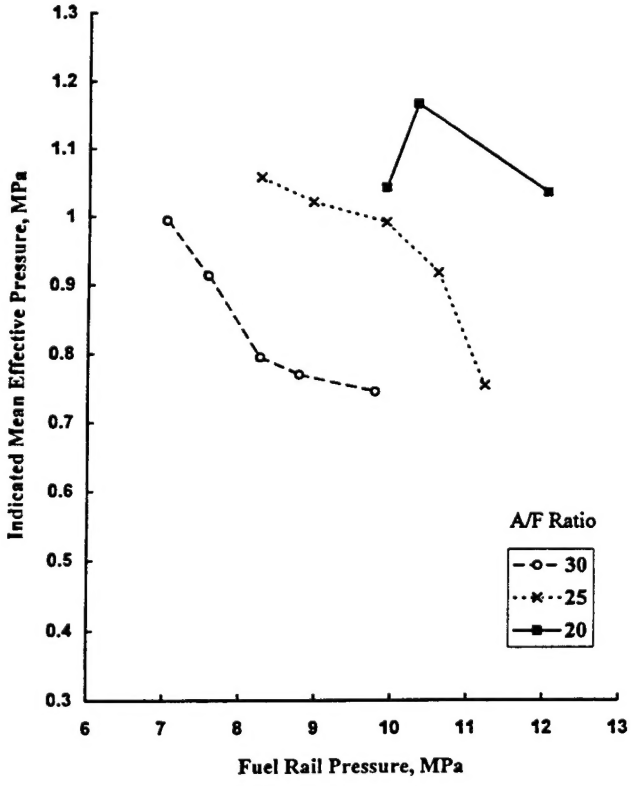

Fig. 8

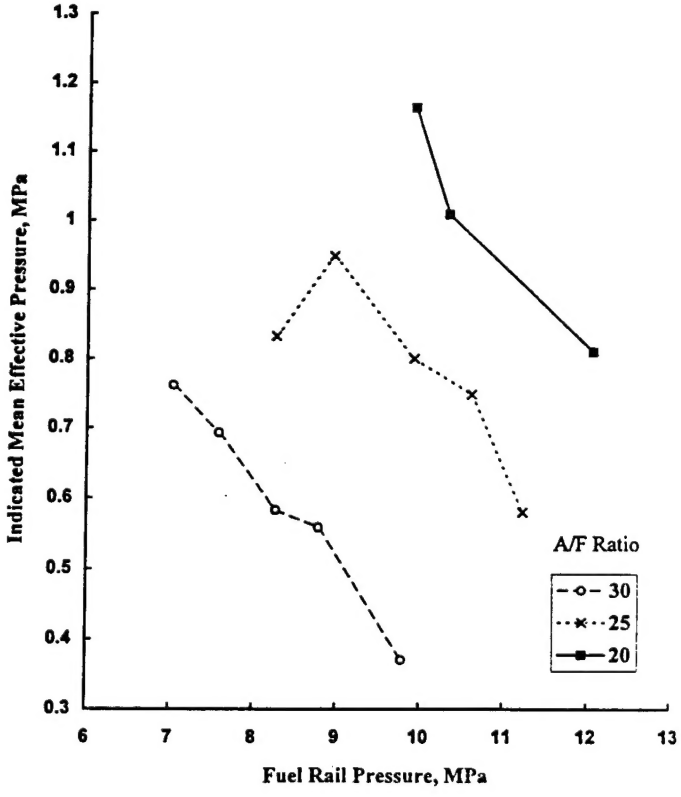

Fig. 10

Figs. 7-10. Indicated Mean Effective Pressure (IMEP) as a Function of Air/fuel Ratio and Rail Pressure for Varied Intake Air Temperatures (T_a): Fig. 7, T_a =38°C; Fig. 8, T_a =95°C; Fig. 9, T_a =150°C; Fig. 10, T_a =205°C.

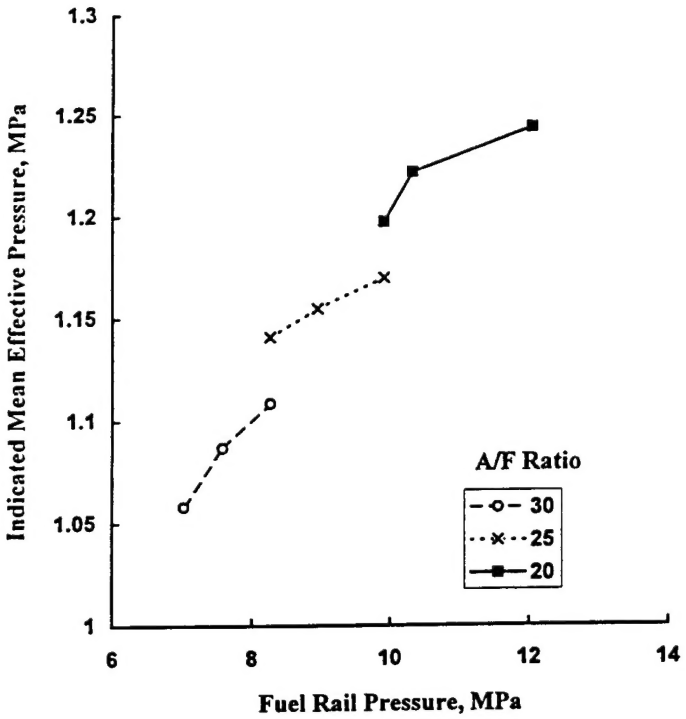

Fig. 11. Indicated Mean Effective Pressure as a Function of Fuel Rail Pressure (1000rpm, 38°C Intake Air Temperature) for Variable Injection Timing.

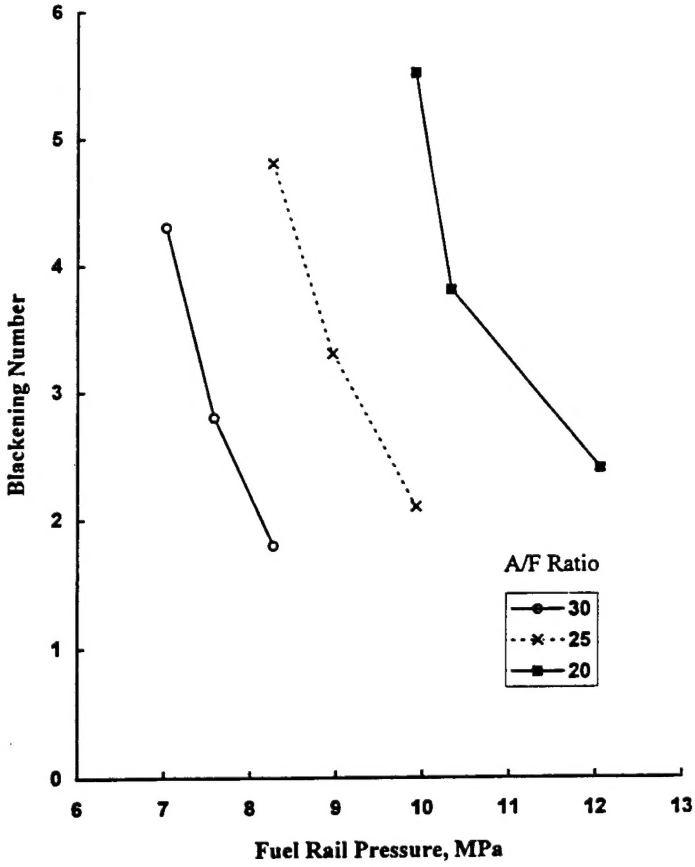

Fig. 12. Smoke Emission, Bosch Blakening Number as Function of Fuel Rail Pressure and Air/fuel Ratio.

temperatures of the intake air in order to assess the engine response when the uncooled (low heat-rejection) design is incorporated, which would have a high engine-block temperature resulting in the intake air heating.

Several reasons for the significantly decreased IMEP with increased intake air temperature may be considered. First of all, since the ignition delay (ID) would decrease with the temperature, a fixed injection time (and even the rate shape) should have been shifted for an optimum power torque output. Next, a decreased ID will result in a smaller amount of heat release from the premixed combustion stage (and thus an increased amount of heat release via the diffusion-controlled combustion) to cause a deteriorated cycle efficiency. Note that when these happen, the formation of soot, in general, is expected to increase, which in fact was the exact observation in the experiment. While such a deterioration of combustion and energy conversion efficiency is considered, recall Fig. 3 showing the calibration results determining fuel flow rate obtained at room temperature using a bench-top apparatus. Those measurements, however, may not be repeated when the intake temperature was increased, because of a probable decrease in the flow rate with increase of the temperature. If this is the case, a decreased IMEP is expected to occur, which needs further investigation.

Also, what was most unexpected was the somewhat decreasing trend of IMEP with increase of the rail pressure (thus the injection pressure), which was contrary to an expectation that combustion would improve when a "better" fuel spray is achieved by an HIP. The decreasing trend was found in *all* temperatures of intake air and air/fuel ratios. Reviewing the measurements, it came to examine the effect of the injection time, which was tested in the beginning and set at 10 bTDC for the experiment (Fig. 4). This was because when the injection pressure was varied, the change in ignition delay was considered to be altered enough to affect the energy conversion efficiency. Note that the need for shifting the injection time is unusual in the conventional CI-DI engines equipped with a mechanical injection unit, which mostly maintain the injection time at a fixed CA.

Figure 11 shows the results obtained in a similar measurement performed as above by varying the injection time that produces the best torque for each engine condition especially at respective injection pressures. The overall trend was quite the same at other intake air temperatures, which indicates an obvious need for adjusting the engine fuel system to deliver a new injection time in order to obtain the best IMEP. This observation led us to recall the adjustment of ignition time in the SI engine under different engine conditions.

Since an HPD from a CI engine is meaningful if the exhaust smoke emission is acceptably low, its measurement was conducted (using a Bosch smoke meter) and the results are plotted in Fig. 12. As expected the higher the injection

pressure, the lower the smoke emission. When the injection pressure was at 210 MPa, the measurement with air/fuel ratio of 20 was almost as low as that obtained for air/fuel ratio of 30 (injection pressure of 145 MPa, or 21,000 psi). The result suggests that an additional reduction is possible if the injection pressure is further increased in all air/fuel ratios investigated. It is reminded that these measurements were much lower than those observed in the same engine with the (low-pressure) conventional PT injector.

A HIGH-POWER-DENSITY CI ENGINE

The present study was directed towards investigation of some engine design strategies to achieve an HPD DI-CI engine, in particular when the engine is equipped with ceramic components for uncooled operations. Several issues may be discussed in consideration of achieving the goal.

An increased air utilization appears to be highly promising by the use of an HIP as demonstrated in the present study. It was possible to operate an engine having an injection pressure of 210 MPa by using an HIP at air-fuel ratio as high as 18-1 to produce smoke emissions comparable or lower than those from a DI-CI engine equipped with a conventional low pressure injection unit. The high air utilization, however, resulted in several consequences, including high engine block and exhaust temperatures, and increased noise. Note that the temperatures will become higher when an uncooled engine design approach is employed, whose impacts on the goal of developing an HIP are in need of discussion.

Most of all, the volumetric efficiency will greatly deteriorate, in an uncooled high air-utilization engine, to cause a low mean effective pressure as studied in the present work. The use of a high performance turbocharger or supercharge, therefore, may become a precondition for an HPD uncooled engine, which also may have to use inter-cooling. In addition, the high engine temperature will undoubtedly increase the injector as well as the fuel temperature. The results obtained in the present study suggest it is probable that the fuel flow rate out of the injector may be affected with the injector temperature. When there is no positive remedy for this, the fuel would attain super critical temperatures. This then will modify the spray formation, affect the lubrication of the injector itself and even damage the nozzle holes by cavitation in the fuel stream.

The high exhaust gas temperature, on the other hand, may be a useful ingredient for achieving an HDP engine by facilitating the incorporation of a turbocharger in the engine. Also, the high exhaust temperature may offer an opportunity for using an exhaust catalytic converter to produce a cleaner emission, which then may make it possible to further increase the air utilization.

The development strategies of an uncooled HDP DI-CI engine using ceramic components is certainly a great challenge involving various technical problems as briefly discussed above. There is no question that they would not be easy to surmount, but they offer an exciting opportunity for advancing the engine technology.

ACKNOWLEDGMENT

The present work has been performed under the sponsorship of the U.S. Army Research Office (Contract No. DAAH04-95-1-0430, and DAAH04-96-1-0459).

REFERENCES

1. Clasen, E., Campbell, S., and Rhee, K.T., "Spectral IR Images of Direct Injection
Diesel Engine Combustion with High Pressure Fuel Injection," SAE Paper-950605,
1995.
2. Clasen, E., Song, K., Campbell, S., and Rhee, K.T., "Fuel Effects on Diesel Combustion Processes," SAE Paper-962066, 1996.
3. Chang, C., Clasen, E., Song, K., Campbell, S., Jiang, H., Rhee, K.T., "Quantitative Imaging of In-cylinder Processes by Multispectral Methods," SAE Paper-970872, 1997.
4. Abata, D., Stroia, B.J., Beck, N.J., and Roach, A.R., "Diesel Engine Flame Photographs with High Pressure Injection," SAE Paper-880298, 1988.